Integration of drone data and field investigations to investigate avalanche potential in steep cliffs, with examples from Western Norway

Master Thesis
Basin and Reservoir Studies

Anine Eikrem Helland

University of Bergen

Department of Earth science

November 2019

Abstract

The geology, topography and climate in Norway makes it vulnerable to avalanches and can cause great socio-economic consequences, human losses and structural damages. To keep these fatal consequences on its minimum it is important to monitor and map slopes prone to avalanches. However, this can be expensive, demanding and dangerous due to terrain conditions and inaccessibility to the slopes. The last years a simpler, safer and cheaper method has been developed, by collecting data using unmanned aerial vehicle (UAV) and create 3-D models of cliffs and avalanche fans.

In this thesis a workflow is evaluated, where a combination of photogrammetric models (acquired by using a drone), field observations and lichenometry, is used to understand avalanche potential in steep slopes. Three well-exposed, accessible cliffs, prone to avalanches has been investigated in; Vinddal in Bergen, Taulen in Voss and Mundal in Sogndal.

This study shows that, by combining photogrammetric models acquired using a drone, field observations and lichenometry, information about the characteristics of the cliff and the slope can be acquired, and thus help to understand the avalanche potential.

The results show that rockfall and rockslide are the most important processes in both Vinddal and Taulen, whereas in Mundal, in addition to rockfall and rockslide, snow avalanches and debris flow were also recognized. Vinddal is considered to be the most active area. Several fresh rocks in the middle and upper part of the fan indicated that smaller rockfalls still frequently happens, but avalanches large enough to reach the distal part of the fan is rather unlikely to happen in the near future. In Taulen the avalanche activity is estimated to be low, even though dangerous fracture sets and overhanging blocks are observed. However, a camp site and a farm are located close to the cliff, and can suffer great damages from a potential avalanche. In Mundal the activity and type of avalanche is highly depending on the season (weather).

Using drones to collect data in the field is a safe and effective approach. Within a few hours, the drone had acquired data from large areas of both the cliff and the slope. High quality 3-D data enabled detailed analysis of the cliff (e.g. fracture patterns) and the slope deposit (e.g. size distribution). Further, vegetative analysis and lichenometry conducted in the field, provided an age estimate of several deposited rocks, that was later used to estimate avalanche frequency and activity in each of the studied areas.

Acknowledgment

First and foremost, I wish to thank my supervisor Christian Haug Eide at the Department of Earth Science, for his good supervision, inspiration and feedback. I really appreciate how easy it has been to come by your office for a chat. I would also like to thank Casey William Nixon for shearing his knowledge and for the many hours he has spent helping me. I am also grateful to Thomas Thuesen and Torbjørn Haga for their assistance during fieldwork and helpful input that have improved my work. Further, I am grateful for financial support for fieldwork provided by the Department of Earth Science at the University of Bergen.

Thanks to my fellow students, family and friends, who have all contributed in different and highly valuable ways. A special thanks to my mom, Gro, and my dad, Reidar, for their support, helpful input and reviews.

Contents

1 Introduction

The geology, topography and climate in Norway makes it vulnerable to avalanche and other natural hazards. Avalanches are rapid gravitational movements of soil and rock debris, characterized in steep slopes. It is one of the most important causes of natural disasters in Norway, and can cause great socio-economic consequences, human losses and structural damages. During the last 150 years about 2000 humans have died in such events (Sulebak, 2007). To keep these fatal consequences on its minimum it is important to monitor and map slopes prone to avalanches (Lied, 2014). However, there are challenges associated with this. Mapping and monitoring avalanche slopes can be demanding and dangerous due to, among other things, terrain conditions and inaccessibility. In order to reduce these challenges, a simple and safe method is required, making it safer and easier to investigate and monitor slopes (Abellán et al., 2014).

The traditional methods of monitoring movement and changes on a cliff are based on point-based measurements, such as GPS. These methods have high precision and are highly accurate, but do not provide information on the entire area, only at a few measuring points. In addition, the measuring points must be placed where there are movements, and since this area often is unknown, an extra method that can identify the area in motion is crucial (Norang, 2016). Moreover, these methods require high mobilization and operational costs, and are therefore only feasible for mountain areas large and dangerous enough to provide the necessary economies of scale. By using a less expensive and simpler method, it is possible to also monitor and investigate smaller mountain areas, and thus a wider range of areas.

In this thesis, a drone is used to create photogrammetric models of slopes susceptible to rockfall and rockslide. This is an easy, safe, detailed and efficient method to investigate large, dangerous cliffs exposed to avalanches. With high quality 3-D models, information about important characteristics from both the cliff and the slope can be acquired. Further, by combining these models with field investigation and lichenometry, a better understanding of the avalanche potential, including activity, frequency and hazard, in steep slopes is acquired.

Three areas exposed to avalanches in Western Norway is studied; Vinddal in Bergen municipality (figure 1-1A and 1-2A), Taulen in Voss municipality (figure 1-1B and 1-2B) and Mundal in Sogndal municipality (figure 1-1C and 1-2C). Data from each area is collected by using a drone, and further used to create photogrammetric models that provides detailed information about the cliffs and the avalanche deposits. Additionally, field investigation,

lichenometry, vegetative analysis is conducted in order to get a more detailed analysis of the avalanche deposits and understand the avalanche potential. The lichenometry measurements are performed in two graveyards, one at Oppheim kyrkje in Voss (figure 1-1D) and one at Åsane Gamle kirke in Bergen (figure 1-1E).

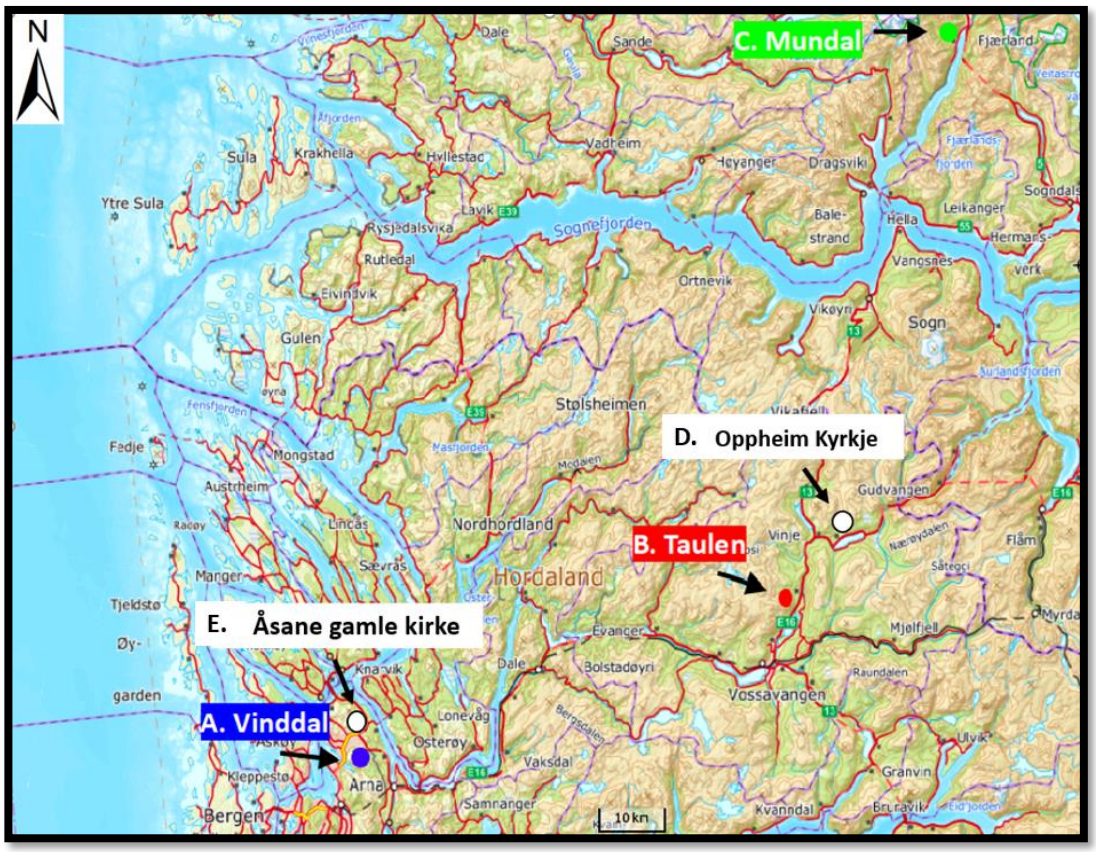

Figure 1-1: Map of western Norway showing the three study areas and the two graveyards investigated. A: Vinddal, B: Taulen, C: Mundal, D: Oppheim kyrkje and E: Åsane Gamle kirke (Modified from Kartverket, 2019b)

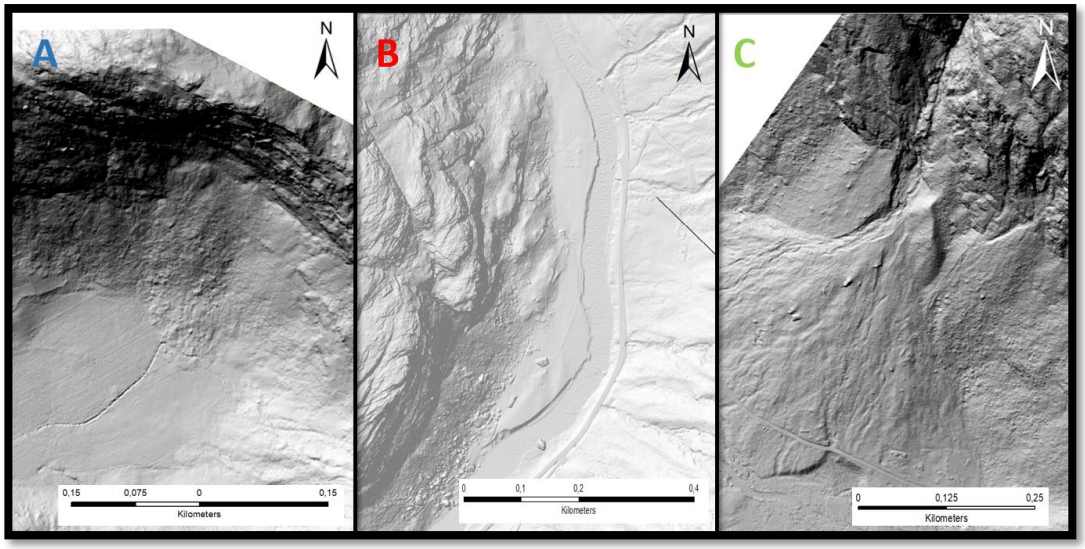

Figure 1-2 Three hillshade maps from the three study areas; A: Vinddal, B: Taulen, C: Mundal.

1.1 Project goals

The goal of this thesis is to evaluate a workflow for understanding avalanche potential in steep slopes, by combining photogrammetric models acquired using a drone with low-cost field observations and investigation of nearby gravestones. The project has the following 4 objectives: (1) Investigate 3 well-exposed, accessible cliffs that are prone to avalanche processes and with little human modification, (2) characterize the structural characteristics of the cliff face (fractures, bedding) for each of the three areas using photogrammetric models, (3) investigate distribution and size of fallen blocks by using orthophotos from the studied areas, (4) investigate relationship between age and vegetation in graveyards close to the studied sites, and combine these datasets with vegetative analysis during fieldwork, to estimate the avalanche frequency and activity at the studied sites.

2 Theoretical background

2.1 Avalanche activity in western Norway from last ice age until today

There have been relatively rapid changes between ice ages and interglacial periods during the quaternary period (the last 2.6 million years (Ma)). The Quaternary period is normally divided into two epochs, the Pleistocene (2.6 Ma - 11 700 years before present (PB)) and the Holocene (11 700 years BP - today). The Pleistocene is characterized by alternations between ice ages and interglacials, while Holocene, which is the current era, represents the last interglacial period (Mangerud et.al., 2011).

The Fennoscandian ice cover in western Norway reached its maximum prevalence in last glacial maximum (LGM) and lasted between 20-23 ka BP (1ka=1000 years) (Mangerud et.al, 2011). After this the deglaciation started and lasted until the ice sheets melted away in Holocene. During the deglaciation there were several glacial advances as a result of frequent and short climatic fluctuations (e.g. Andersen, 1980). The largest glacial advance happened during Younger Dryas (12 900 – 11 700 years BP) where the glacier front moved towards the coast, covering among others, all the study areas; Sogndal, Voss and Bergen (Hughes et.al., 2016). After Younger Dryas, the ice cover quickly melted away as a result of milder climate and calving in the fjords (e.g. Andersen, 1980; Hughes et al., 2016). During Holocene, smaller sized ice caps has existed in the western part of Norway (Dahl and Nesje, 1993, 1996; Bakke et.al 2005). Today, western Norway is still partly glaciated, where several small glaciers drain into the fjords and lake systems.

Mountain areas that has been affected by multiple glaciations tend to be highly susceptible to colluvial processes such as rockfalls, rockslides, rock avalanches, snow avalanches and debris flow (e.g. Böhme et.al.,2015). According to Blikra and Nemec (1998), areas that was covered with ice during Fennoscandian Ice Sheet re-advance in Younger Dryas is assumed to have higher intensity of these colluvial processes.

Within certain periods in Holocene the avalanche activity in western Norway has been higher. Bøe et al. (2004) and Bellwald et al. (2019) suggests that this is a result of seismic activity and/or climatic conditions. In an article, by Bellwald et.al. (2019), 125 mass transport deposits were identified and dated, resulting in a table showing the avalanche activity within different time intervals (Table 2-1). The period between Early Holocene (11 700 years BP) to ~ 8 200 years BP is characterized by high avalanche activity in western Norway as a result of the glacial

impact on the landscape and the recovery of glacial isostasy, which reactivated shallow fault planes and increased earthquake activity (Gudmundsson, 1999).

In the following period, mid-Holocene (8 200 - 4 200 years BP), the avalanche activity was lower, which may be a related to a period with low seismic activity (Bellwald et al., 2019). Further, in the beginning of late Holocene, from about 4 200 year BP, the avalanche activity increases again. This may be explained by the climatic changes and/or increased earthquake activity (Bøe et al., 2004).

Tabell 2-1: Time intervals with normal or high subsea avalanche activity and/or tsunami. Events written in italics represents events with great uncertainty. Modified from (Bellwald et al., 2019).

Time interval (cal.yr. BP)	**Event(s)**	**Suggested trigger mechanism**	**Avalanche time with high or normal activity**
11 000 – 9700	High avalanche activity	Glaci-isostatic processes, earthquake activity and high sedimentation rate	High: Snow avalanche, rock fall/slide/avalanches and landslides
8300 – 7700	Low avalanche activity (Storegga-tsunami)	Earthquake activity. (Big submarine avalanche)	
4200 – 4100	High avalanche activity (*Trænadjup-tsunam)*	Earthquake activity. (*Big submarine avalanche*)	High: snow avalanche
3600 – 3200	High avalanche activity	Climatic condition and earthquake activity	High: snow avalanche Normal: clay slide
3100 – 3000	Normal avalanche activity	Climatic condition and earthquake activity	Normal: snow avalanche
2700 – 2200	High avalanche activity (*avalanche in Storeggagropen*)	Earthquake activity	High: rock fall/slide/avalanche Normal: landslide and snow avalanche
1800 – 1000	Normal avalanche activity	Climatic condition and earthquake activity	Normal: snow avalanche

2.2 Avalanche risk and building regulations

Risk assessments in areas that are exposed to geohazards are important to prevent material damages, and damages or loss of human lives. Gaining knowledge of hazardous areas and taking this into account in planning and development is the most effective way to do this (NGU, 2019b). Based on the avalanche activity, Norway have clear sets of regulations and rules for in which areas it is allowed to build in. In order to prevent the fatal consequences an avalanche event can cause, Norway has developed two organizations; 1) NGI, considered as the avalanche experts, evaluating and determining danger zones, and 2) NVE, the national avalanche authority, with the responsibility to make sure that the rules and regulations are complied with (NGI, 2019a).

Due to Norway's special geographic conditions it is impossible to not develop society in avalanche prone mountain areas. In order to adapt to the avalanche risk, two stage approach has been developed. The first step, carried out by NGU, is mapping mountain areas where potential unstable slopes can collapse in the future (NGU 2019a). The second step, carried out by NVE, is to preform periodic displacement measurements in all areas that show movement and where people live within the hazard zone (despite risk level being considered as acceptable). In areas where the risk level is considered as unacceptable, continuous monitoring and early-warning practices are put in place (NGU, 2019a).

When mapping, several methods can be used, such as studying historical frequency, field work and digital tools (aerial photos, high resolution images and digital elevation models). In order to estimate avalanche risk in steep terrain, NVE have created two types of maps; the susceptibility map and the hazard zone map, which are compared in figure 2-1 and 2-2. The susceptibility map (aktsomhetskart) are normally generated by using GIS based on a terrain model and experience-based runout/outflow calculations (NVE, 2016). Because the runout area often is based on an analysis of the 25 m elevation model, some areas within the hatched zone, specially the outer edge, can have a very small possibility of being hit by avalanches (NVE, 2019b). The susceptibility map is often used in land planning to prevent building in areas exposed to avalanches. Without these susceptibility maps, development in dangerous avalanche prone areas can cause major economic losses and loss of human lives. However, refusing to build in areas that have very low probability of avalanches leads to inefficient land use and discontent with the public authorities.

The hazard zone map (faresonekart) is more detailed than the susceptibility map. It illustrates danger zones for different avalanches based on the repeat intervals given by zooning plans and building applications (reguleringsplaner og byggesaker). A combination of a detailed terrain model, information on local geology and geomorphology, and information about earlier avalanches in the area, are used to create the hazard zones (NVE, 2016). Each hazard zone represents maximum runout distance with repeat interval of once every 100, 1000 and 5000 years, thus provide an important tool in governmental zooning plan and building development plan (reguleringsplaner og bebyggelsesplan) (NVE, 2016). Within the zone of repeat interval 1/100 it is allowed to develop constructions where people do not normally live, and the economic or other social consequences are small (e.g. garages). Within the repeat interval of 1/1000 it is allowed to build construction where there is normally an estimated maximum of 10 people, and where there are medium economic or other social consequences (e.g. houses). Within the repeat interval of 1/5000, development of constructions with major economic or other social consequences are allowed (e.g. hospitals and schools). Because the danger zone map is created based on a more detailed analysis, larger areas are defined as safe compared to the susceptibility map (NVE, 2016).

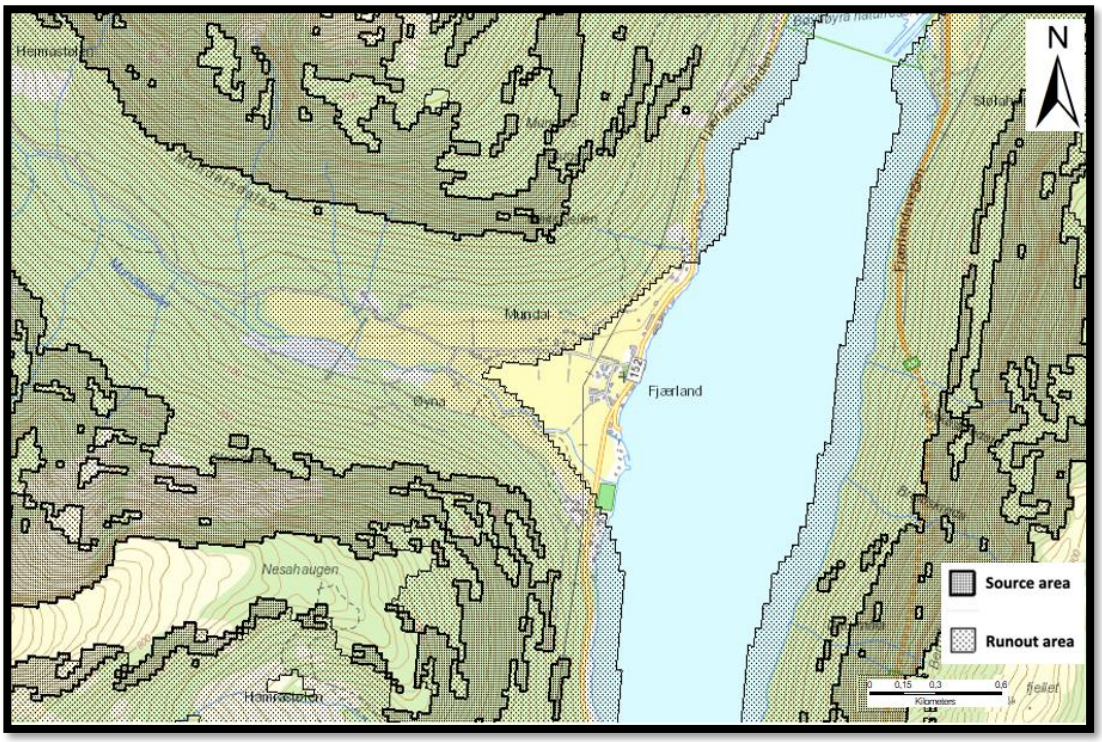

Figure 2-1: Susceptibility map for rockfall in Mundal (1:7500). The darkest hatched areas = possible source area for rockfall. The lighter hatched areas = a theoretical possibility to be hit by a rockfall. Adapted from NVE (2019c

Figure 1:)

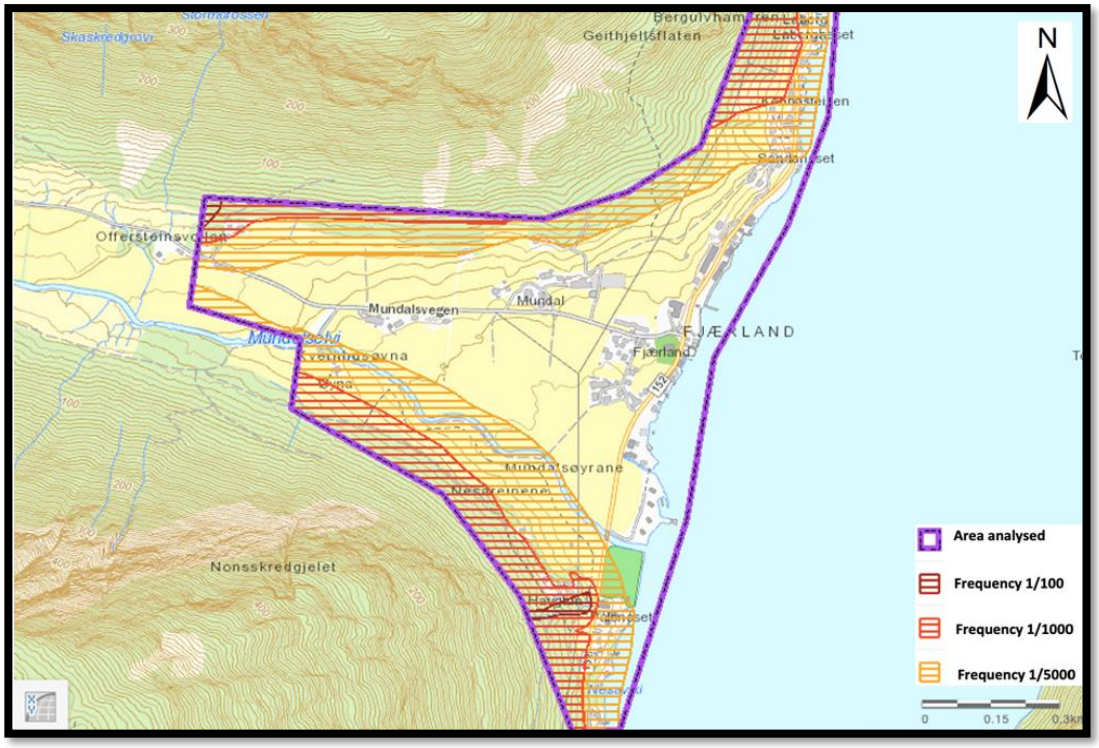

Figure 2-2: Hazard zone map for rockfall in Mundal with danger zones 1/100, 1/1000 and 1/5000 years. Note that the areas with an estimated frequency of rockfall events every 1/5000 years are much smaller than the areas marked as susceptible to rockfall in the susceptibility map in figure 2-1. Adapted from NVE (2017).

2.2.1 Identify, assess and map avalanche risk

A simplified description of the procedure for identifying, assess and map avalanche risk in steep terrain is illustrated in figure 2-3. The chart explains what part of the process that must be evaluated and performed by expert, and what part of the process that can be performed by the municipality itself or by a plan consultant. For each step the chart concludes, based on the risk, if further mapping and evaluation is necessary. As soon as the avalanche risk have been clarified there is no need move on to the next step (NVE, 2019a).

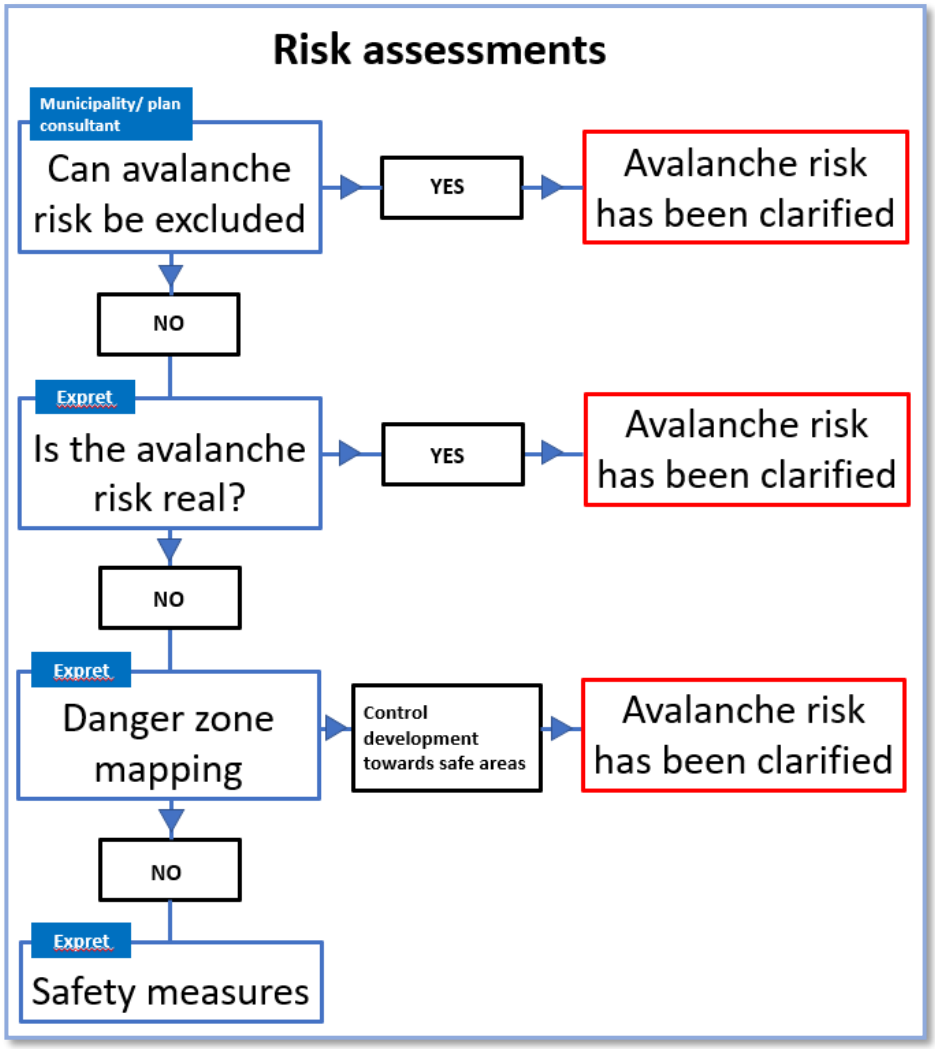

Figure 2-3: Chart illustrating the process of identifying, assess and map the avalanche risk in an area (NVE, 2019a)

2.3 Mass movements

Mass movement, also called mass wasting, is the down-slope movement of soil and rock debris affected by a force that drives the masses towards lower ground (Sigmond et.al. 2013). This force is called the shear stress and is primary a function of the force exerted by the weight of the material under the influence of gravity (figure 2-4). The angle of incline and the weight of the masses is the most important factors determining the shear stress. With increasing slope angle and weight, the shear stress increases, and opposite. The forces that keeps the mass stable and counteract a mass movement are called the shear strength and includes frictional resistance and cohesion among the particles in the mass (Sulebak, 2007). If the shear stress is greater than the shear strength, detachment and mass movement occurs (Sigmond et al., 2013; Sulebak, 2007,). The likelihood of this happening increases during periods of heavy rainfall. The water

increases the pore pressure in the earth material and the water pressure in cracks, resulting in a decrease in shear strength and a destabilized hill slope.

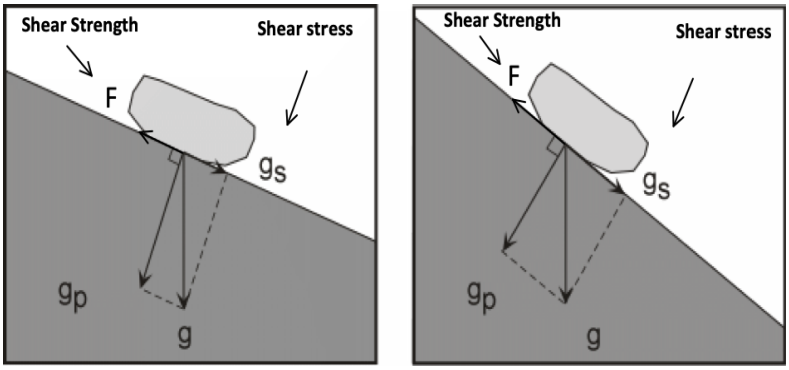

Figure 2-4: Illustration of forces affecting mass movements. When shear stress exceeds the shear strength the mass starts to move. Modified from Nelson (2015)

2.3.1 Classification of mass movements

Mass movement can be classified in many ways as there are different types of processes and materials involved in the various types. Several criteria can be considered, such as the geometry/geomorphology of the mass, water content, velocity of the mass movements, type of material etc. As a result, several different classification methods for mass movement has been created (Selby and Hodder, 1993).

According to Hungr et.al (2001), the classification done by Varnes (1978) and Hutchinson (1968, 1988) are the most common used classification systems in the English-speaking world. Varnes (1978) classifies mass movements based on movement and material type (figure 2-5), while Hutchinsons (1988) classification system is based on morphology, and divides the mass movements into eight main groups (A-H) with subgroups based on, among other things, velocity and the material (figure 2-6) (Selby and Hodder, 1993).

TYPE OF MOVEMENT		TYPE OF MATERIAL		
		BEDROCK	ENGINEERING SOILS	
			Predominantly coarse	Predominantly fine
FALLS		Rock fall	Debris fall	Earth fall
TOPPLES		Rock topple	Debris topple	Earth topple
SLIDES	ROTATIONAL	Rock slide	Debris slide	Earth slide
	TRANSLATIONAL			
LATERAL SPREADS		Rock spread	Debris spread	Earth spread
FLOWS		Rock flow (deep creep)	Debris flow (soil creep)	Earth flow
COMPLEX		Combination of two or more principal types of movement		

Figure 2-5:Abbreviated version of Varnes classification of slope movements (Varnes, 1978)

A	Rebound		
		1	Movements associated with man-made excavations
		2	Movements associated with naturally eroded valleys
B	Creep		
		1	Superficial, predominantly seasonal creep; mantle creep
		2	Deep-seated, continuous creep; mass creep
		3	Pre-failure creep; progressive creep
		4	Post-failure creep
C	Sagging of mountain slopes		
		1	Single-sided sagging associated with the initial stages of landsliding
		2	Double-sided sagging, associated with the initial stages of double landsliding, leading to ridge spreading
		3	Sagging associated with multiple toppling
D	Landslides		
		1	Confined failures
		2	Rotational slips
		3	Compound failures (markedly non-circular, with listric or bi-planar slip)
		4	Translational slides
E	Debris movements of flow-like form		
		1	Mudslides (non-periglacial)
		2	Periglacial mudslides (gelifluction of clays)
		3	Flow slides
		4	Debris flows, very to extremely rapid flows of wet debris
		5	Sturzstroms, extremely rapid flows of dry debris
F	Topples		
		1	Topples bounded by pre-existing discontinuities
		2	Topples released by tension failure at rear of mass
G	Falls		
		1	Primary, involving fresh detachment of material; rock and soil falls
		2	Secondary, involving loose material, detached earlier; stone falls
H	Complex slope movements		
		1	Cambering and valley-bulging
		2	Block-type slope movements
		3	Abandoned clay cliffs
		4	Landslides breaking down into mudslides or flows at the toe
		5	Slides caused by seepage erosion
		6	Multi-tiered slides
		7	Multi-storeyed slides

Figure 2-6: Hutchinson classification of avalanches (Modified from Hutchinson, 1988)

In Blikra and Nemec (1998) the stratigraphic structure of post-glacial avalanche deposits in western Norway is examined and classified based on depositional processes. The depositional processes are divided into four categories; rockfall and debris fall, debris flow, snow flow and waterflow. Their stratigraphic structure and deposition processes are summarized in figure 2-7 (Blikra and Nemec, 1998).

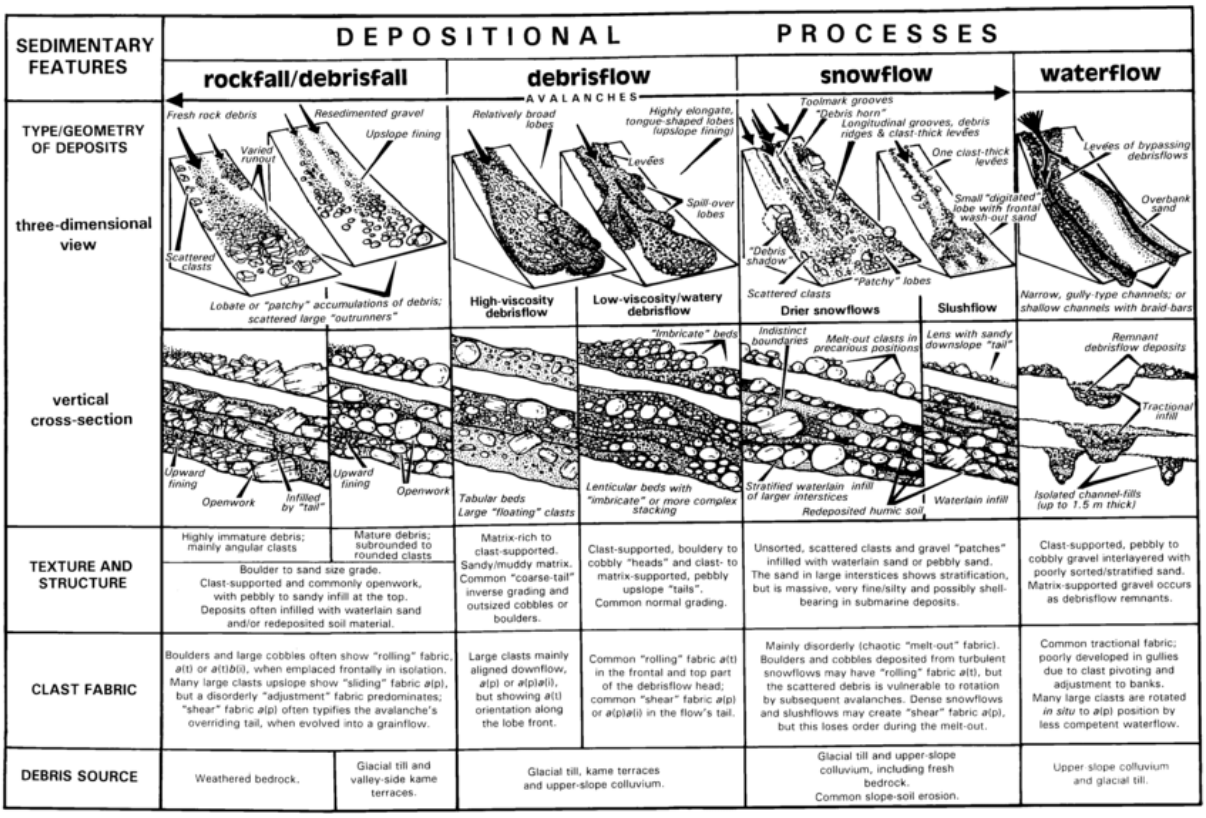

Figure 2-7: A summary of Blikra and Nemec (1998) classification system. It shows the main depositional processes and the stratigraphic structure of the post-glacial avalanche deposits in western Norway (Blikra og Nemec, 1998).

The classification system developed by NGU (2014) is based on type of material (rock/soil, vegetation, water, snow/ice), movement (flow, slide, fall, slump, creep) and velocity (very fast to slow). The result is illustrated in figure 2-8, where the type of material divides the mass movement into three categories with under groups. Rockfall, rockslide and rock avalanches are classified based on the volume of falling material (Domaas and Grimstad, 2014). Rockfall involves a single rock or mass of rocks with a maximum volume at 100 m^3 that travel with high velocity down a very steep slope. If the volume of falling material are between 100-10 000 m^3 it is called a rockslide and includes both small and large rocks. Mass movement with volume larger than 10 000 m^3 are defined as rock avalanches (Blikra et al., 1989; Domaas and Grimstad, 2014). Furthermore, this thesis will focus on rockfall and rockslide, and possible deposits from smaller snow avalanches and debris flow, based on this classification system.

Bedrock	Soil		Snow
Rockfall (<100 m^3)	Landslide		Loose/powder snow avalanche
Rock slide (100 - 100.000 m^3)	*Coarse grained*	*Fine grained*	Slab avalanche
Rock avalanche (>100.000 m^3)	Debris flow Debris avalanche	Clay slide Quick clay slide	Slush flow Wet snow avalanche

Figure 2-8: NGU's classification system of mass movements. Modified from NGU (2014).

2.3.2 Avalanches in Western Norway

The extensive fjord system in Western Norway is a result of deep erosion during multiple glacial cycles and the Holocene isostatic rebound (Vorren and Mangerud, 2007). It consists of high and steep sections of exposed rocks, and sections of marine sediments that may be susceptible to avalanches.

As illustrated in figure 2-9, showing registered avalanche events, valleys close to glacial lakes and around fjords in western Norway is very exposed to avalanches. This is quite unique compared to the rest of the world (Vorren and Mangerud, 2007). Due to climatic and topographic factors, the population in western Norway tend to concentrate in these avalanche prone valleys and fjords, thus is very exposed to avalanches and displacement waves generated by rock slope failures and clay slides (Hermanns et al., 2012).

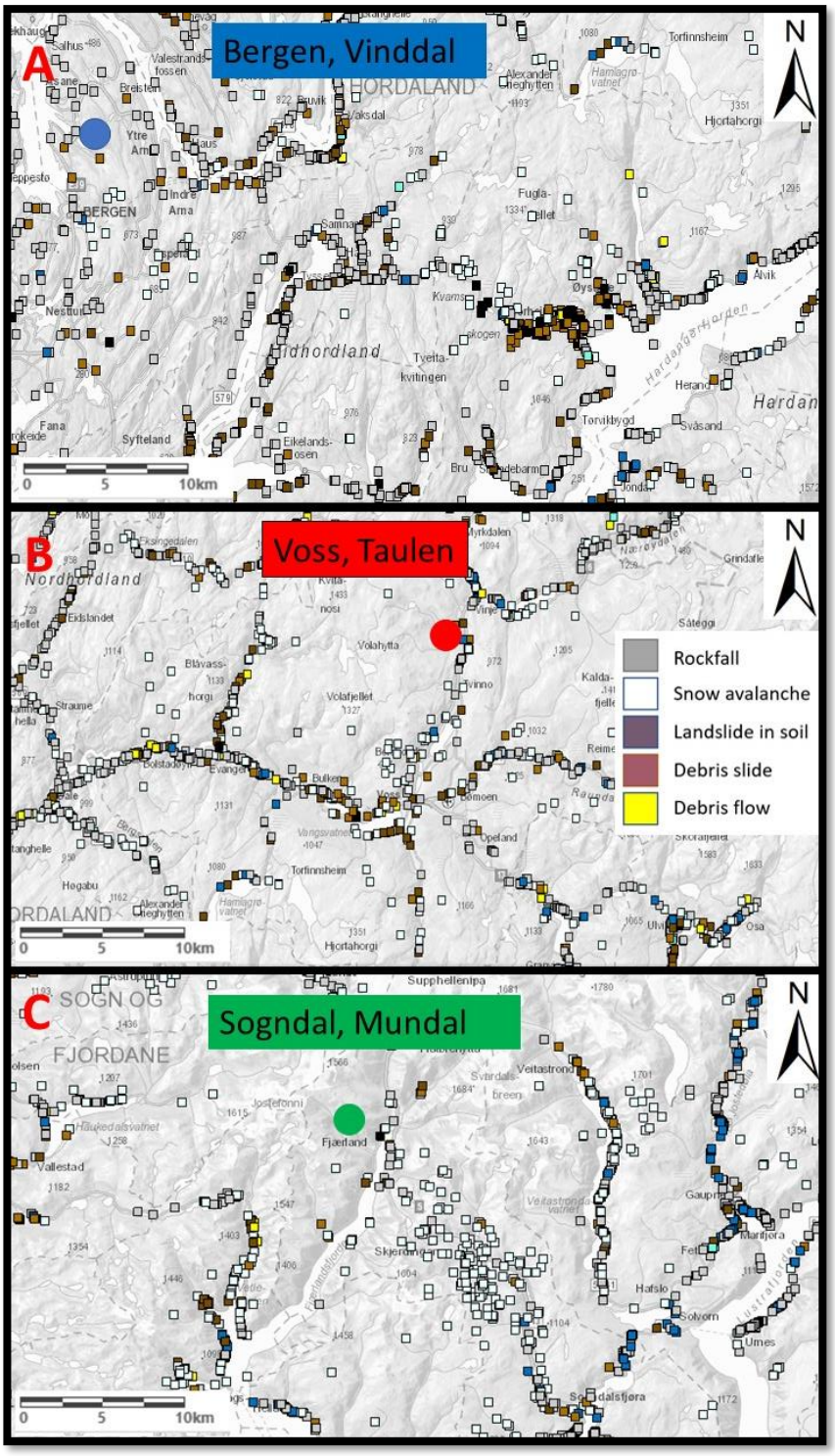

Figure 2-9: Avalanche events in western Norway; A) Mundal, B) Taulen and C) Vinddal. Modified from NVE Atlas (2019)

According to the fifth assessment report from united nations (UN) Intergovernmental Panel on Climate Change (IPCC) (2014), research shows that the climate on Earth is changing. Further, Hanssen-Bauer et al. (2015) used this report to estimate the climate change until 2100, with 1971-2000 as the reference period. Since 1900, the temperature in western Norway has increased by 0,4°C and is estimated to continue to increase by 3,7 °C within 2100 AD (figure

2-10) (Hanssen-Bauer et al., 2015). With an increasing temperature, more of the precipitation will fall as rain instead of snow, resulting in earlier snow melting, decrease in snow avalanches frequency and thus a lower risk of dry snow avalanche. However, the risk of wet snow and slush avalanches will increase as well as the snow avalanche danger in high mountain areas (Hanssen-Bauer et al., 2015).

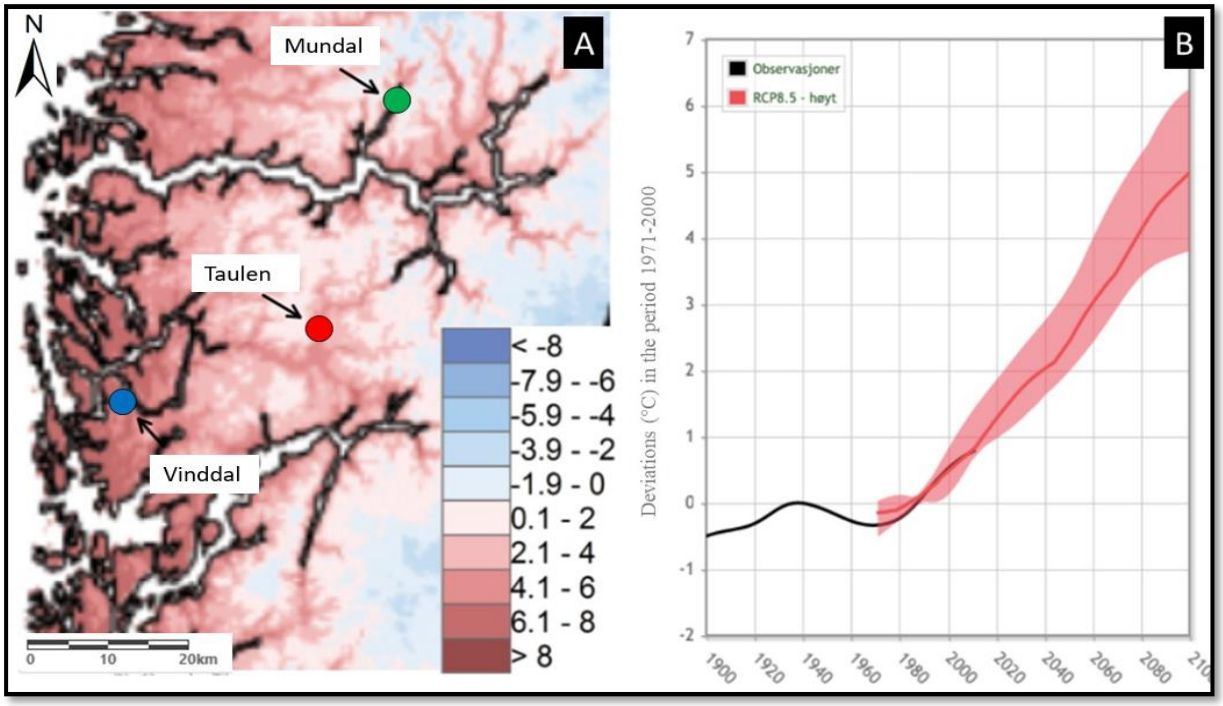

Figure 2-10: A) Map showing change in mean temperature (°C) from the period 1971-2000 to 2071-2100. B) A graph showing the temperature changes from 1900 to 2100. Black curve= observations form 1900-2014, red curve= median value based on a variety of regional climate model (RCM) simulations. The curves are smoothed to illustrate variations on a 30-year scale. Shaded area indicates the spread between low and high climate projections (10 and 90 percentiles) (Hanssen-Bauer et al. 2015).

The average annual rainfall in Norway has increased by approximately 18% since 1900 AD and is estimated to continue to increase by 20-25% until 2071-2100 AD (figure 2-11) (Hanssen-Bauer et al., 2015). Heavier precipitation and an increase in rainfall days will affect avalanche activity for avalanches such as; snow avalanches, debris flows, rockslides and rockfalls (Jaedicke et al., 2008). In addition, future climate change may lead to a change in the current avalanche pattern, that is, both avalanche type and the geographical occurrence of avalanches. Consequently, the complexity in predicting future avalanche events increases. However, there are great uncertainty related to how anthropogenic climate change will affect the climate system, hence also the avalanche activity (Hanssen-Bauer et al., 2015).

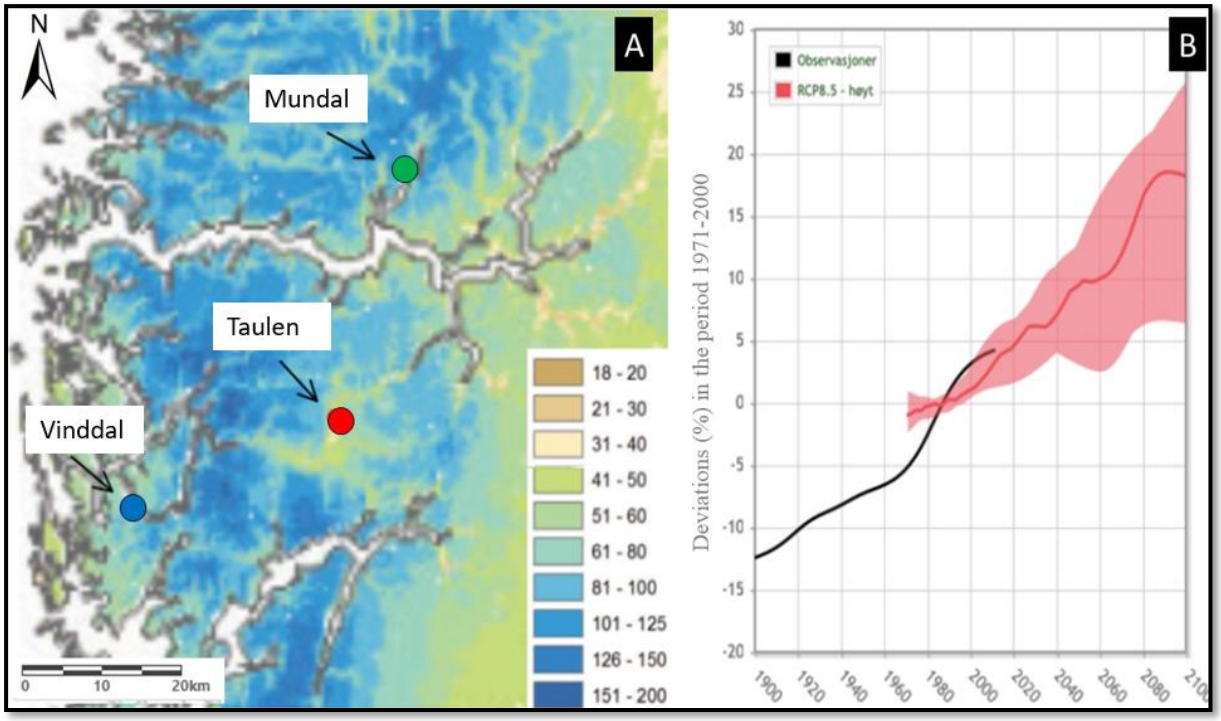

Figure 2-11: A) A map showing relative change (%) in annual rainfall in the period 1971-2000 to 2071-2100. B) A graph showing change in rainfall from 1900 to 2100. Black curve= observations from 1900-2014. Red curve= median value based on a variety of regional climate model (RCM) simulations. The curves are smoothed to illustrate variations on a 30-year scale. Shaded area indicates the spread between low and high climate projections (10 and 90 percentiles) (Hanssen-Bauer et al., 2015).

2.3.3 Rockfall and rockslide

Rockfall and rockslide is a daily occurrence in mountain areas. It can occur on all types of slope over 30° with loose rocks (NGI, 2019b), from natural cliffs, excavated rock faces, or steep exposures of coarse-grained soils (Braathen et al, 2004). It is a gravitational movement of a mass containing fragmented bedrock (Blikra et al., 2002) and, because of the unpredictability of the magnitude and frequency, it poses a great danger to human lives and infrastructure. Rockfalls and rockslides are defined based on volume of fallen rocks, where rockslides consist of volume between 100 m^3 - 10 000 m^3 and rockfall have a volume less than 100 m^3 (Blikra et al., 1989).

Depending on the slope gradient, the falling rocks descend the slope in different modes of motion. The three most important modes are; rolling (<45°), bouncing (45°-70°) and freefall (>70°) (figure 2-12) (Ritchie, 1963). The velocity of the moving rocks mainly depends on the slope gradient, but factors like the size of the rocks and the material covering the slope, such as scree, vegetation and soil, are also important factors (Ritchie, 1963).

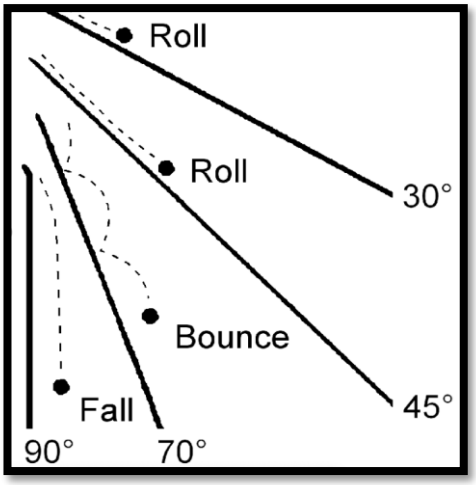

Figure 2-12: General modes of motion of rocks during their descent on slopes related to the mean slope gradients (modified from Ritchie, 1963)

The clasts move through a series of impacts during a rockfall or rockslide, which may result in a retardation of the clasts, acceleration or stop it instantly. The runout distance is controlled by the size of the falling clast (weight), clast shape, slope gradient and roughness of the slope surface (Parsons and Abrahams, 1987).

However, the collision frequency and concentration of clast is low, which allows a relatively free movement downslope for the largest clast and segregating according to sizes, leading to a fall sorting (Campbell and Gong, 1986). Fall sorting is characterized by a distal coarsening of block sizes, away from the cliff. The fan apex is normally thinner than the outer edge of the fan, and often consist of finer gravel, infiltrated with granule sand (Evans and Hungr 1993). If several of rockfalls or rockslides descend the slope along the same track, the effective runout distance of the successive avalanche may be shortened, resulting in an overall upward coarsening (Statham and Francis, 1986; Parsons and Abrahams, 1987; Nemec, 1990). The deposit can range from randomly and scattered clustered cobbles or boulders, to distinctive tongue-shaped beds of immature coarse gravel with an upslope fining (Blikra and Nemec, 2002b).

2.3.3.1 Source area

The source area for rockfalls and rockslides usually has a steep gradient and are characterized by blocks that are separated from in situ bedrock by steep, edge-slope-parallel fractures (figure 2-13A). Fractures with a high angle to the slope commonly limit the block on one or both sides, or split the main block into segments (Dorren, 2003). If the fractures surface the slope in the lower part of the block it is most likely kept in place solely by frictional forces between the cliff

and the block. This implies that if the driving forces overcomes the frictional forces, the block immediately accelerates, resulting in freefall.

Individual blocks that rotate outwards in the upper part make an opening of about 1-3 m wide crevasses near the precipice edge. This rotation is called toppling, where the final failure causes direct fallout without sliding (figure 2-13B) (Goodman and Bray, 1976).

A back-stepping in the unstable area can also occur as a result of new fractures forming prior to, or as the block is released. Thereby, the source area consists of several blocks separated by sub-parallel fractures or of single blocks. The block sizes varies, but the largest blocks can have vertical and horizontal dimensions of an order of several hundred meters (Dorren 2003).

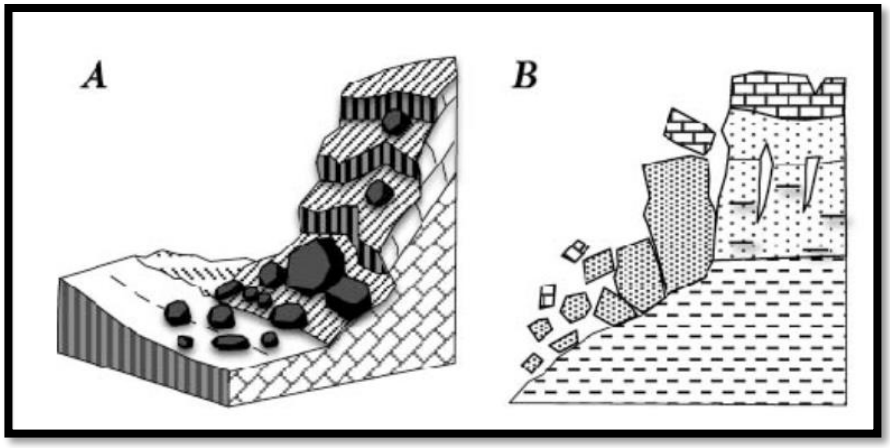

Figure 2-13: A) illustration of a rockfall, B) illustration of toppling. Modified from Guzzetti, F. (2015)

2.3.3.2 Factors causing rockfalls

The slope morphology and the direct surroundings of the potential falling rocks are the most important factors determining whether a rock may fall. All bedrock slopes are exposed to weathering to various degrees, which often leads to opening of joints and fracturing. The degree of rockfall or rockslide promotion depends on the environmental factors causing physical and chemical weathering, and on the bedrock type (Schumm and Chorley, 1964). According to Gardner (1983), glacial over-steepened rock slopes are particularly vulnerable to low magnitude and high frequency rockfall and rockslide events.

Several studies have highlighted the influence of different triggering factors. According to Douglas (1980), the geotechnical properties of the bedrock material play an important role. Luckman (1977) concluded that rockfalls and rockslides are controlled by the geological- and the morphological character of the cliff, and the rock surface temperature fluctuations. Another cause was investigated by Zellmer (1987), Bull et al. (1994) and Vidrih et al. (2001). They

studied the influence if seismic activity and concluded that it could be a triggering factor. A study done in the Yosemite Valley, by Wieczorek et al. (1995, 2000), concluded that rockfalls and rockslides was triggered by several different factors, such as rainstorms, earthquakes, freeze–thaw cycles of water in joints, rapid snow melt, wedging and root penetration, or stress relief following deglaciation. In addition to environmental factors, human factors, such as undercutting of slopes during quarrying or excavations for infrastructure, also trigger rockfalls and rockslides. In comparison to geological factors they are minor, but locally it can be of great importance (Selby, 1982). As a conclusion there are a wide range of factors that can cause rockfall sand rockslides, but the most crucial factors is a combination of the geology, the climate, the topography and the time.

2.3.4 Snow avalanches

In Norway snow avalanche is the avalanche type that kills most people and composes as one out of three avalanche events registered in Norway (Colleuille and Engen, 2009). It is a rapid flow of snow down a hill or mountainside and can occur in areas with a slope between 25° and 60°, that are not covered by trees. Snow and weather conditions are the main factors determining the frequency of snow avalanches. Thus, getting a better understanding of the past and the future climate, is important when studying avalanche frequency (Vasskog, 2011).

There are several ways to group snow avalanches, but in this thesis NGU's classification system is used (figure 2-8). The snow avalanche is divided into three groups: loose/powder snow-, slab-, slush flow/ wet snow avalanches. Loose/powder snow avalanches can be triggered by any start mechanism and occur in any snow type, but usually in fresh dry powder snow. They can travel for long distances along a flat valley floor and for short distances uphill. In addition, they can be extremely large with masses of 10 million tons and a velocity that can reach 300km/h (NVE, 2014). The second group, slab avalanche, is triggered in areas with a slope gradient between 25-50° and is formed in snow with great firmness, resulting in eruption of large snow masses (Luckman, 1977). The final group, slush flow/wet snow avalanches, has a high water content, resulting in progressed high speed (Blikra et al., 1989). These avalanches are most common in the spring, when the supply of water is high because of snow melting or precipitation. The runout distance varies, but because of the high water content it can be released in relatively gentle slopes (Lied and Kristensen, 2003).

2.4 Drone

In mountain areas with high and steep slopes, geological mapping has in the past been complex, time-consuming and an expensive process (Fischer et al. 2012; Joyce et al. 2014). Today unmanned aerial vehicle (UAV), or in simpler terms drones, are used as a tool to study and characterize steep mountain areas in a simple and effective manner. Drones are often used for regional research such as deformation analysis (Shi and Liu 2015), avalanche monitoring (Torrero et al. 2015), territory analysis (Farfaglia et al. 2015) and for mapping geological structures at a small scale (Vasuki et al. 2014). With its ability to fly at low altitude and with a slow, controlled speed it offers many advantages in comparison to the traditionally piloted vehicles (Bemis et al., 2014).

Like other photogrammetry-based techniques, drone mapping capture 3-D information of features by taking two or more photographs, in different angels or positions, of the same object. Further, by using geological software, these photos can be used to generate high quality 3-D models (Bemis et al., 2014), thus capture exceptional detailed geophysical data (Sadeghipoor et al. 2015). Accordingly, the drone has enhanced the mapping efficiency and offers an improved accuracy, flexibility and precise mapping of geological structures over both small and large areas.

2.4.1.1 Dji Mavic Pro

The drone used in this study is called Dji Mavic Pro and is equipped with a 4K camera stabilized by a 3-axis mechanical gimbal and 12-megapixel resolution. With a flight time at 25 minutes per battery, 300-400 images can be collected. The transmitter has maximum transmission distance at 4 km and is connected to a phone that controls the drone by using the app Dji GO 4. The following table 2-2 summarizes the key specifications of the drone (DJI, 2019).

Tabell 2-2 Key specifications for Dji Mavic Pro

Item	Specification
Type	DJI Mavic Pro RC Quadcopter
Max speed	40 mph (65 kph)
Max flight time	27 minutes
Battery capacity	3830 mAh
Flight mode	Wireless control
Max transmitting distance	4 km
Camera	Effective pixels:12.35 M (Total pixels:12.71M), image size: 4000×3000
Stabilization	3-axis (pitch, roll, yaw)

2.5 Determining age of fallen blocks

Dating prehistoric avalanche deposits, is a general problem, especially the last 1000 years and newly events (0-100 years). This is mainly due to difficulties in obtaining dateable organic material directly related to the avalanche event. Developing new and improved methods for a more accurate dating of avalanche deposits are useful, as they can give an indication as to whether historical avalanches were triggered during periods of tectonic activity or climate change. Several of methods that has been developed today is based on the assumption that rock surfaces become weathered with time (Nesje et al., 1994). In this study, lichenometry and vegetative analysis is used to estimate an approximate age of blocks deposited in avalanche fans, and thus estimate the avalanche frequency.

When a rock is deposited it goes through three stages of weathering; the initial stage, the mid-successional stage and the late- successional stage (Garibotti et al., 2011). The initial stage is dominated by the pioneer species, such as crustose lichens. They are successful colonizers, with high growth rate and dispersal ability. They typically colonize recently exposed areas and disappears in older sites. After dominating the community for about 50-80 years they start decreasing in coverage and moss starts developing, marking the transition from the pioneer to the mid-successional stage. After about 140 years the moss usually covers 90-100% of the rock surface, creating a continuous moss matt (Irene et al., 2011). In sites older than 140 years, the invasion of a large diversity of vascular plant species characterize the late-successional stage (Garibotti et al., 2011).

2.5.1 Lichenometry

Lichenometry is an absolute dating technique used for dating relatively recent event (Armstrong, 2004). The method is based on the assumption that lichens growing on a rock surface (or other suitable surfaces) can be used to obtain an approximate age of the exposed rock surface. By knowing the time between the exposure of the rock surface and its colonization by lichens, and the grow rate of a given species in an area, the minimum age can be determined by measuring the diameter of the largest lichen (Innes, 1985).

Lichenometry can be performed by either the direct method or the indirect method. The direct approach involves measuring the growth rate over a period of time (years), while the indirect approach involves measuring the size of lichen colonies with known dates of origin (Innes, 1985)

For the present master project, the indirect approach is used. This requires a substrate with different known ages, in this case gravestones, and measurements of the diameter of the largest lichen growing on them (Mottershead, 1980; Benedict, 2009). The start point for lichen growth is estimated to be the burial date from the gravestone. After measuring several lichen diameters growing on different gravestones, a graph with lichen diameter vs age can be created. This graph can further be used to date rocks with unknown age, such as boulders derived from a cliff zone. As lichen size and cover is time dependent, it can be used to give an approximate age for the arrival of each boulder, thus allow an approximate estimation of avalanche frequency and activity (Evans and Slaymaker, 1996)

2.5.1.1 Lichen

The period of colonization varies depending on lichen species and its growth rate, and by the development of available nutrients through weathering (Hale, 1961). The big variety of lichen types can be divided into three main groups; Crustose lichens, Foliose lichens and Fruticose (Beschel, 1961). Due to the crustose lichens long life span, slow growing rate and normally symmetrical growth (Hale 1967), three different lichens that belongs to this group is studied in this thesis. First is the Rhizocarpon geographicum (kartlav) (figure 2-14A). They normally appear as green patches on rocks in mountainous areas. Each lichen grows adjacent to each other, leading to the appearance of a map/patchwork field or circular shape. When circular, or roughly circular, this species is widely used for dating (Nash et.al., 2004). Further in this study the Rhizocarpon geographicum will be referred to as the green lichen. The second type is the chalky white to pale grey crusty lichen called Lecanora Rupicola (kantlav) (figure 2-14B). It is highly variable and usually forms determinate patches or mosaics on rocks (Nash et.al., 2004). In this thesis Lecanora Rupicola is referred to as the white lichen. The last one is the Aspicilia Cinera (Kantlav) (figure 2-14C), a gray lichen that mostly grows on rocks. It appears in variable forms and can be round, angular or irregular. This lichen is one of the first to appear on stony deposits and are therefore often used in lichenometry (Nash et.al., 2007). Further the Aspicilia Cinera is referred to as the gray lichen.

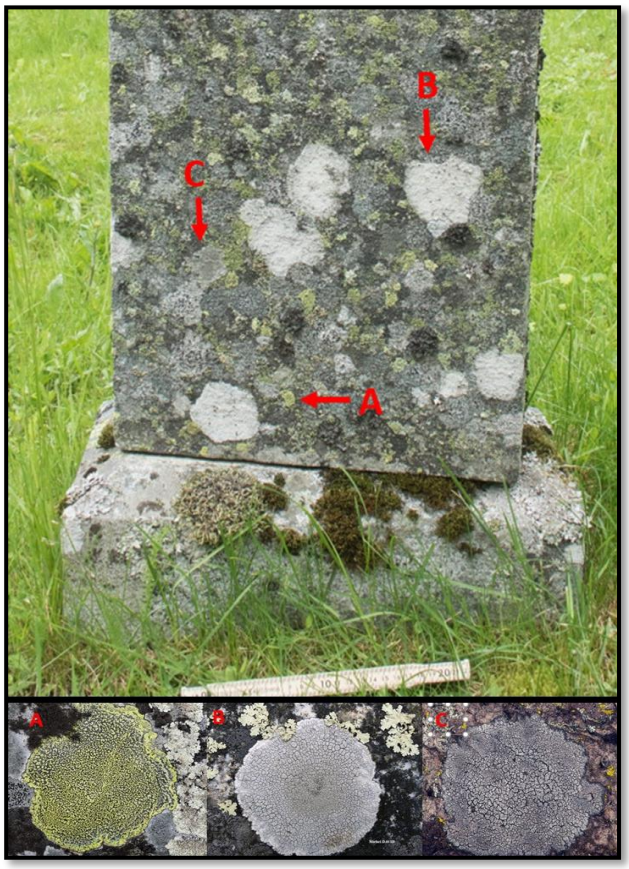

Figure 2-14 The oldest gravestone investigated in this study is from Oppheim Kyrkje (87 years) and close up pictures of; (A) Rhizocarpon geographicum (the green lichen) (Photo by: Kristian Aasbrenn, 2017), (B) Lecanora rupicola (the white lichen) (Photo by: Michel David, 2019) and (C) Aspicilia Cinera (the gray lichen) (Photo by: Richard Droker).

2.5.2 Vegetation

Vegetative analysis preformed in avalanche areas are used in order to gain indications of the avalanche frequency, energy and age. It is based on the concept that vegetation, growing in the runout zone and along the flanks of an avalanche track, may experience damage due to impact of snow or rocks. Depending on the size of the avalanche, the geomorphic situation and avalanche type, the extent and type of damage vary (Burrows and Burrows 1976). When rocks and debris, carried from upslope, strike a standing tree, it results in a scar on the uphill side of the stem and branches. The trees start forming callous tissue around the margin of the scar, and gradually add new wood and bark. Consequently, avalanche areas with visible damaged and scared trees indicate a possible active area with resent avalanche activity (Burrows and Burrows 1976, Carrara 1979).

A direct impact of large boulders, snow or windblast from large avalanches can break the main tree stem, or tear and fracture roots (Jenkins and Hebertson, 1994). Areas with high and frequent avalanche activity often appears as vertical swaths of open vegetation down steep mountain

slopes, with a dominant vegetation of different types of ages, or a lack of vegetation (Martinelli, 1974; Burrows and Burrows, 1976; Johnson, 1987; Patten and Knight, 1994; McClung, 2003)

In this project, only simple vegetative analysis, based on field observations, is conducted in three areas exposed to avalanches. Observations, such as fallen or bent trees, scars or damages, vegetation beneath and around rocks (fresh or rotten) and the overall prevalence of vegetation, is used to estimate the avalanche frequency and activity.

2.5.3 Cosmogenic nuclides

Using terrestrial cosmogenic nuclides (TCN) for surface exposure dating is an established and reliable method to date landforms. This method can sample and date directly fluvial- or glacial-polished bedrock surfaces, bedrock landforms, fault footwall faces, and avalanche bedrock detachment surface. NGU applies TCN dating within avalanches to determine ages of avalanche events and sliding surfaces, and past long-term displacement rates (NGU, 2015).

This dating method is based on the fact that when a mineral is exposed to cosmic rays the cosmogenic nuclides build-up predictably with time. Thus, by measuring the concentrations of cosmogenic nuclide, it is possible to determine how long rocks or sediments have been exposed at or near the surface of the Earth (Lal, 1991; Gosse and Phillips, 2001). The nuclides can be measured in a variety of minerals and in the wide variety of nuclides available (with different half-lives or stable), thus a broad spectrum of geomorphological problems can be addressed (Ochs and Kober, 2008). Another big advantage with TCN dating is that the dateable material is produced by the avalanche event itself by exposing fresh material surfaces to the cosmic rays. With today's modern instruments the uncertainty limit lies below 10% of the age and every surface older than 1000 years can be dated. However, this dating method is expensive, and the entire process takes a long time (NGU 2015), therefore, this method will not be carried out in this thesis.

3 Geological background

3.1 Geomorphology of Western Norway

The study areas investigated in this thesis are all located in the western part of Norway; Vinddal in Hordaland, Taulen in Hordaland and Mundal in Sogn og Fjordane. The valleys and fjords in this part of Norway normally follows the fractures in the bedrock, with a direction either perpendicular or parallel to the coastline. South for Stad the coastline has a north-south direction and north for Stad, a northeast-southwest direction.

3.2 Bedrock geology of Western Norway

The bedrock in western Norway generally reflects the tectono-stratigraphy of the Scandinavian Caledonides and can be divided into three units (figure 3-1); 1) the Precambrian basement (Western Gneiss Region), 2) the Fortun/Vang nappe, and 3) the Caledonian nappes (Fossen, 2014).

The Precambrian basement (Western Gneiss Region) was exposed to the Caledonian deformation and metamorphism, and consists of intrusive complexes and subordinate metasedimentary rocks, such as pre-Cambrian gneisses and migmatites (Fossen, 2014). Both Vinddal and Mundal is a part of this Region, where banded- and metamorphosed migmatitic gneiss dominates in Vinddal (Tveit and Helliksen, 1997) and local banded dioritic to granitic gneiss dominates in Mundal (AA and Sønstergaard, 1995).

The first trust nappe overlying the basement is the Fortun/Vang nappe. The rocks in this nappe originate from the Baltic shield before the collision between the Baltic plate (Northern Europe and Russia) and the Laurentian plate (North America and Greenland) (Kvale and Ingdahl, 1985). Consequently, the Fortun/Vang nappe consist of metamorphosed sedimentary rocks, such as mica schist and phyllite, of Cambrian to Ordovician age. Taulen is a part of this region, thus is dominated by quartz schist (metasandstone)/metaconglomerate.

The uppermost nappe is the remnants of the Caledonian nappes called the Jotunheimen Complex and was thrusted above the Fortun/Vang nappe and the Precambrian basement (Fossen, 2014)

The Jotunheimen Complex and the Precambrian basement consist of mechanically strong rocks that do not easily break up unless there are zones of weakness or a joint zone present in the

rocks (Grue et al., 2017). The phyllite and mica schist found in the Fortun/Vang nappe are generally weak rocks that will easily weather and can break up the same way as the mechanically strong rocks in the Jotunheimen Complex. The valley sides are characterized by exfoliation fractures, due to the pressure relief when the large ice sheets retracted for about 10.000 years ago. These fractures are normally parallel to the valley side and dip away from the hillsides (Grue et al., 2017).

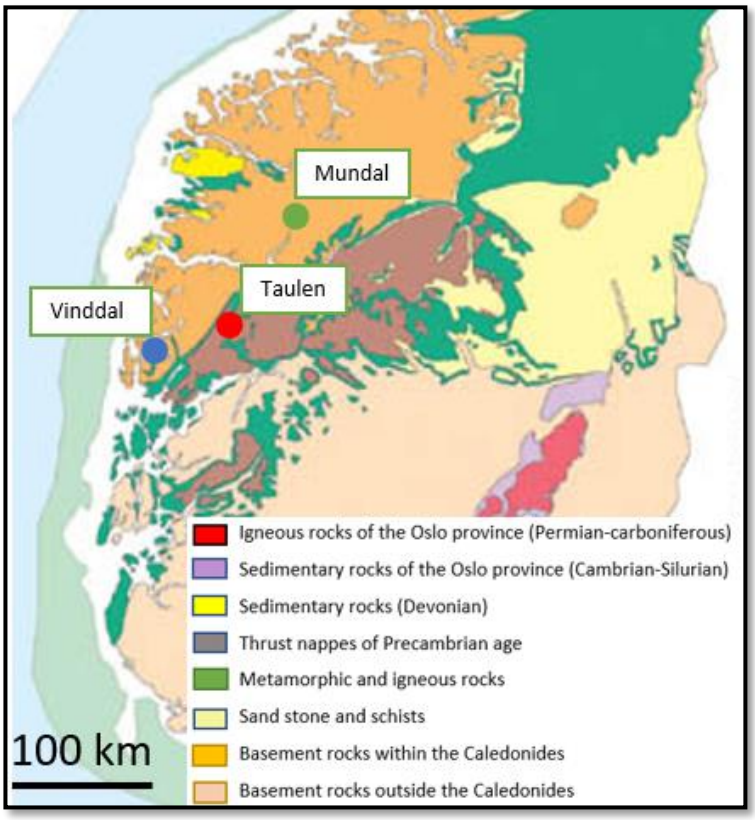

Figure 3-1: Bedrock geology of western Norway.

3.2.1 Climate

The climate and weather condition are two of the most important factors that can trigger an avalanche. Throughout history, avalanches have happened during or right after special weather conditions, such as heavy rainfall within short period of time or strong wind (Iden et.al., 2009). Because of Norway's location in relation to the Westerlies (Vestavindsbeltet) and the Gulf Stream, it has a warmer climate than the latitudes would indicate. The annual average temperature in southern Norway shows two main features; high temperatures along the coast and low temperatures in the hinterland (figure 3-2) (Iden et.al., 2009).

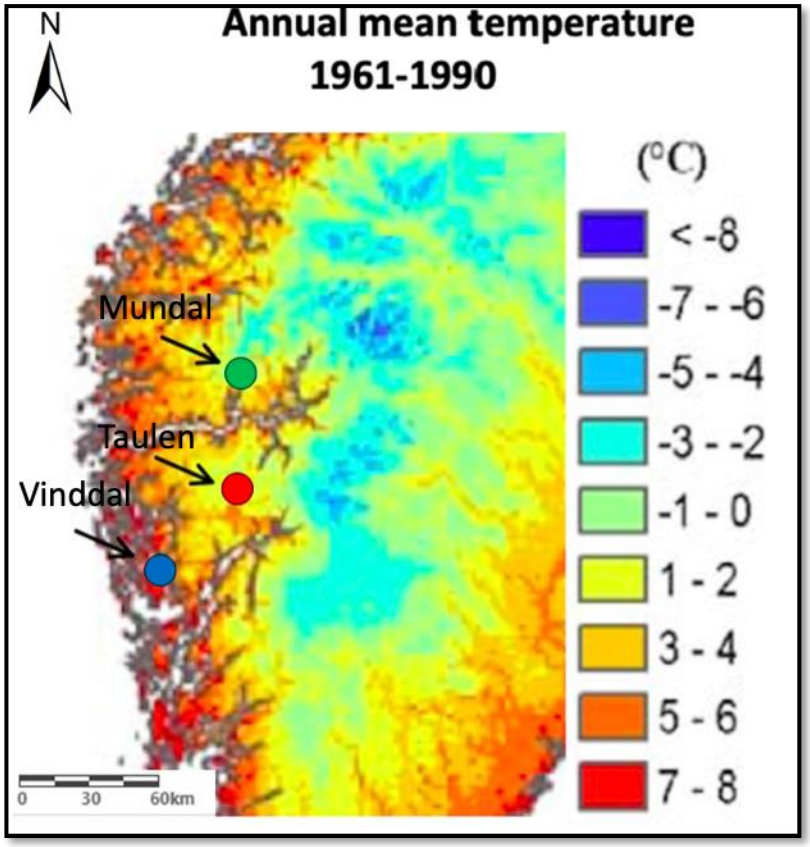

Figure 3-2: Normal annual mean temperature in the western part of Norway during the last normal-period 1961-1990. Modified from Iden et.al 2009.

The climate on the west coast of Norway is characterized as cold and wet. Throughout the year, clouds, rain and wind dominates as a result of weather fronts coming from the Atlantic Ocean and the orographic rainfall. The weather fronts forms in low pressure at the polar front and moves towards Norway from the southwest and west. When the humid air masses face the cold polar, precipitation occurs. Another type of precipitation is the orographic rainfall, which happens when air masses hit the coast of Norway and, because of the mountains, is being forced to increase latitude. When lifted, the air masses is unable to retain the moisture and precipitation occurs (Liljequist, 1970). Consequently, due to weather fronts coming from the Atlantic and orographic rainfall, the annual average precipitation in westerns Norway is much higher compared to the hinterland (figure 3-3).

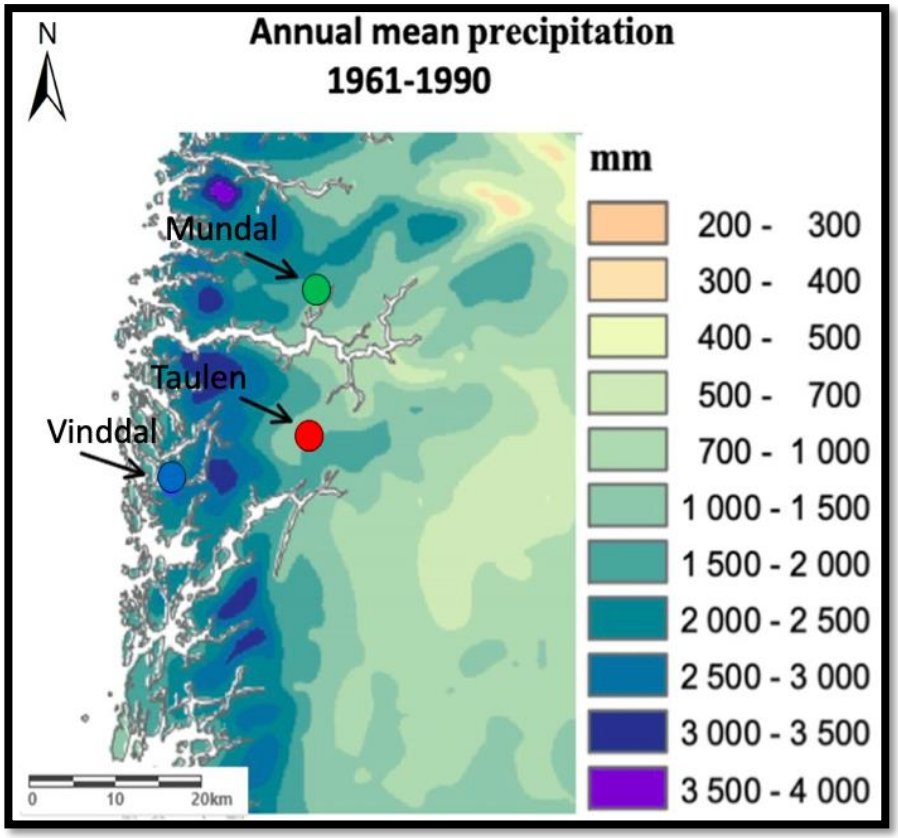

Figure 3-3: Normal annual mean precipitation in the western part of Norway during the last normal-period 1961-1990. Modified from Iden et.al 2009.

Both Voss and Mundal is located further east than Bergen and thus, because of the mountains, are partly shield from the weather fronts and the orographic rainfall (Liljequist, 1970). Consequently, Mundal and Voss have a more continental climate; less wind, less rain, low humidity, large daily temperature difference, hot summers and cold winters. Bergen, on the other hand, is located along the coast, and thus have a more maritime climate; lots of wind, lots of rain. high humidity and small daily and annual temperature differences (Liljequist, 1970).

In table 3-1 and 3-2, the monthly and annual mean temperature (in C°) and precipitation (in mm) is listed. Voss and Mundal have large temperature differences between summer and winter, while in Bergen the temperature is more consistent throughout the year. Accordingly, because of the mild winters, Bergen have the highest average temperature. Moreover, Bergen has a significantly larger average amount of precipitation during a year compared to Voss and Mundal (Aune, 1993).

Tabell 3-1 Monthly and annual mean temperature (Celsius) during the last normal period 1961- 1990., from station 5054 (Bergen), 5156 (Voss), 5584 (Mundal). (Aune, B., 1993)

Temperature (C°)													
Station	**Jan.**	**Feb.**	**Mar.**	**Apr.**	**May.**	**Jun.**	**Jul.**	**Aug.**	**Sept.**	**Oct.**	**Nov.**	**Des.**	**Av.**
Bergen	1.5	1.6	3.3	5.9	10.5	13.5	14.5	14.4	11.5	8.7	4.7	2.6	7.7
Voss	-4.7	-3.2	0	4.2	9.8	13.5	14.9	13.9	9.6	6.9	1.0	-2.1	5.3
Mundal	-3.3	-3.0	-0.1	3.7	9.6	13.3	14.3	13.3	9.3	5.7	0.6	-2.1	5.1

Tabell 3-2 Monthly and annual mean precipitation (mm) during the last normal period 1961- 1990, from station 5054, 5156, 5584 (Førland, J.F., 1993).

Precipitation (mm)													
Station	**Jan.**	**Feb.**	**Mar.**	**Apr.**	**May.**	**Jun.**	**Jul.**	**Aug.**	**Sept.**	**Oct.**	**Nov.**	**Des.**	**Av.**
Bergen	190	152	170	114	106	132	148	190	283	271	260	235	188
Voss	127	87	95	51	54	69	77	92	159	162	151	156	107
Mundal	198	138	158	82	71	88	102	129	238	245	217	239	159

3.3 Study site

3.3.1 Vinddal, Bergen municipality

Vinddal is a valley located in the northern part of Bergen and belongs to the Caledonian mountain range. The area consists of an 80° steep, NE facing cliff at about 400 masl and a 35° steep slope (figure 3-4A). The slope hosts a short steep fan that most likely has been formed by gravitational processes such as rockfall, rockslides and snow avalanches (Tveit and Helliksen, 1997). The fan extends 215 meters from the fan apex, at 250 masl, to the fan apron, at 150 masl (figure 3-4B), and is approximately 110 m broad. Metamorphic gneiss and the plutonic rocks; anorthosite, gabbro- anorthosite and mangerite, dominates in the area (Askheim, 2016). In addition, a vain consisting of diorite/trondhjemite is observed in the middle part of the cliff (figure 3-5). Figure 3-6 shows three pictures of Vinddal; a hillshade map from ArcGIS (A), an orthomosaic from ArcGIS (B) and a quaternary geological map (C).

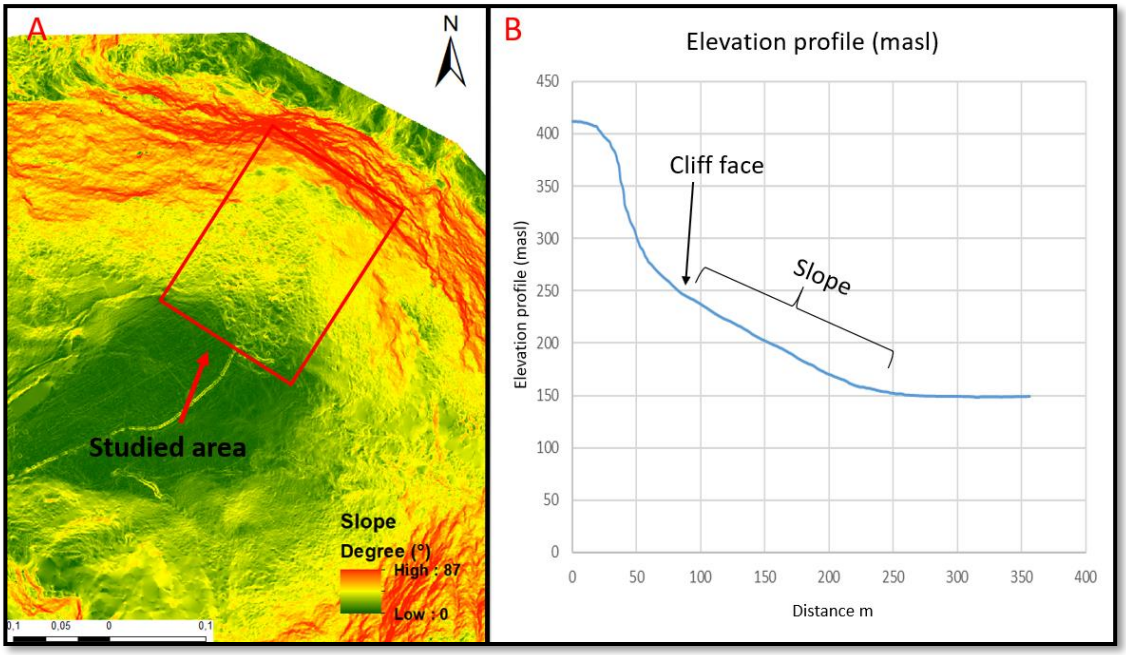

Figure 3-4: A) Slope map of Vinddal from ArcGIS, showing areas where the slope is steep (red) and shallow (green), B) Elevation profile from Vinddal

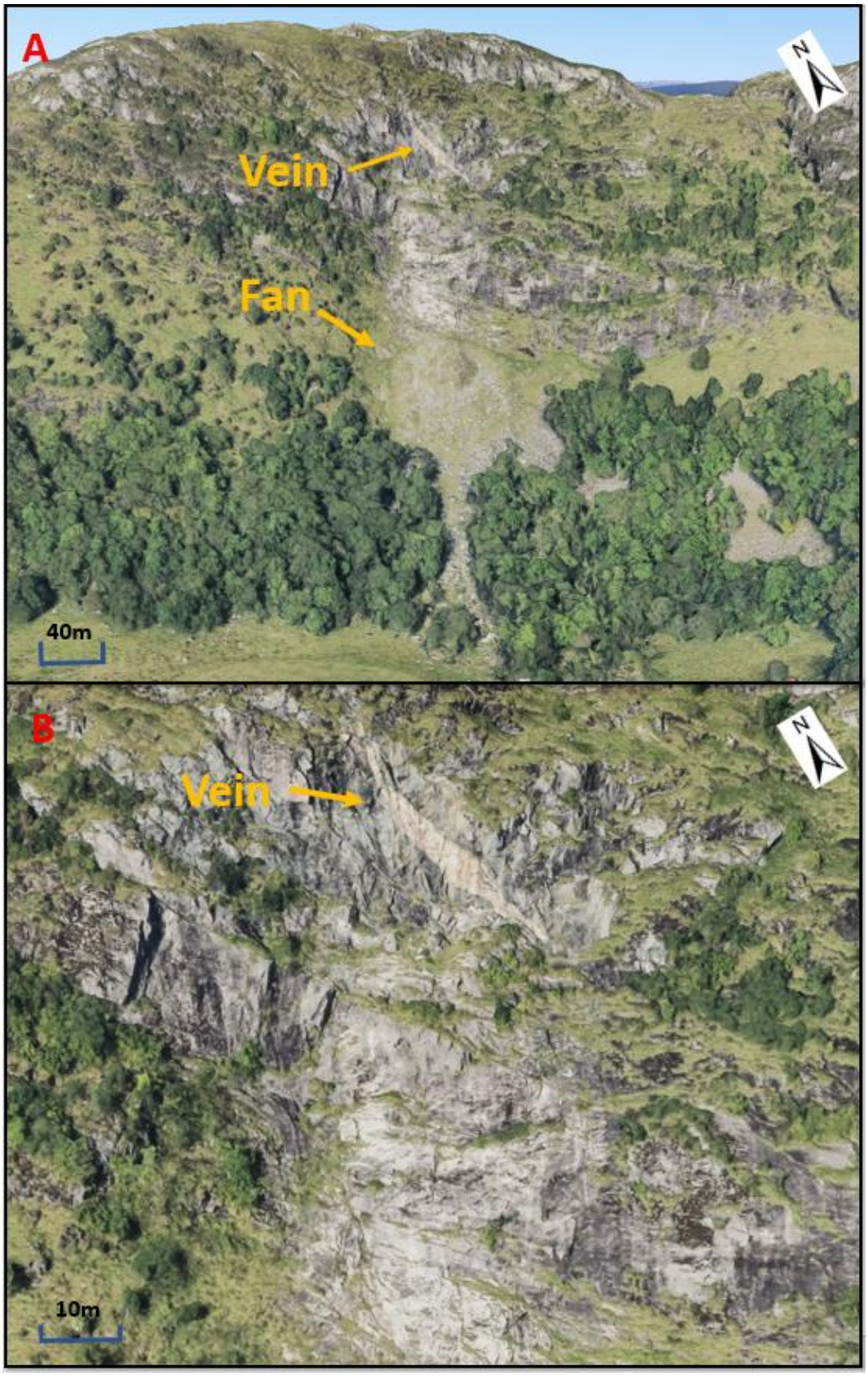

Figure 3-5: Pictures of the cliff and the fan area. A) cliff and the avalanche fan. B) Closer picture of the vein. Modified from Google Earth, 18.10.19

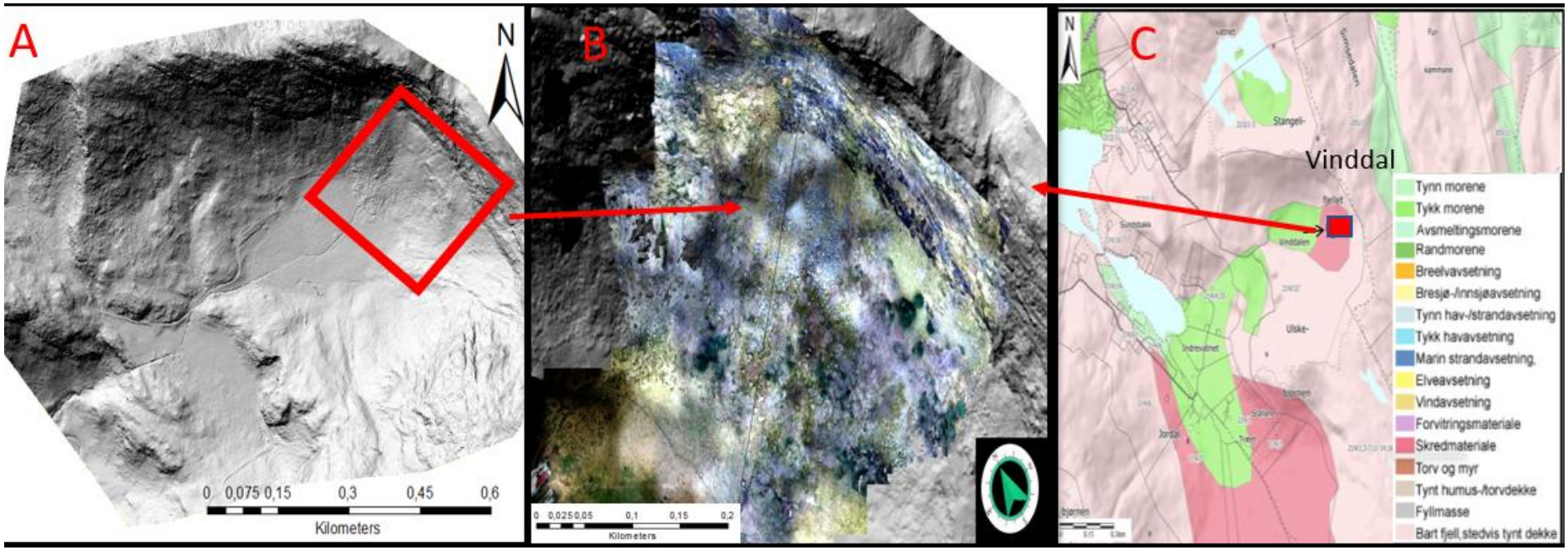

Figure 3-6: A) Hillshade map of the study area in Vinddal, B) Orthomosaic derived from drone photos of Vinddal, C) Quaternary geological map of Vinddal. Modified from NGU (2019c).

3.3.2 Taulen, Voss municipality

Taulen is a part of a valley located in the northern part of Voss municipality. The area consists of a NW facing 80° cliff at about 400 masl (figure 3-7A) with several overhanging areas (figure 3-8A). Close to the cliff a camp site with 14 cabins and a farm is located are located (figure 3-8B). The slope has a 30° inclination and hosts a fan that stretches 148 m from the fan apex, at 224 masl, to the fan apron, at 150 masl (figure 3-7B), and has a width of approximately 410 m. The uppermost and middle part of fan is more or less covered by avalanche deposits, while in the lower part only a couple of large blocks are located between the farm and the camp site. The fan deposited in Taulen probably originates from gravitational processes, such as rockfall, rockslides and snow avalanches (Tveit and Helliksen, 1997). The bedrock is dominated by magmatic- and metamorphic rocks, such as granites, gneiss, quartzite and quartz slate.

Because of human activities and a great amount of vegetation, the data is limited in the northeastern part of the area. However, the southwestern part shows better data, and is probably untouched by human activities. Figure 3-9 show three pictures from Taulen; a hillshade map from ArcGIS (A), an orthomosaic from ArcGIS (B) and a quaternary geological map (C).

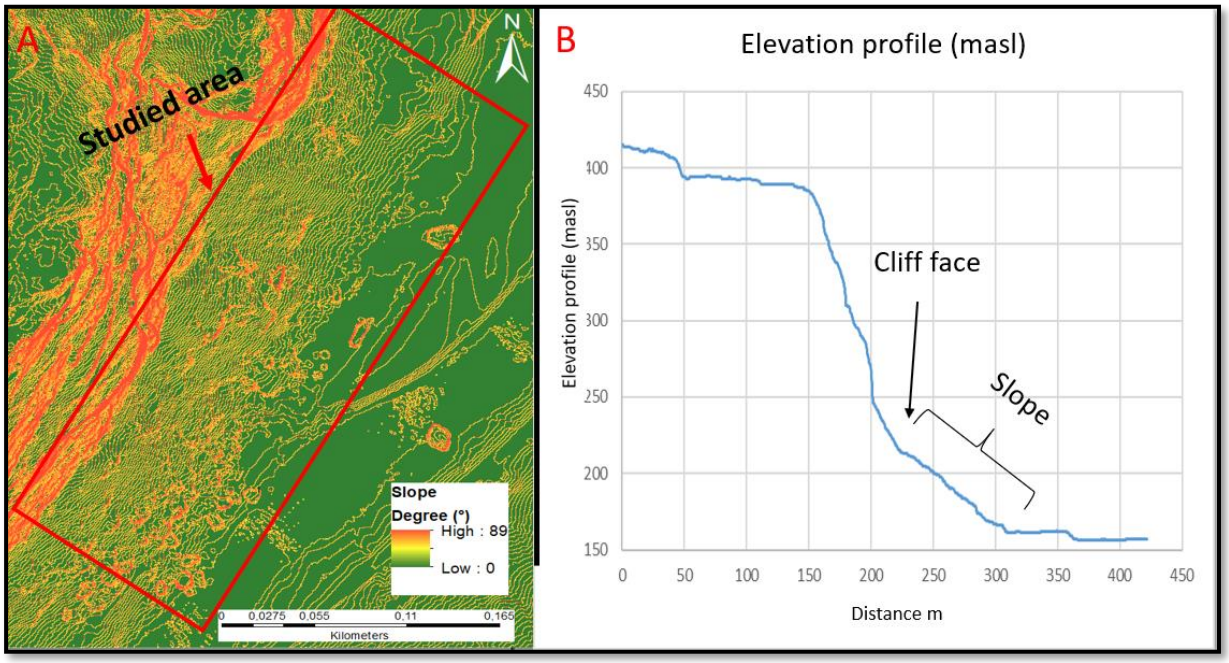

Figure 3-7: A) Slope map of Taulen from ArcGIS, showing areas where the slope is steep (red) and shallow (green), B) Elevation profile from Taulen

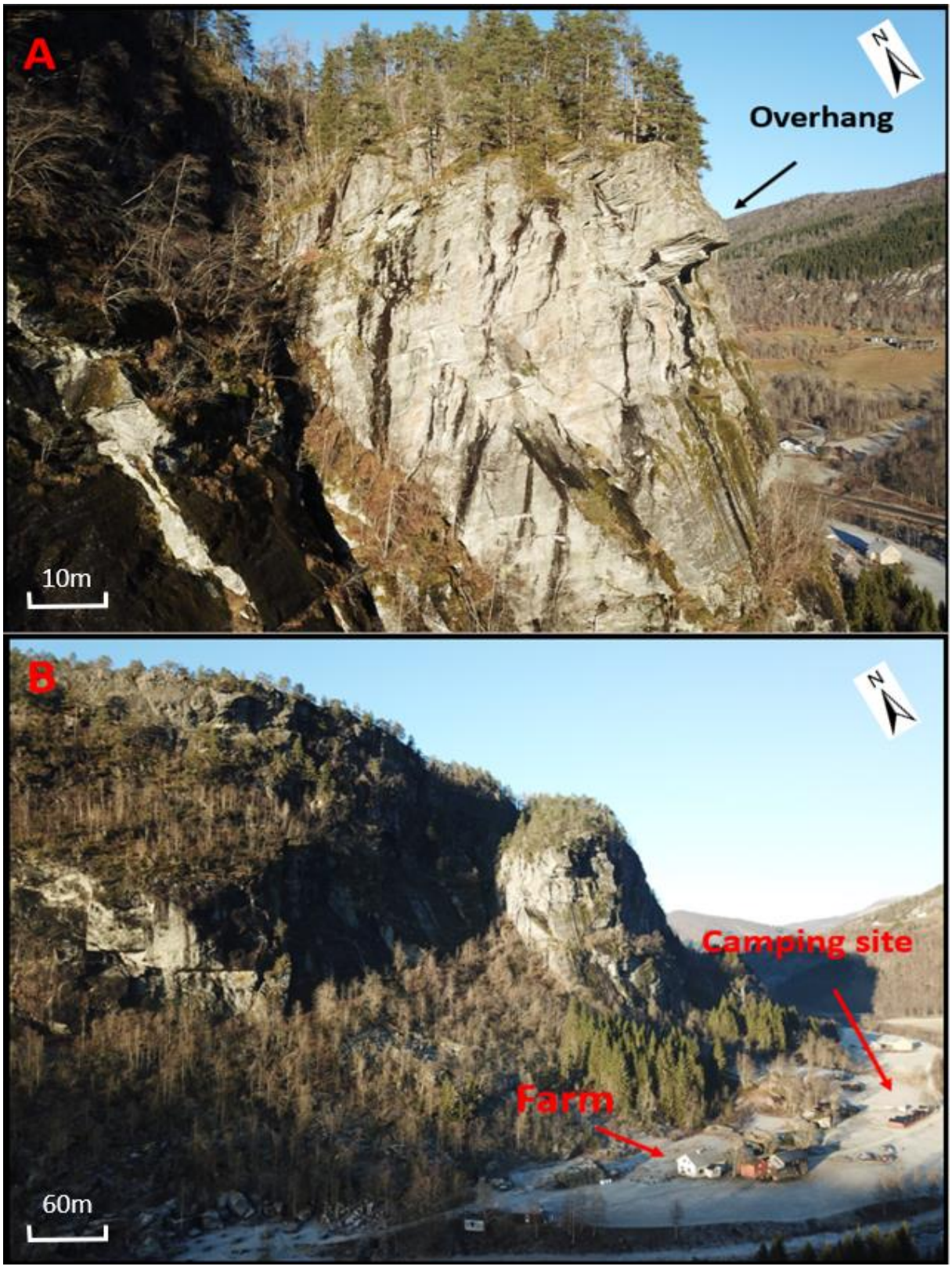

Figure 3-8: Pictures from Taulen. A) Example of an overhang in Taulen. B) Overview of Taulen

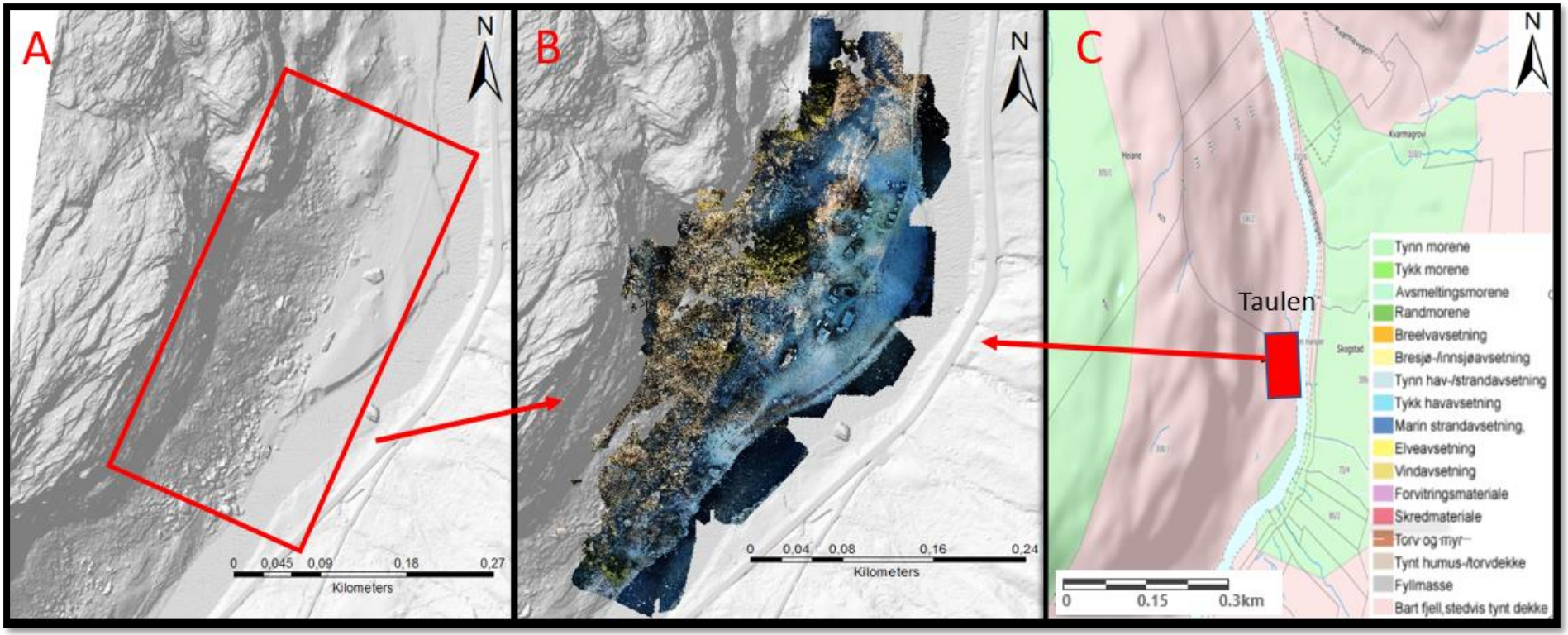

Figure 3-9: A) Hillshade map of the study area in Taulen, B) Orthomosaic derived from drone photos of Taulen, C) Quaternary geological map of Taulen- Modified from NGU (2019c)

3.3.3 Mundal, Sogndal municipality

Mundal is located in Fjærlandsfjorden, which is an arm on the north side of the Sognefjord (Aa and Sønstegaard, 1995). The area consists of an 80° steep cliff at about 1400 masl that is facing east (figure 3-10A). A prominent valley (figure 3-11) hosts a steep (30°) fan that stretches 450 m from the fan apex (300 masl) to the valley floor (100 masl) (figure 3-10B), and has a width of approximately 540 m. The bedrock in the area is dominated by metamorphic rocks, such as local banded dioritic- and granitic gneiss (Hermanns et al, 2011). The fan is mainly covered by rocks originating from gravitational processes, such as rockfall, rockslides, snow avalanches, and possibly debris flow. According to the quaternary geological map made by NGU (2019), the valley floor is a glacifluvial/fluvial river plain (Aa and Sønstegaard, 1995). Figure 3-12 show three pictures of Mundal; a hillshade map from ArcGIS (A), an orthomosaic from ArcGIS (B) and a quaternary geological map (C).

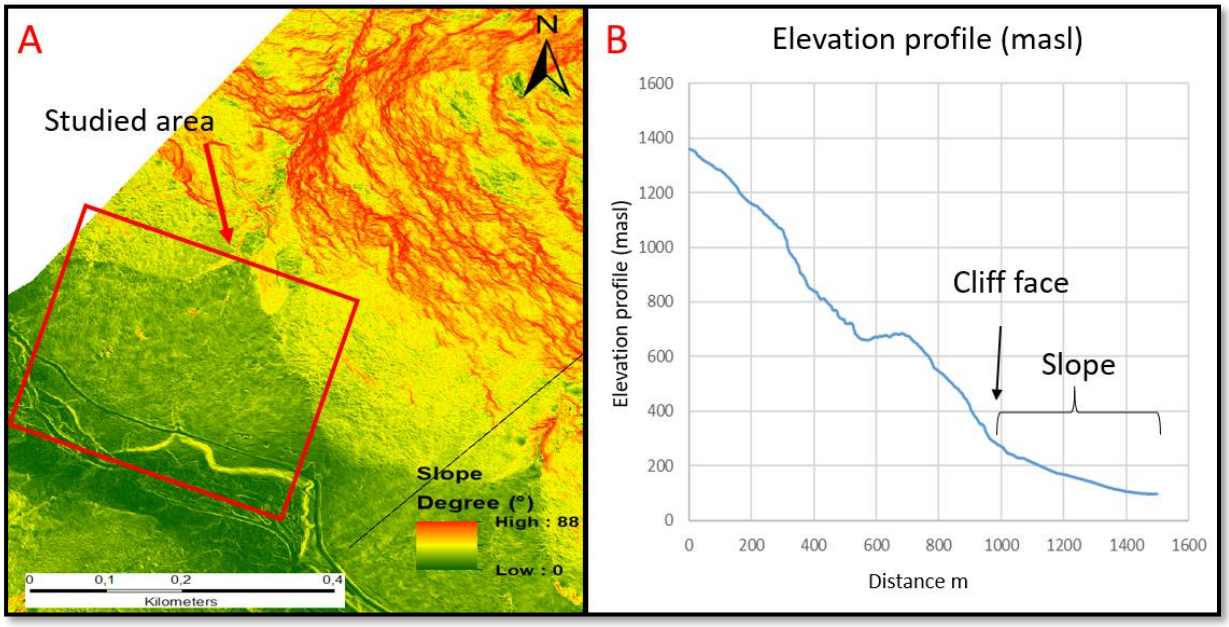

Figure 3-10: A) Slope map of Mundal from ArcGIS, showing areas where the slope is steep (red) and shallow (green), B) Elevation profile from Mundal

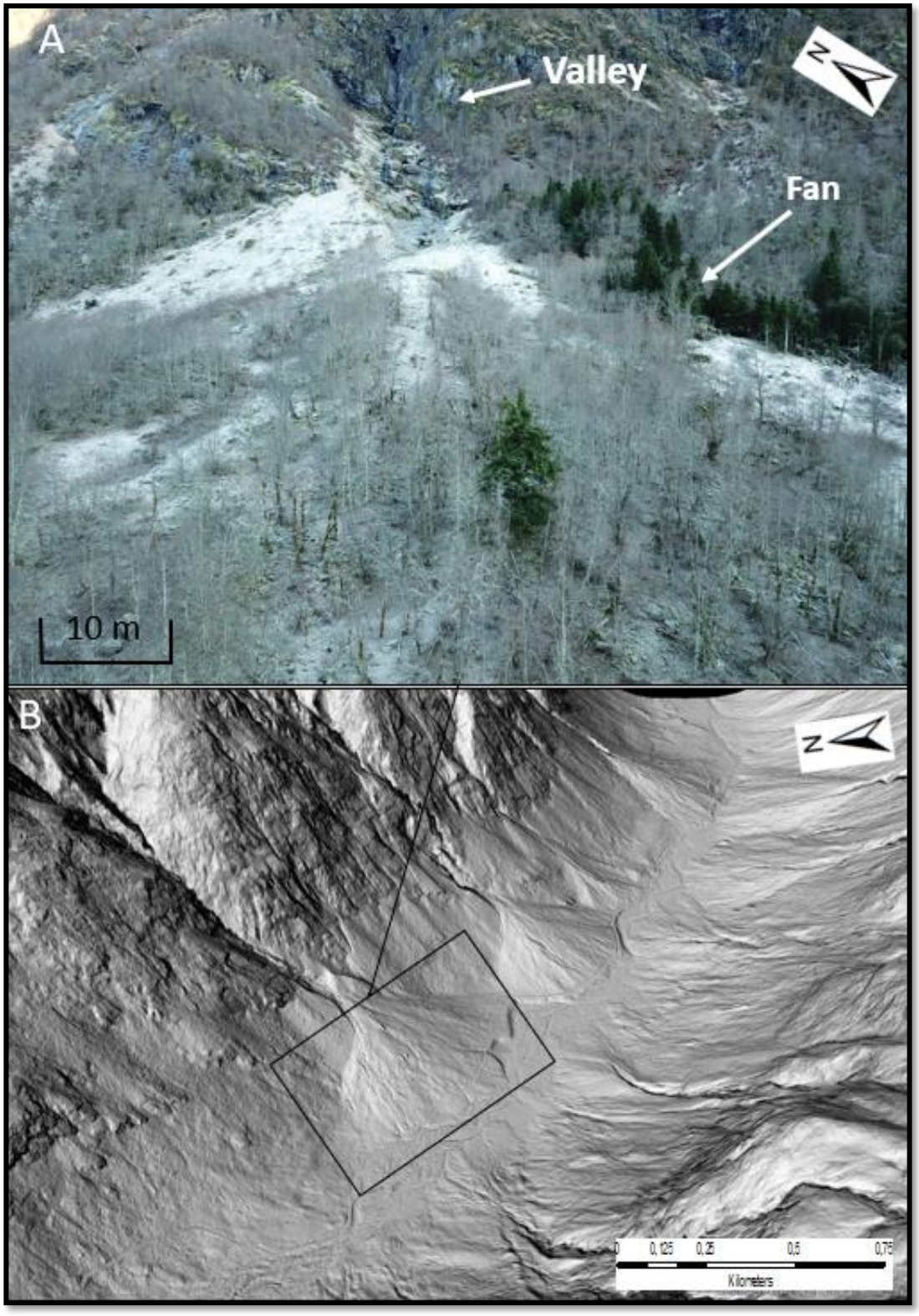

Figure 3-11: A) drone picture of the fan in Mundal, B) Hillshade picture of Mundal, where the fan investigated is marked.

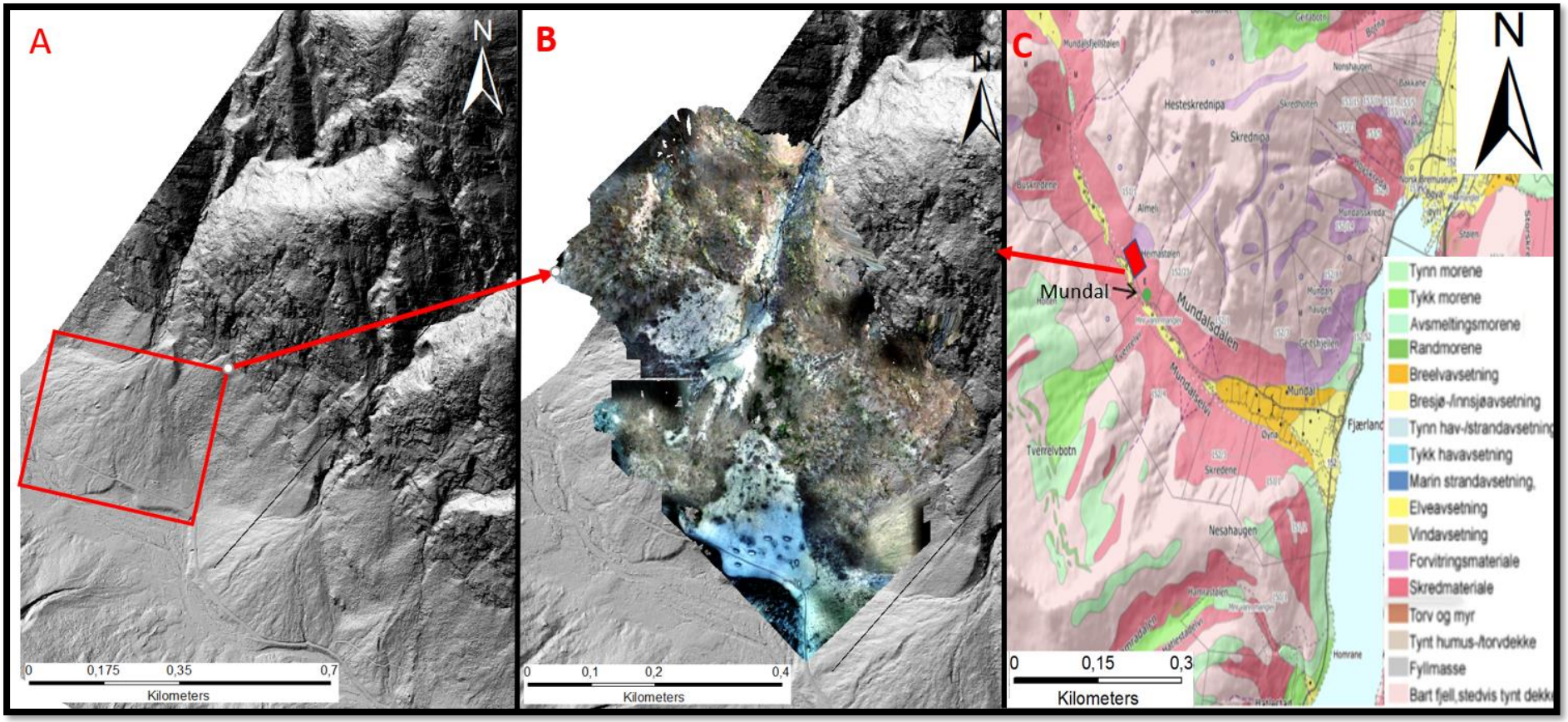

Figure 3-12: A) Hillshade map of the study area in Mundal, B) Orthomosaic derived from drone photos of Mundal, C) Quaternary geological map of Mundal. Modified from NGU (2019c)

4 Methodology

The methodology of this study is a combination of UAV survey, lichenometry and vegetative analysis, and fieldwork (Figure 4-1). The UAV survey provides high resolution 3-D models for each of the studied areas, thus a detailed analysis of the cliff and the slope can be acquired. Moreover, the lichenometry measurements were conducted in two graveyards close to the studied sites. During field work at Vinddal and Taulen, lichenometry and vegetative analysis were used to estimate the avalanches activity and frequency. Additionally, areas where the 3-D model showed no or bad data, such as areas with abundant vegetation or bad resolution (30-50 cm versus a resolution c. 10-20 cm in most places), were also investigated. By combining UAV survey and fieldwork, an informative and detailed analysis of the fan area and the cliff was completed.

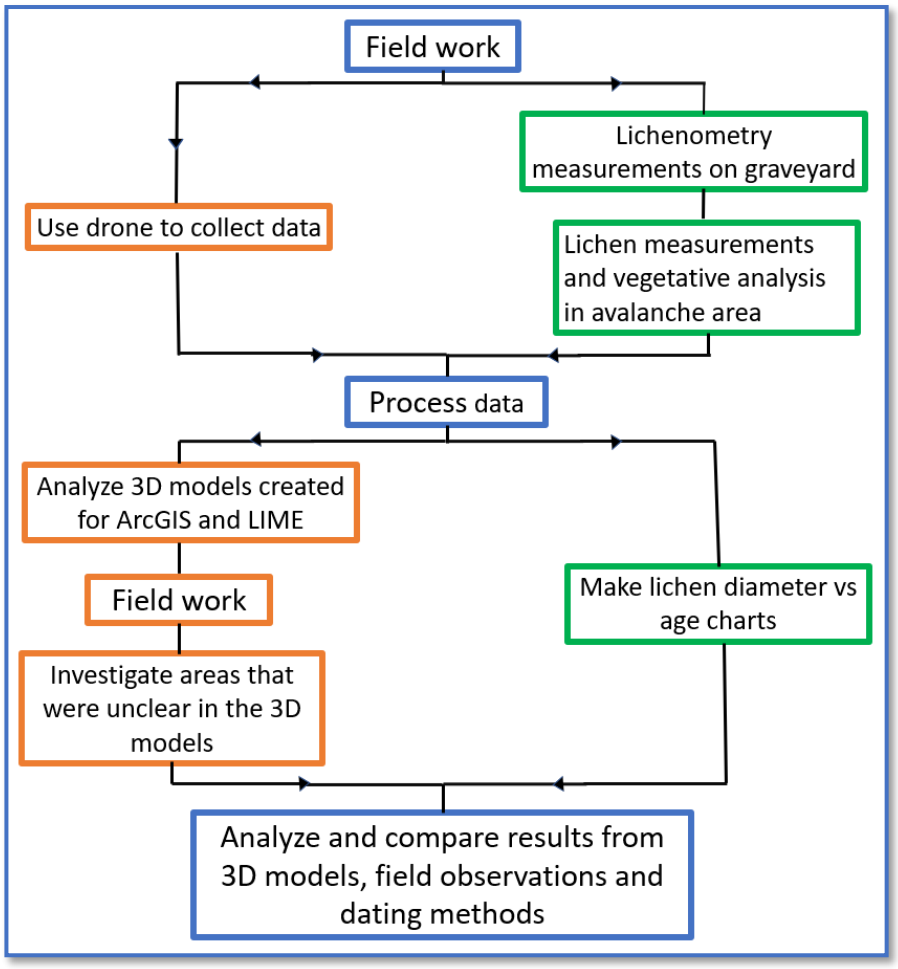

Figure 4-1: Flow chart showing the workflow of all procedure for data acquisition processing and interpretation in this thesis. In general, the study can be divided into two parts; 1) drone data acquisition and processing and 2) lichenometry study and analysis.

4.1 Drone data

4.1.1 Drone data acquisition

The drone was used at three different locations where the only equipment needed was the drone (Dji Mavic Pro), 6 batteries, the remote and a phone used as a screen when connected to the remote. About 40 km^2 - 206 km^2 terrain was covered at each site and the images were acquired at an elevation in the range of 400-1000 masl and with an 80% overlap. At each location, 1000-2000 images were collected in a 1-2 hours long flight time. As each battery had a maximum flight time of 20-30 minutes, 4-6 batteries were needed.

4.1.2 Drone data processing

In order to make the 3-D models, the drone data had to be processed following several steps in Agisoft before exporting the models to ArcGIS and LIME (figure 4-2). The first step was to review all the pictures collected by the drone and delete those pictures that were unclear or bad. Secondly, the pictures were transferred to Agisoft Photoscan by selecting the *Add Photos* command from the *Workflow* menu and select the pictures to be processed. As the coordinate system for the future model is set using camera positions, it is important to see if it looks reasonable by using the command *View/Show hide items/cameras.*

The next step is to select *Align Photos* command from the *workflow* menu. The photoscan will at this point find matching points between overlapping images, estimate camera position for each photo and then build a sparse point cloud model. This cloud is vaguely shaped like the terrain of the studied area, but with a great amount of misplaced point. These misplaced points do not fit into the terrain and need to be deleted by using the *select-function* to mark the misplaced points. Next step is to build a dense point cloud by selecting *Build dense point cloud* command in the *workflow* menu. As in step three, points that do not fit in to the terrain need to be deleted. In addition, the outermost points in the cloud is deleted making sharp edges.

Based on the dense point cloud a digital elevation model (DEM), orthomosaic, a mesh and a texture can be generated. The DEM and Orthomosaic is further exported to ArcGIS, and the Mesh and Texture is exported to LIME.

To build a DEM the *Build DEM* command is selected from the *workflow* menu. In the Build DEM dialog, the following values are set: Type: geographic, Coordinate system: WGS 84 / UTM Zone 32N, Source data: dense cloud, Interpolation: enabled, Resolution (m): 0.05. To make an orthomosaic, select *Build orthomosaic* command in *Workflow* menu and in the Build

orthomosaic dialog the following values are set: Type: geographic, Coordinate system: WGS 84 / UTM Zone 32N, Surface: DEM, Blending mode: mosaic, Enable hole filling: yes, Pixel size: 0.01 m. In the next step the DEM and Ortomosaic is export to ArcGIS by selecting *Export DEM/Orthomosaic and Export JPEG/TIFF/PNG* command from *File* menu. In the DEM/Orthomosaic dialog the «WGS 84 / UTM Zone 32N» coordinate system is used.

To build a Mesh the *Build Mesh* command was selected from the *workflow* menu. In the Build Mesh dialog, the following values were set: Surface type: arbitrary. Source data: dense cloud, Face count: custom, 1 500 000. To build a texture the *Build Texture* command was selected from the *workflow* menu. In the Build Texture dialog, the following values was set: Mapping: generic, Blend: mosaic, Texture size: 4096x30.

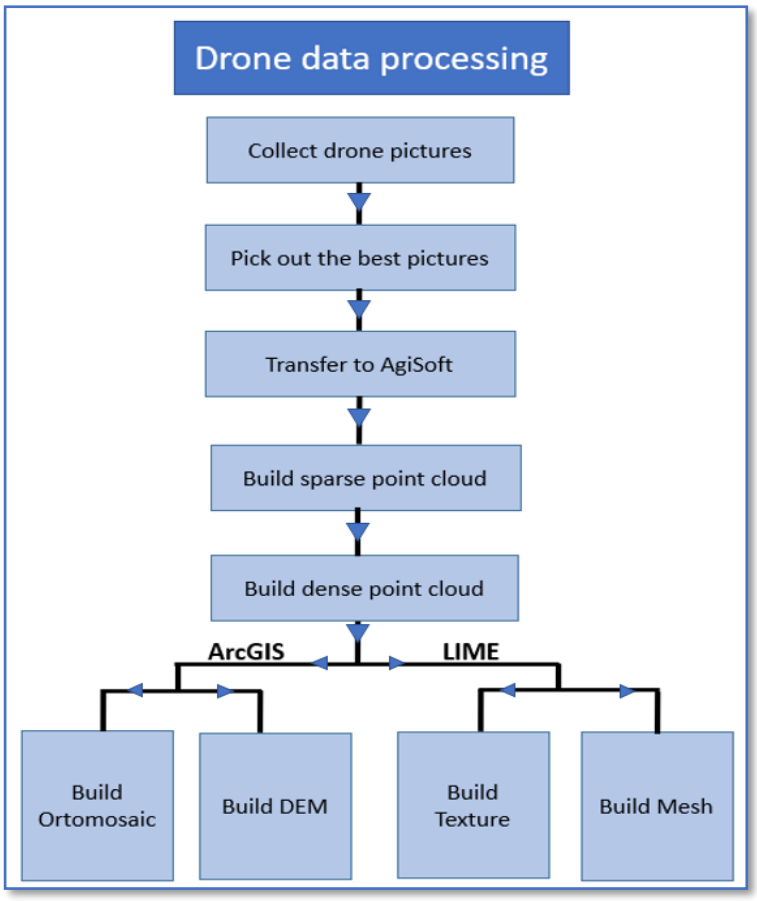

Figure 4-2: Flow chart showing all procedure for data processing

4.2 Map data

The models created in Agisoft were, as explained in chapter 4.1 above, exported to ArcGIS and LIME. In these programs a further analysis of the avalanche area (ArcGIS) and the cliff (LIME) was conducted.

4.2.1 Spatial analysis in ArcGIS

In addition to the DEM and the ortomosaic created in Agisoft, a hillshade map and a slope map were made from 0.5 m data from Kartverket in all the three studied areas.

All the rocks deposited from the avalanche were digitized by creating a polygon, using the *editor tool* to draw polygons around each block (figure 4-3). The benefit of digitizing the blocks in ArcGIS, is that information such as amount, size distribution, density distribution, length and orientation of the block population can be extracted, thus makes it possible to conduct a detailed analyze of the area.

To analyze the spatial distribution of block intensity and block size, two maps were made; an intensity distribution map and a block size distribution map. First, a feature class creating a point in the center of each interpreted rocks has to be made. To do this *Features* and *Feature to point* are selected in the *Data Management tool*, from the ArcToolbox. In the following Feature to point dialog the interpreted blocks are selected as input feature. Next, the intensity distribution map is created by selecting *Kernel Density* from *Spatial analysis tools* in the ArcToolbox. In the Kernel Density dialog, the following values are set: Input point: feature to point, Population field: area, Output cell: 10, Search radius: 10, Output values: expected count. To make the block size distribution map a second similar intensity map has to be made, except that in the Kernel Density dialog the population field is selected as none instead of area. Next, *Math* and *Divide* is selected from *Spatial analysis tools* in the ArcToolbox. In the Divide dialog, the following values are set: Input raster 1: Kernel density (population: area), Input raster 2: Kernel density (population: none).

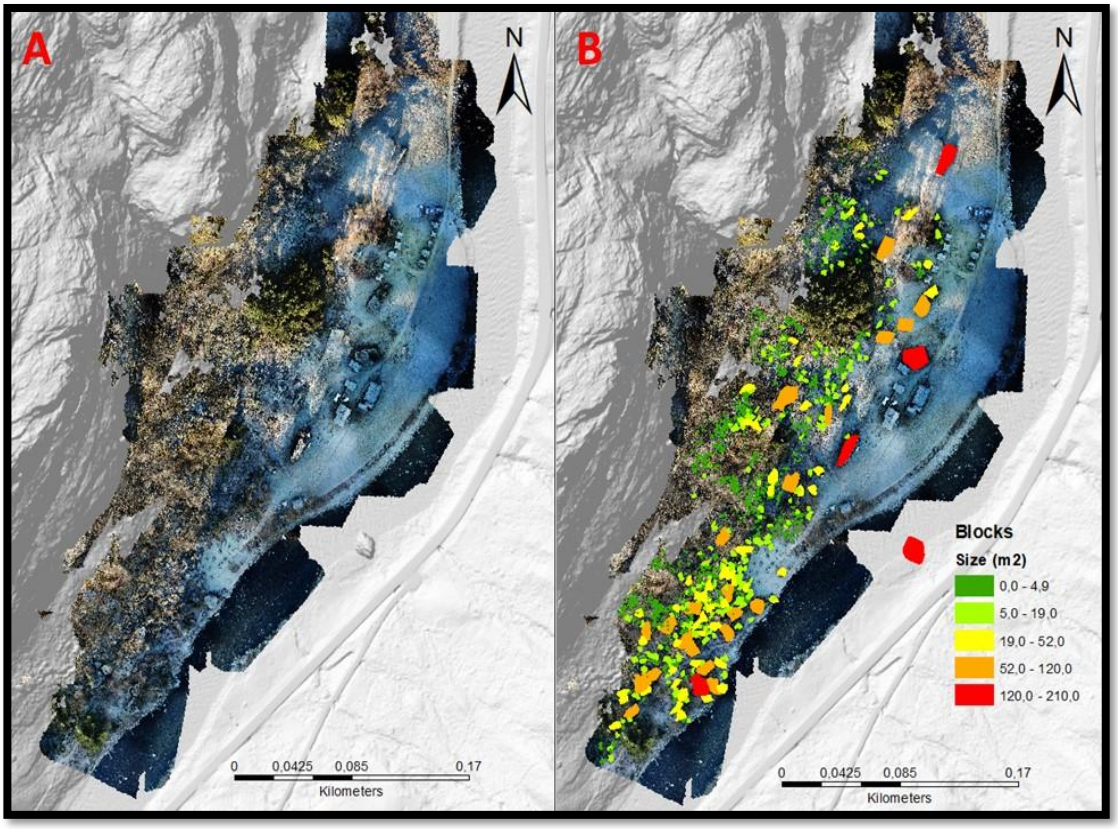

Figure 4-3:ArcGIS model from Taulen showing (A) the fan area without interpretation and (B) the fan area where the blocks are interpreted.

4.2.2 Fracture analysis in LIME

One 3-D model for each study area was created in LIME by using Agisoft to build a mesh and a texture (as explained in chapter 4.1). Further, interpretation tools in LIME (Buckley et.al., 2019) were used to digitize and measure geological features by using the *3D element* command. By selecting the command *create a line,* several fractures and beddings were digitized and located, providing an overview of the bedding and fracture patterns (figure 4-4). By selecting the command *create a plane,* several planes were also digitized and information about dip, dip direction and strike were acquired.

4.2.2.1 Linear scan line

The fracture population at Vinddal was mapped on the cliff sections and sampled using the linear scan line method. This method includes sampling several fractures that intersect a line, thus provide a spatial analysis of the fracture frequency and spacings (figure 4-4) (data in appendix) (Hudson and Priest 1983). The linear scan lines were created in LIME by selecting the *create a line* command from the *3D element* menu. In total, 22 horizontal scan lines were sampled at different elevations; 5 in Vinddal, 8 in Taulen and 9 in Mundal (data in appendix).

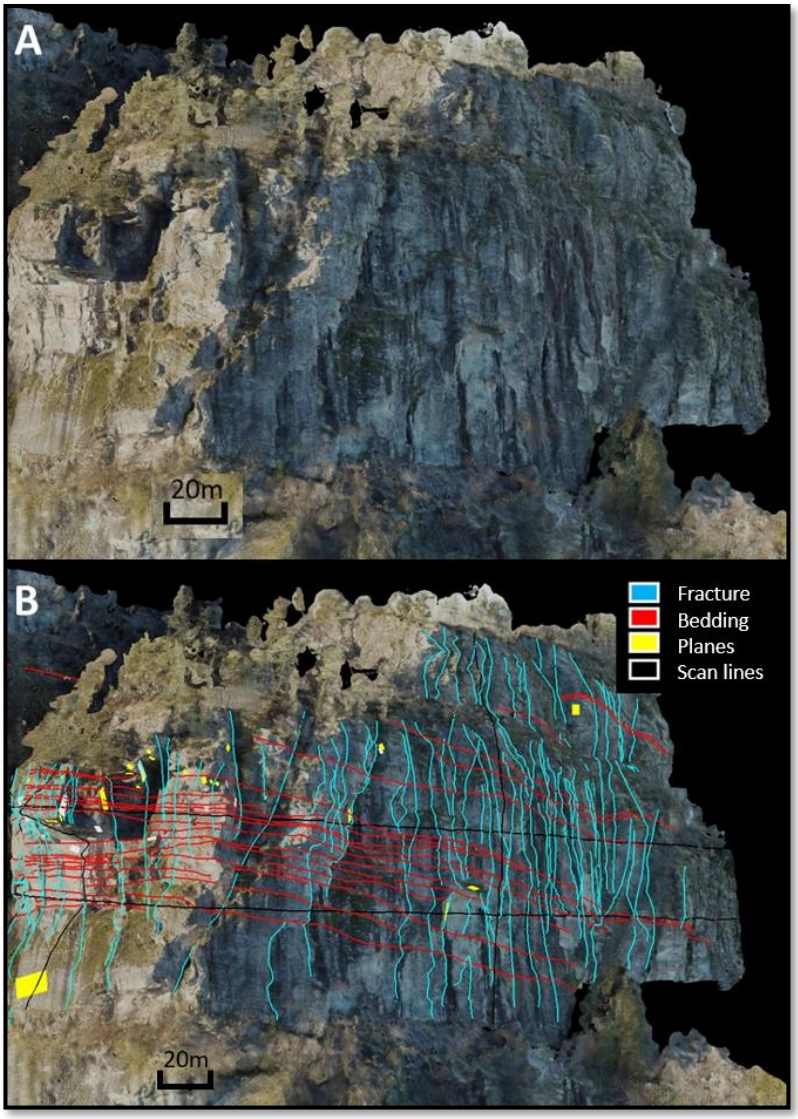

Figure 4-4: LIME model from Taulen showing (A) the cliff without interpretation and (B) the cliff with interpreted fractures, beddings and planes, and horizontal scan lines.

4.2.2.2 Fracture population characteristics

The characteristics of the fracture population were conducted by calculating four important parameters; true fracture spacing, true fracture frequency, the coefficient of variance (CV) and a heterogeneity parameter (V). Further, three frequency-size plots are presented in order to describe the spacing for both the fractures and the rock sizes.

According to Terzaghi (1965), estimation of frequency and spacing based on linear scan lines produces an orientation and spacing bias. To correct this, Terzaghi proposed a correction factor in order to adjust the fracture orientations, and thus reduce the bias caused by the sampling orientation.

To calculate the correct spacing between the fractures, the equation illustrated in figure 4-5A is used. It shows a scan line at angle α with the plane, D' is the apparent spacing along traverse and D is the true spacing between the planes (data in appendix) (Terzaghi, 1965).

The correct fracture frequency (the number of fractures per unit distance) is calculated from the equation illustrated on figure 4-5B (data in appendix). The figure shows a linear scan line at an angle α with the normal (n) to a set of fractures. λ_1 is the fracture frequency measured along fracture normal and λ_1' is the measured frequency along the scan line. By calculating the λ_1 the bias caused by the sampling orientation can be corrected (Terzaghi, 1965).

The coefficient of variance (Cv) is defined as the ratio of the standard deviation to the mean. This parameter measures the degree of clustering (zones where fractures are closely spaced) or anti-clustering for each scan line (Gillespie et al. 1999, 2001). If the Cv is equal to 1 (Cv=1) the distribution is identical to a Poisson (random) distribution (Cox and Lewis 1966). If the Cv is less than 1 (Cv<1) the fractures are anti-clustered (more regular) and if Cv is more than 1 (Cv>1) the fractures are clustered (less regular) (McCaffrey et.al., 2003). Complimentary to this, the heterogeneity parameter (V) is calculated to test in which extent the observed data conform to a uniform distribution. The calculation is based on a cumulative frequency plot, where the maximum deviation above (D^+) and below (D^-) the straight line is summarized; ($V= |D^+| + |D^-|$) (figure 4-5C). V value close to zero indicate a uniform (homogeneous) distribution, and a V value close to 1 indicates a non-uniform (heterogeneous) distribution (Sanderson and Peacock, 2019).

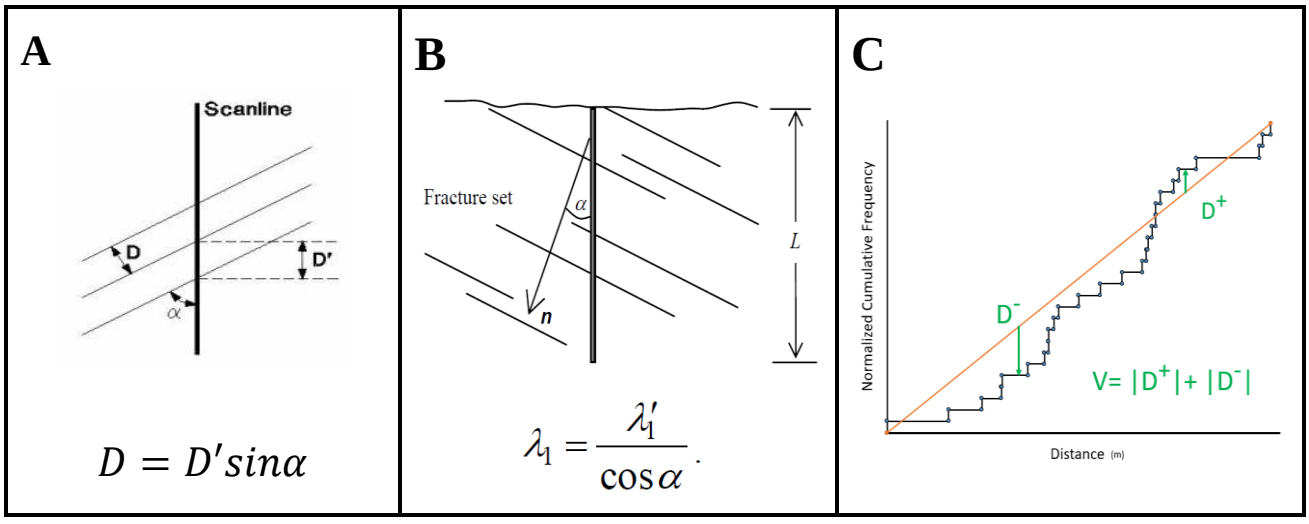

Figure 4-5:A: a linear scan line at an angle a with the fractures and the equation used to find true spacing between the fractures (modified from (rocscience, 2019). B: a linear scan line at an angle a with the normal n to a set of fracture and an equation used to find correct fracture frequency (modified from Wang and Mauldon, 2006). C) A cumulative frequency diagram, showing the maximum deviation above (D+) and below (D-) the line, and the equation used to find the heterogeneity parameter V.

In order to describe the spacing population for the fractures and the rock sizes, three different frequency-size plots are presented; negative exponential (figure 4-6A), a power-law exponential (figure 4-6B) and log-normal distribution (figure 4-6C) (Gillespie et al. 1993, 1999). Determining which of the statistical distributions the fracture- and block population follows can be technically challenging (Jones and Handcock, 2003). In this thesis, whether a given distribution is appropriately described by a negative exponential, a power-law or log-normal distribution, is determined by a visual inspection of each plot.

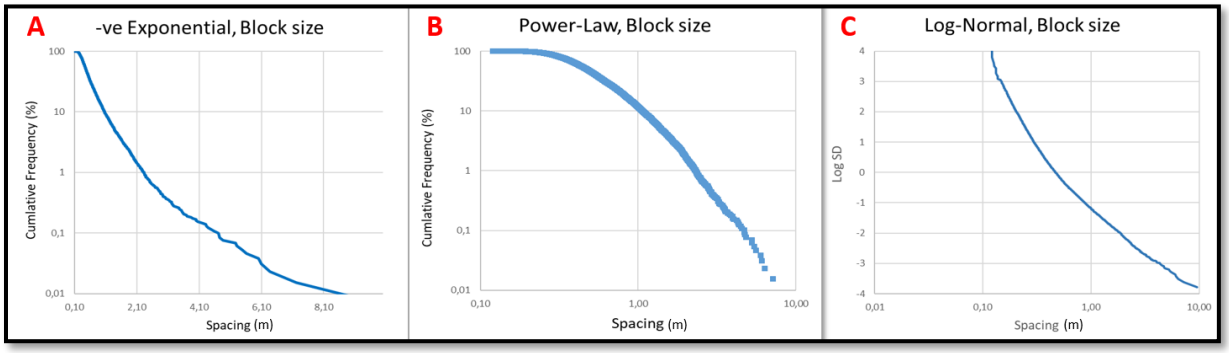

Figure 4-6: Examples of three different frequency-size plots A) negative exponential, B) power-law exponential and B) log-normal distribution

4.3 Field investigations from sites

As the drone data has a limited degree of resolution (commonly 10-20 cm) and leave areas with abundant vegetation difficult to interpret, fieldwork was conducted. Two of the three studied areas were investigated; Vinddal and Taulen. Information about block size, degree of biological weathering, tree damages, vegetation and signs of recent rockfall activities (such as green vegetation beneath rocks) were acquired. For practical and systematic reasons, the collecting of data started at one side of the distal part of the fan, moving up towards the cliff, continuing along the cliff before walking down again, ending at the bottom of the other side of the fan. Figure 4-7A and B illustrate the fieldwork route for Vinddal and Taulen, where the letters along the route represent stops where closer observation were made.

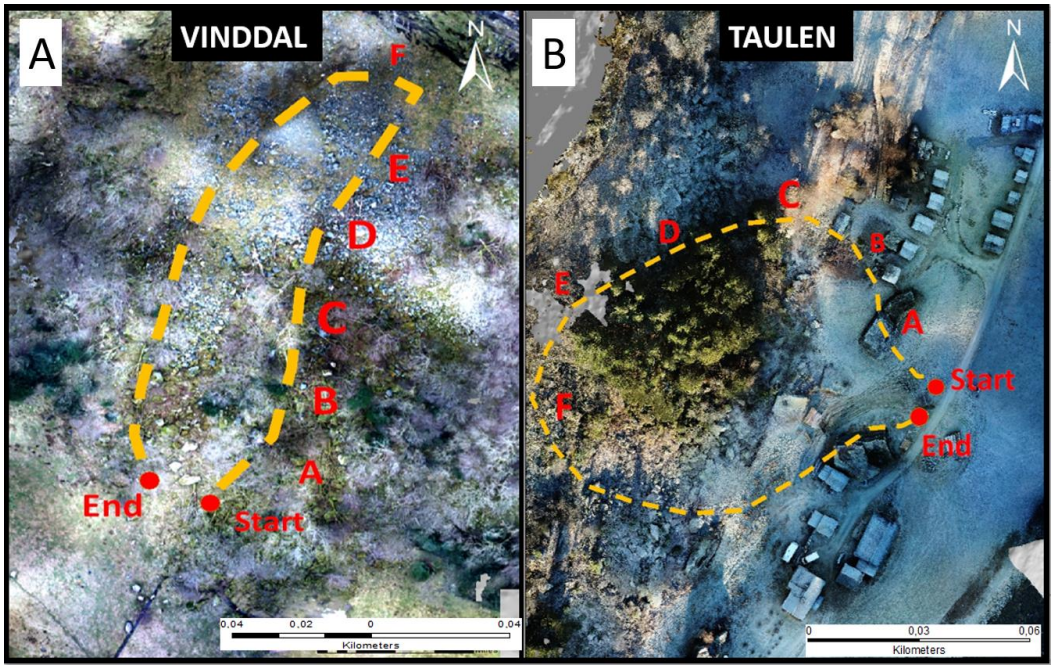

Figure 4-7: (A) Fieldwork route from Vinddal. (B) Fieldwork route from Taulen

4.4 Field investigations from graveyards

A total of 43 gravestones with varying ages were measured at two graveyards; Oppheim kyrkje on Voss (339 masl) (figure 4-8) and at Åsane Gamle kirke in Bergen (117 masl) (figure 4-9). These locations were chosen because of its proximity to the studied areas, thus the growth condition should be comparable.

The three lichens studied (green, Rhizocarpon geographicum lichen; white, Lecanora rupicola lichen; gray, Aspicilia Cinera lichen), were chosen because they all fulfilled the four important requirements making them suitable for dating; (1) easy to recognize, (2) common, (3) slow growing, and (4) grow in a disk shape (figure 4-10). As the lichen growth rate may also depend on the bedrock surface, only gravestones made of granite, granitic gneiss and light granite were investigated. The best usable surface was on the back side, as this was the part that most likely had been undisturbed by human's activity.

To develop an accurate chronology, every gravestone that fulfilled the requirements was investigated for disk-shaped free growing lichen. Further, the largest diameter of the green-, gray- and white lichen was measured and recorded. Additionally, the total coverage of lichens on each gravestone was documented.

Figure 4-8: Map showing where Oppheim kyrkje is located compared to the studied area at Taulen (1:50 000). Modified from NVE 2019

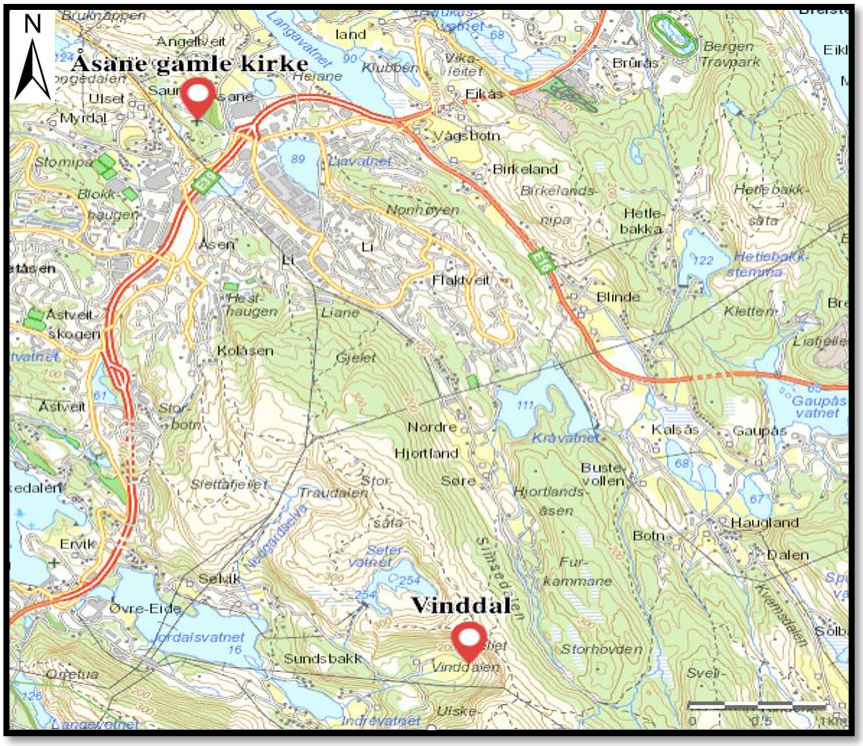

Figure 4-9: Map showing where Åsane Gamle kyrkje is located compared to the studied area in Vinddal (1:50 000). Modified from NVE 2019

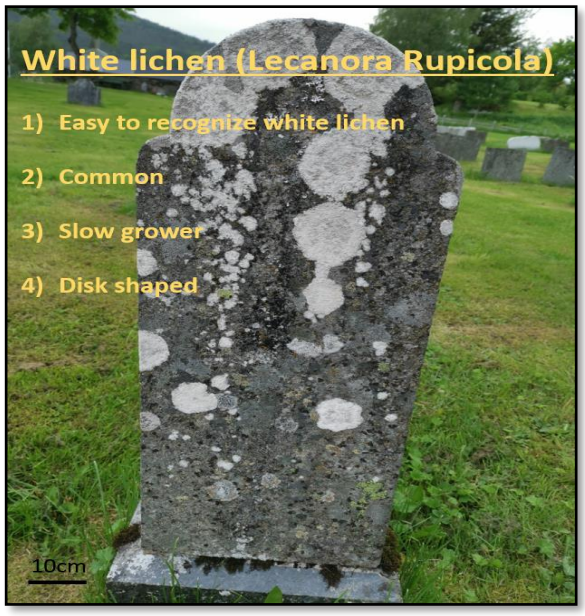

Figure 4-10: A gravestone that fulfill all the requirements for lichen investigation (picture taken at Oppheim kyrkje)

4.5 Potential sources of error

4.5.1 Fracture and bedding data

The linear sampling method used for fracture analysis and attribute sampling, induce some potential sources of error. Firstly, the angle between the scan line and the fractures can create an orientation bias. Furthermore, all fracture orientations were sampled using LIME, which is limited by the resolution (commonly 30-50 cm). This can cause errors related to inaccurate interpretation, thus wrong estimations of the orientation and spacing of fractures.

4.5.2 Block size and block distribution

Resolution problems are also relevant in ArcGIS (commonly 10-20 cm), where errors during interpretation can result in wrong rocks size and intensity maps. In addition, areas covered by vegetation are not possible to map, thus some areas are not accounted for.

The lichen measurements done on gravestones also contains some potential source of error. Firstly, uncertainty related to if and when the gravestones were cleaned. This is difficult to get a total overview of because, according to the graveyard authorities (Gravplassmyndighetene) for both Bergen and Voss, cleaning of the gravestones is only performed by the relatives. Secondly, the study has a limited number of measurements and the sample surface is quite small. According to Innes (1984) the mean largest lichen per size increases with quadra size. In addition, McCarroll (1994) discovered that there is a significant correlation between boulder size and the largest lichen size.

5 Results:

5.1 Case study 1: Vinddal

5.1.1 Spatial mapping of avalanche

The case study at Vinddal consist of a steep NE-facing cliff with an accumulation of coarse rock fragments at the cliff base, which originates form sediment-gravity processes. A total number of 9541 rocks has been digitized (figure 5-1). The rock deposited, form a fan with measured block sizes ranging from 0.003 m^2 (0.012x0.25 m) to 30 m^2 (5x6 m). Analysis of the spatial distribution of the surface blocks shows that block intensity decreases down the talus slope and away from the cliff face (figure 5-2B). The contour plot highlights a bullseye of high block intensity (number of blocks per m^2), with up to 30 blocks per m^2, at the base of the cliff. Away from the cliff the block intensity rapidly decreases to a consistent level of less than 10 blocks per m^2. The spatial distribution of the average block size shows that small (green) to medium (yellow) sized rocks dominate the fan, where block sizes increases away from cliff (figure 5-2A). The distribution of the blocks on the fan surface indicate a fall-sorting, resulting in a distal coarsening of the rock fragments; the smallest fragments are located at the cliff base and larger boulders are transported further down the slope and occur at the distal edge of the fan.

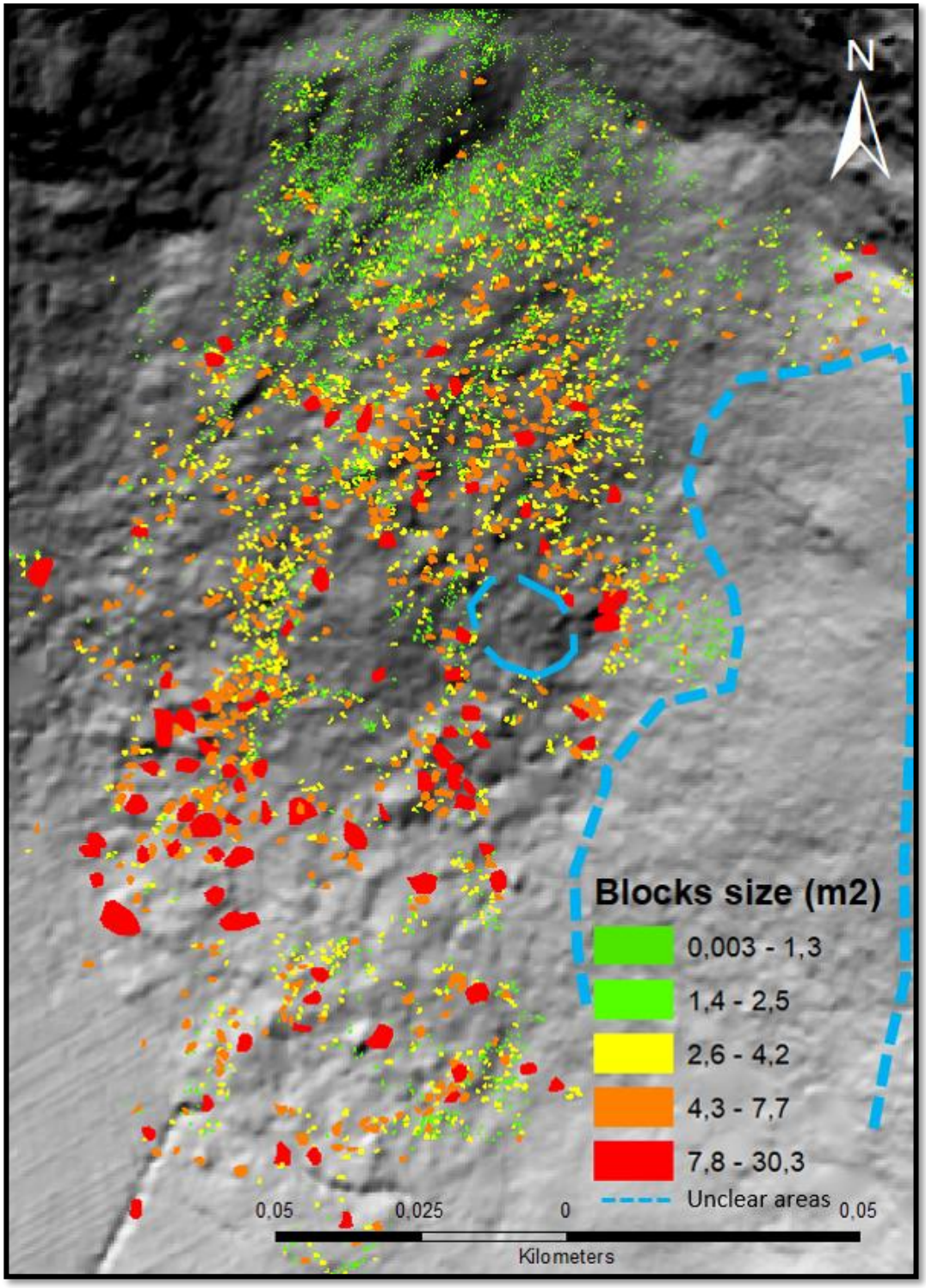

Figure 5-1: Hillshade map and all the 9541 digitized rocks. The blocks are color coded based on their size (m^2). The areas within the dotted lines are inaccessible areas due to vegetation

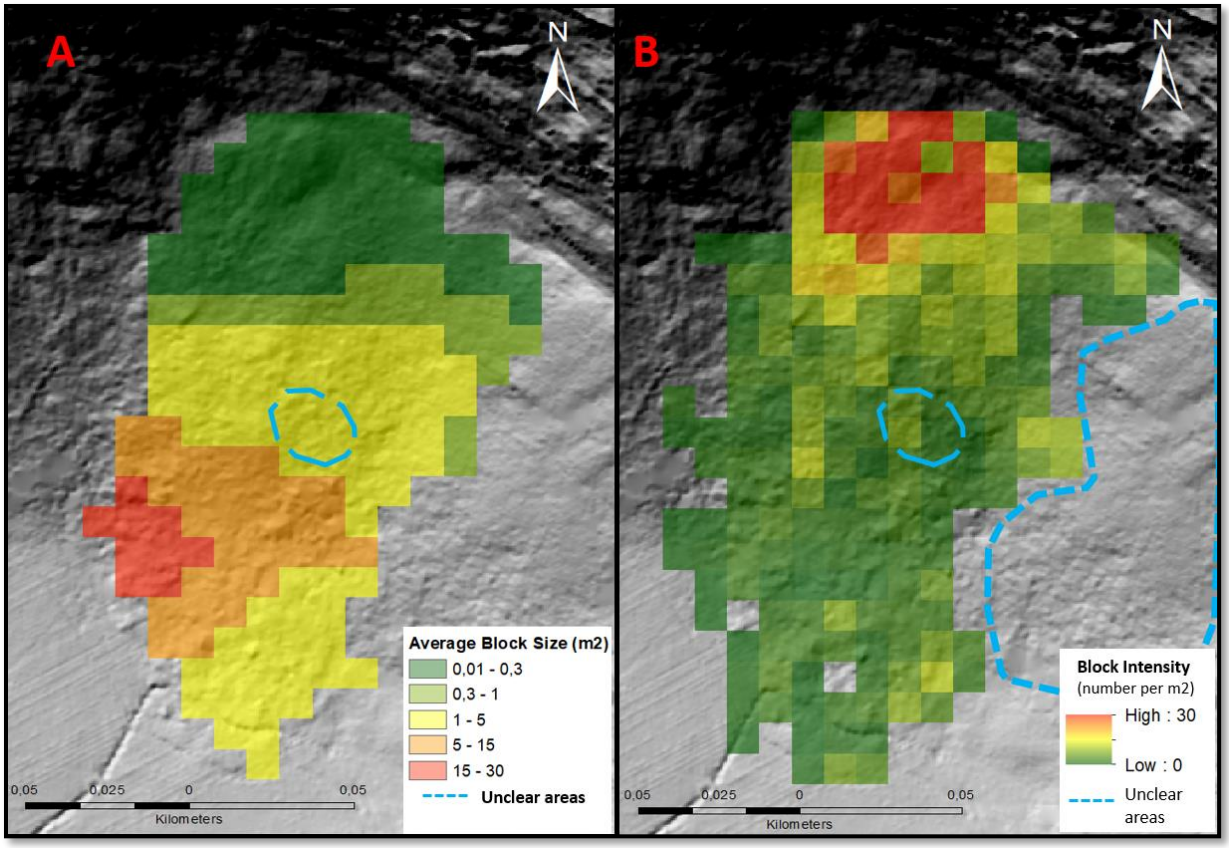

Figure 5-2: Ddistribution maps from the ArcGIS model of Vinddal. A: Block size distribution (average block size per m^2) where the largest blocks = red, and the smallest= green. B: Intensity distribution (number per m^2) where high intensity area = red, and low intensity area = green. The areas within the dotted lines are inaccessible areas du to vegetation.

5.1.2 Fracture population characteristics

The fracture population at Vinddal was mapped on the cliff sections and sampled using a series of line scans. The dip and strike of 20 fractures and 15 bedding planes were measured (data in appendix) and plotted in a stereonet (figure 5-3). Measured fracture orientations indicate a single set trending ~SE-NW, with an average trend at N120°E and a moderate dip of approximately 60° towards SW. The fractures cut through steeply dipping (~80°) bedding that strikes N290°E with relatively consistent bed thicknesses averaging 2.8 m. The cliff itself (green plane) has an ~E-W orientation, slightly oblique to the fracture trend and sub-parallel to the bedding trend (figure 5-4).

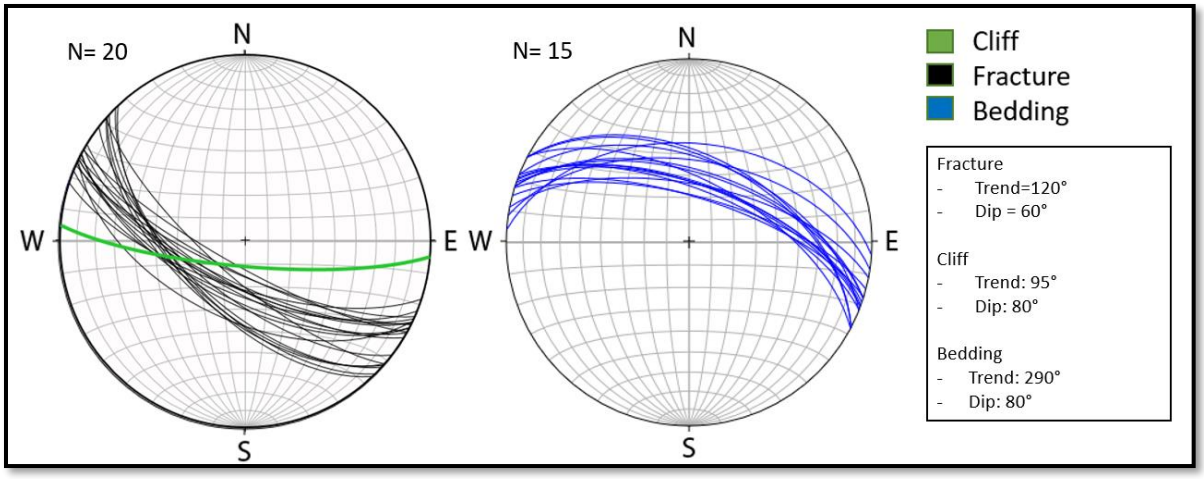

Figure 5-3: Stereonet where fractures and bedding planes are potted. The left stereonet shows fracture planes (black) and the cliff (green). The right stereonet shows bedding planes (blue)

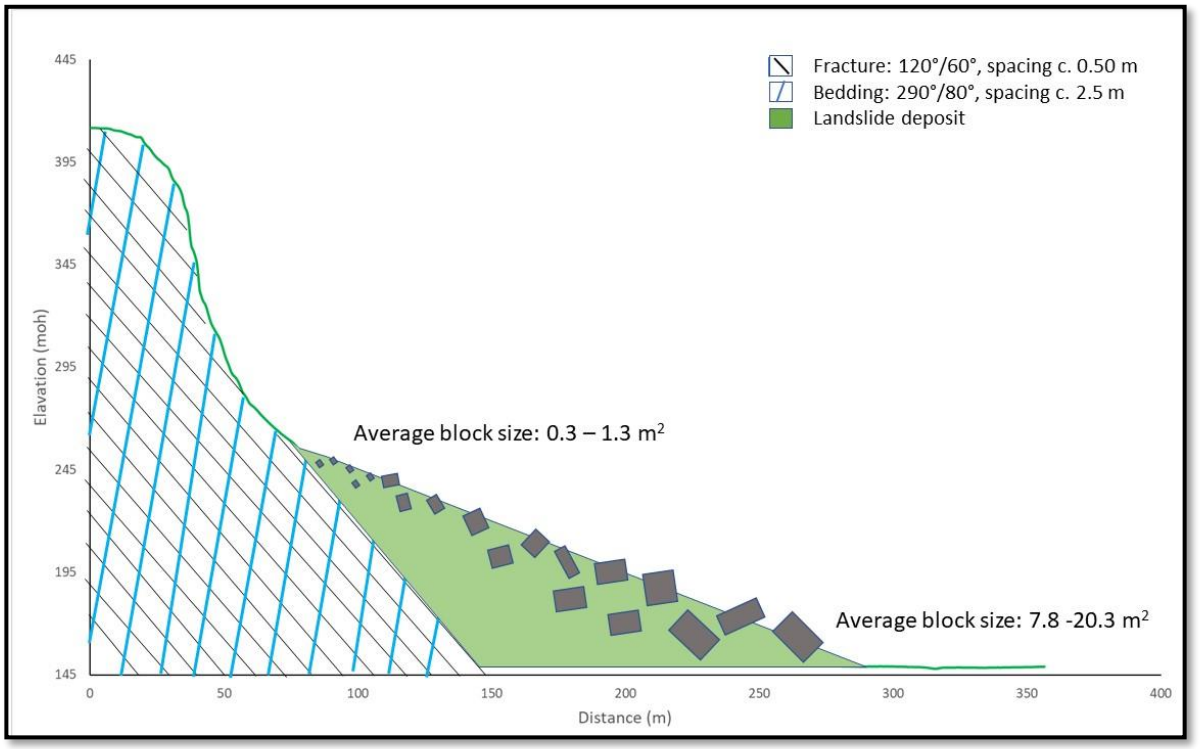

Figure 5-4:: Side view of the cliff showing the fractures and bedding relative to the cliff. The figure is not to scale, but shows relative spacing of fracture and beddings, and trends in block size.

A total of 5 scan lines sample the fracture population in order to provide a spatial analysis of their frequency and spacing (data in appendix) (e.g. Table 5-1). Fracture intensities and fracture spacings vary between scan line localities, ranging from 0.3–1.8 N/m and 0.4–3.4 m respectively. This is illustrated by the scatter of data in figure 5-5A, which compares fracture intensity against the coefficient of variance (CV) for fracture spacing. This variation between scan line localities can be explained by differences in the resolution of the 3-D model rather

than spatial variations, e.g. lower resolutions can lead to under-sampling of fractures. The scan lines from the lower cliff section exhibit lower intensities (~0.4 N/m) coinciding with a low image resolution (150 cm in LIME) (considered further in the discussion, chapter 6.3). Whereas the scan lines from the upper cliff section exhibit the greatest fracture intensities whilst coinciding with higher image resolutions (50 cm). Thus, the scan lines from the upper cliff section are more representative of the fracture population. These indicate an average fracture intensity of ~1.8 m^{-1} with an average fracture spacing CV of ~0.8, suggesting a random fracture spacing (CV = 1) with no clustering of fractures (figure 5-4) (explained in chapter 4.2.2).

The datasets from the uppermost part of the cliff are further presented in Figure 5-5B, which plots normalized cumulative frequency against distance along the scan line, and illustrates the spatial distribution of fracturing. As the fracture frequency is proportional to the slope of the distribution, zones of high frequency are recognized by steep slopes. This means that a zone of clustered fractures will show a stair step curve in the fracture frequency distribution. No such stair steps can be seen along the scan line, indicating a lack of clustering. Furthermore, the maximum departure above ($D^+ = 0.04$) and below ($D^- = -0.09$) the line is used to calculate the heterogeneity parameter ($V= |D^+| + |D^-|$), resulting in a V value of 0.1. This value is quite low indicating a uniform (homogenous) distribution, thus supports the fracture CV spacing values (CV=0.7 and 0.9).

Tabell 5-1 Corrected values for the fracture analysis of each scan line. Green areas represent the scan lines that are the most representative of the fracture population.

Scan lines	elevation (masl)	Resolution (cm)	Total frequency	Average fracture spacing (m)	Fracture intensity (N/m)	CV
1	240	150	53.4	2.4	0.4	1.1
2	260	150	93.4	0.4	0.4	0.9
3	295	150	80.0	3.4	0.3	0.2
4	330	50	128.9	0.6	1.8	0.7
5	340	50	115.6	0.6	1.8	0.9

.

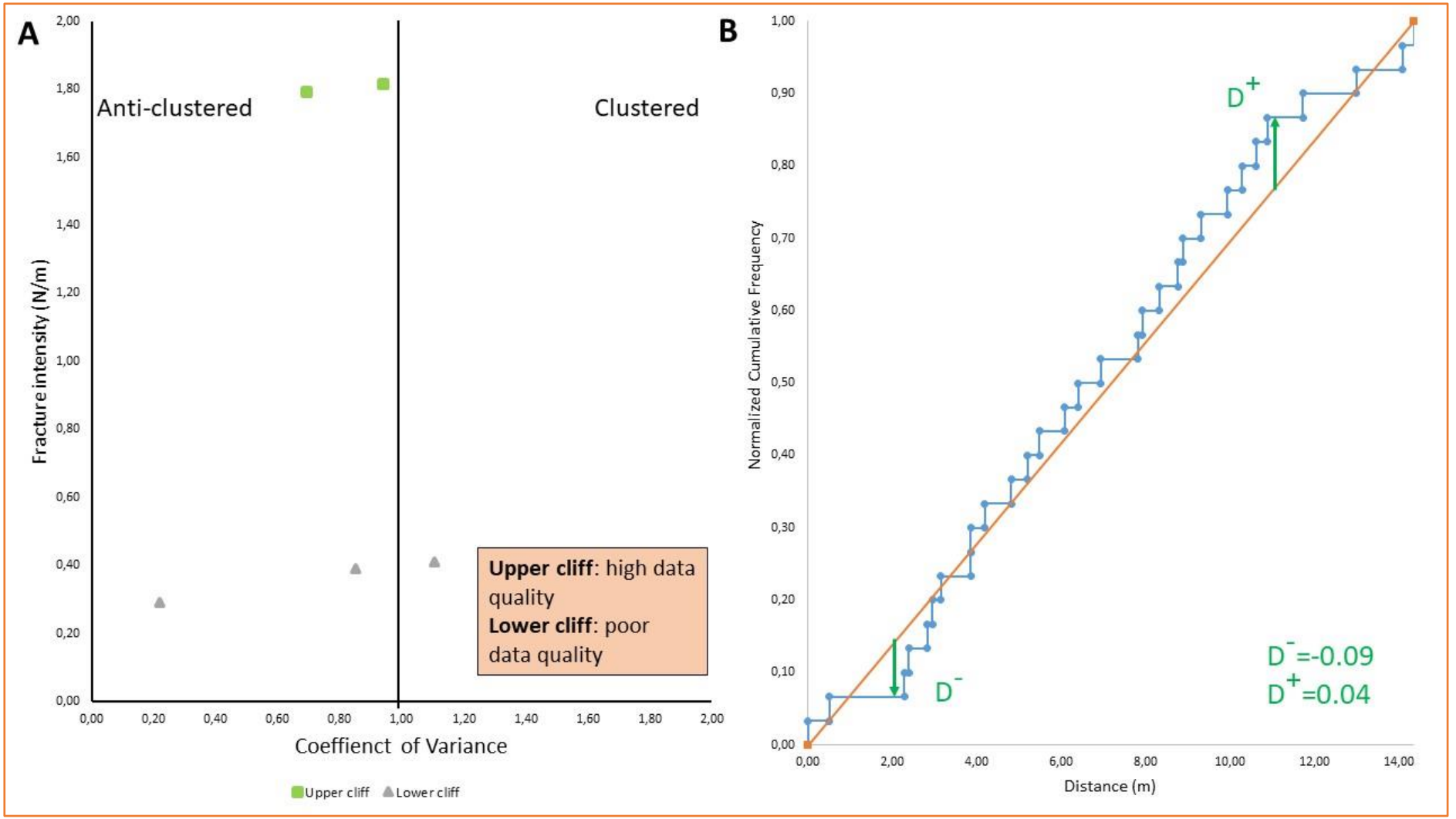

Figure 5-5: (A) The intensity versus coefficient of variance plot from scan lines in Vinddal. The scatter plot shows, based on the most reliable data (scan lines from upper cliff), a random fracture distribution (green squares). (B) Normalized cumulative diagram of the most reliable data (scan lines from upper cliff), showing a curve with no big variations in scale, thus fractures are not clustered. *D+ and D-* represent t*he maximum departure above* and below the line.

5.1.2.1 Block Size vs Fracture Spacing

The box plots in figure 5-6 compare the fracture spacing data from the upper cliff sections with the calculated block dimensions (square root of block size area) of the digitized rock in the avalanche deposits. In this case, both datasets show comparable data ranges and averages. In particular the range of data between the 25^{th} and 75^{th} percentiles. Furthermore, the mean values (marked by x) are very similar, with means of 0.50 m and 0.45 m for fracture spacings and block dimensions, respectively. The whiskers (vertical lines), showing the minimum and maximum values, are also quite close. The decrease in average and maximum size for blocks can be explained by fragmentation (i.e. breaking) of blocks during impacts when falling. Additional. the slightly higher minimum size for blocks is likely explained by that small (< 5 cm) rocks are easily covered by vegetation or larger rocks

Various frequency-size plots are presented in Figure 5-7 for both the block dimensions and fracture spacings, where a straight line fit to the data indicates whether they conform to a negative exponential (figure 5-7A and D), a power-law (figure 5-7B and E) or log-normal distribution (figure 5-7C and F). In this case, both the fracture- and the block populations appear to conform best to a power-law distribution. Deviations from the straight-line fit are due to truncation and censoring effects, such as under-sampling of the smallest blocks and fractures due to the resolution limit of the imagery and underrepresentation of larger blocks due partial burial and/or vegetation cover. The exponents (i.e. the gradients) of the power-law fits are very similar for both the fracture spacings and block dimensions. Although the data conforms to a power-law fit, the exponents are high (>2) indicating a limited scale range in fracture spacings and block dimensions. This means that the mean values for the block dimensions or the fracture spacings are representative of their populations.

Overall the fracture spacings and block dimensions show similar size ranges, averages and frequency-distribution. These similarities indicate that fracture spacings are a major controlling factor on the block sizes within the avalanche deposits at Vinddal.

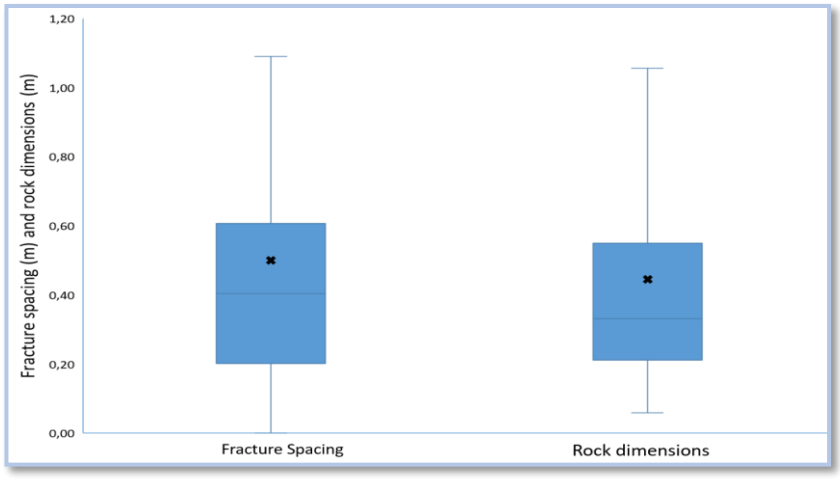

Figure 5-6:Box plot of the fracture spacings and rock dimensions. Middle line in the box = the median, x in the box = the mean, vertical lines = the whiskers (minimum and maximum value). The maximum value is only 95th percentile.

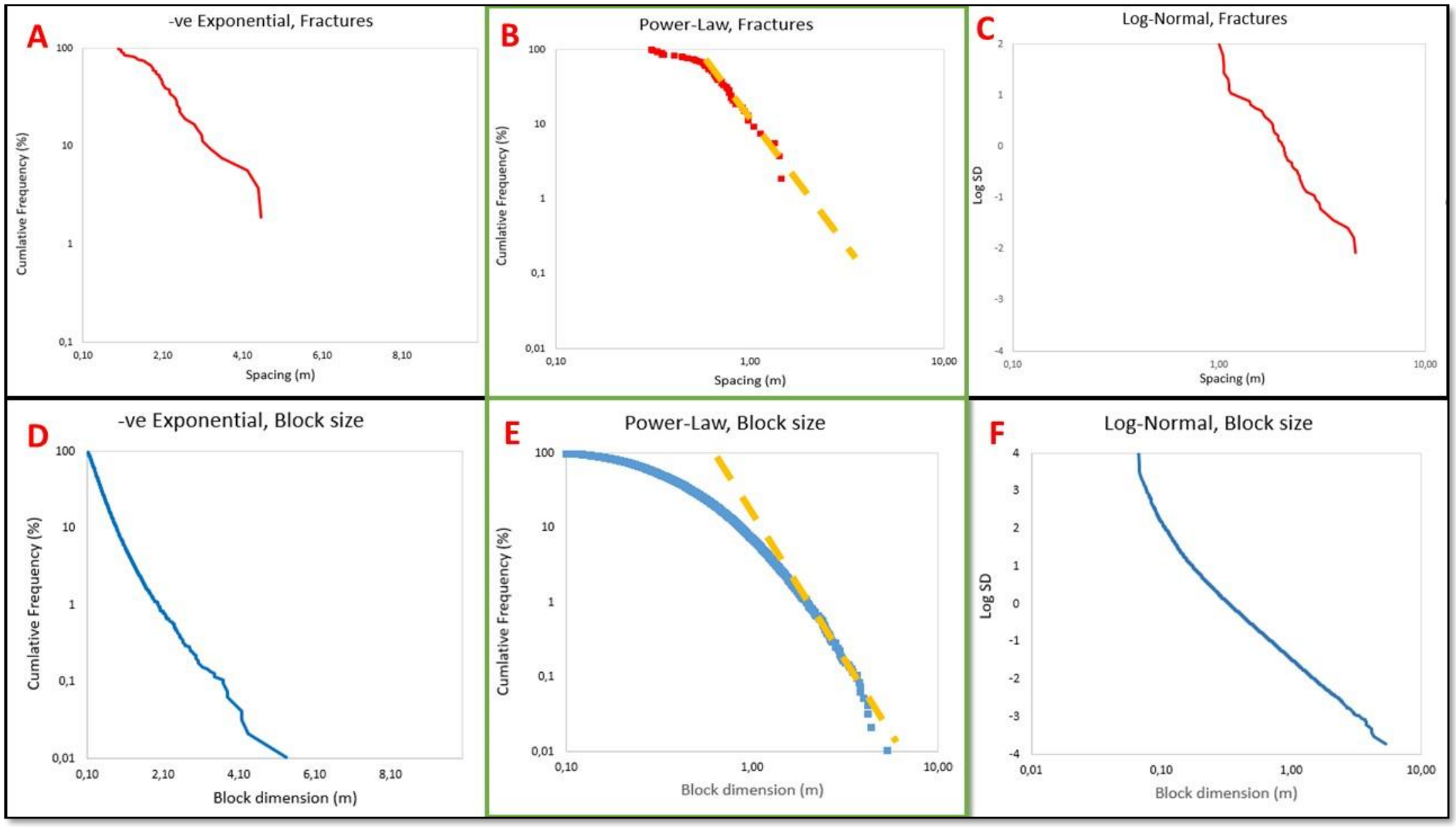

Figure 5-7: Three frequency-size plots for block dimensions and fracture spacings at Vinddal; negative exponential (A,D), a power-law exponential (B,E) or log-normal distribution (C,F). The distributions with green frames are considered the best fit distribution.

5.2 Case study 2: Taulen

5.2.1 Spatial mapping of the avalanche

The case study in Taulen consist of a steep NW facing cliff and an apron, consisting of coarse angular rocks with sharp and jagged corners. A total number of 1948 rocks has been digitized in this locality (figure 5-8). A wide range of block sizes are present in the apron, ranging from 0.01 m^2 (0.1x0.1 m) to 210 m^2 (14x15 m). Analysis of the spatial distribution of the surface blocks shows that block intensity (number of blocks per m^2) decreases down the talus slope and away from the cliff face (figure 5-9B). The contour plot highlights a bullseye of high block intensity with up to 40 blocks per m^2, in the upper and middle part of the cliff (red areas). Away from the cliff, the block intensity rapidly decreases to a consistent level of less than 5 blocks per m^2. Additionally, the spatial distribution plot divides the fan into 4 parts along the fan, which is due to areas covered by vegetation, thus a lack of data (marked with blue dotted line). The spatial distribution of the average block size in figure 5-9A (block size per m^2) shows that small (green) to medium (yellow) sized rocks dominate the upper part of the fan and increases down the slope away from cliff. The distribution of the blocks on the surface of the apron indicate that the fan is fall sorted, resulting in a distal coarsening of rock fragments; the smallest fragments are located at the cliff base and larger boulders are transported further down the slope and occur at the distal edge of the fan.

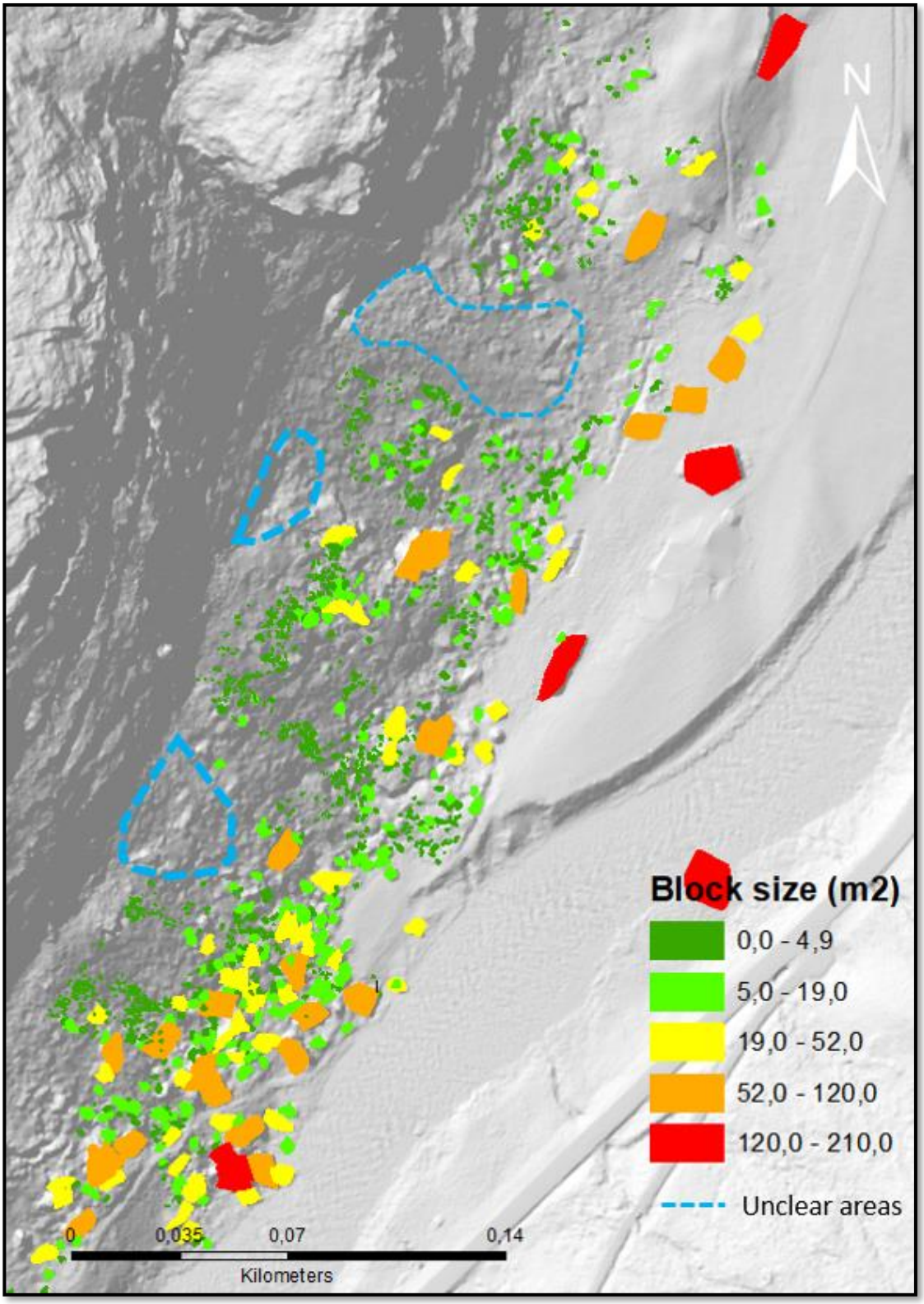

Figure 5-8: Hillshade map and all the 1948 digitized rocks. The blocks are color coded based on their size (m^2). The areas within the dotted lines are inaccessible areas du to vegetation

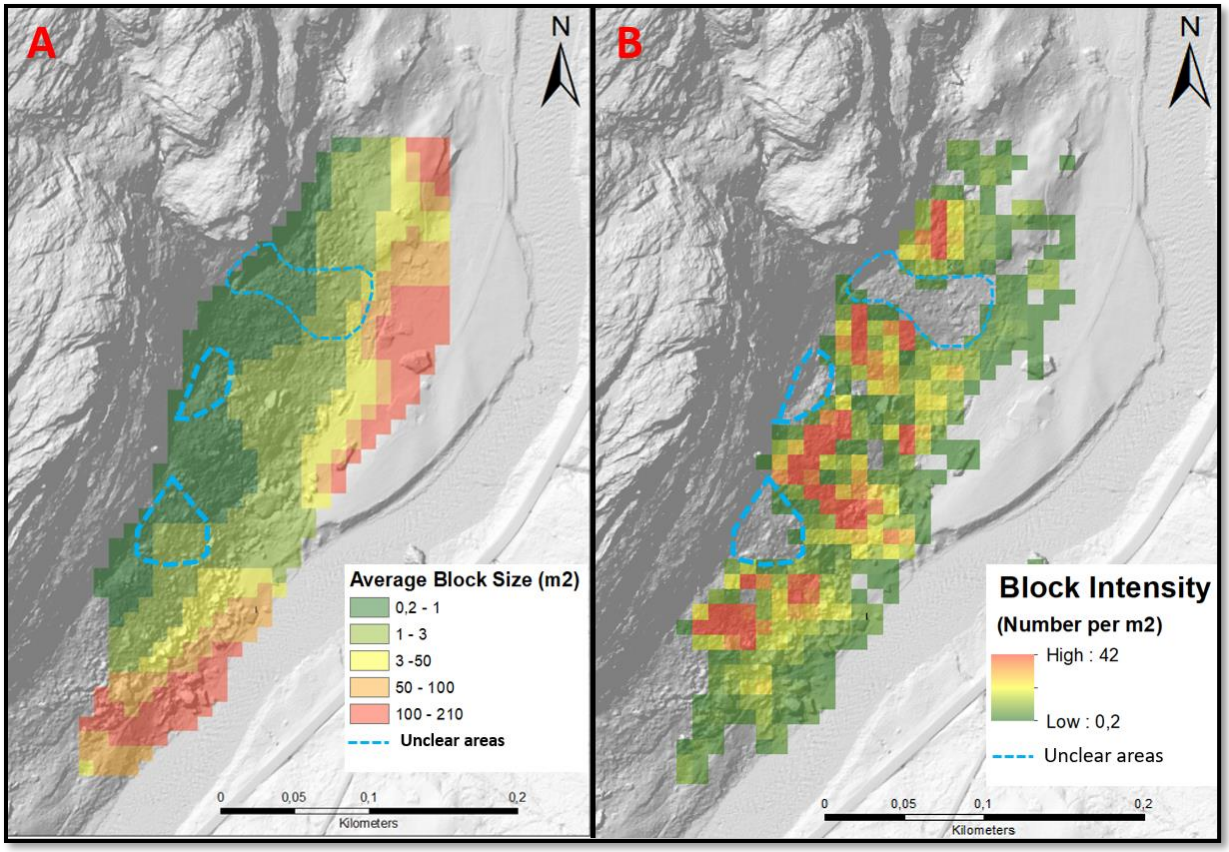

Figure 5-9: Ddistribution maps from the ArcGIS model of Taulen. A: Block size distribution (average block size per m^2) where the larger blocks = red, and the smallest green. B: Intensity distribution (number per m^2) where high intensity area = red, low intensity area = green. The areas within the dotted lines are inaccessible areas du to vegetation.

5.2.2 Fracture population characteristics

The fracture population at Taulen was mapped on the cliff sections and sampled using a series of line scans. The dip and strike of 33 fractures and 13 bedding planes were measured (data in appendix) and plotted in a stereonet (figure 5-10). Measured fracture orientations indicate two, near vertical, orthogonal sets, trending NE-SW and NW-SE. Fracture set 1 has an average trend at N40°E and a steep dip of approximately 75° towards NW. Fracture set 2 has an average trend at N306°E and a steep dip of approximately 87°. The fractures cut through shallow dipping (~20°) bedding that strikes N198°E with an average thickness of 8.9 m. The cliff itself is plotted as three planes (green) due to variation in the orientation of the cliff face. It is oriented ~NE-SW, parallel to the trend of fracture set 1 and perpendicular to the trend of fracture set 2. The bedding is orientation parallel to the cliff face, with a dip that is almost perpendicular to each other (figure 5-11).

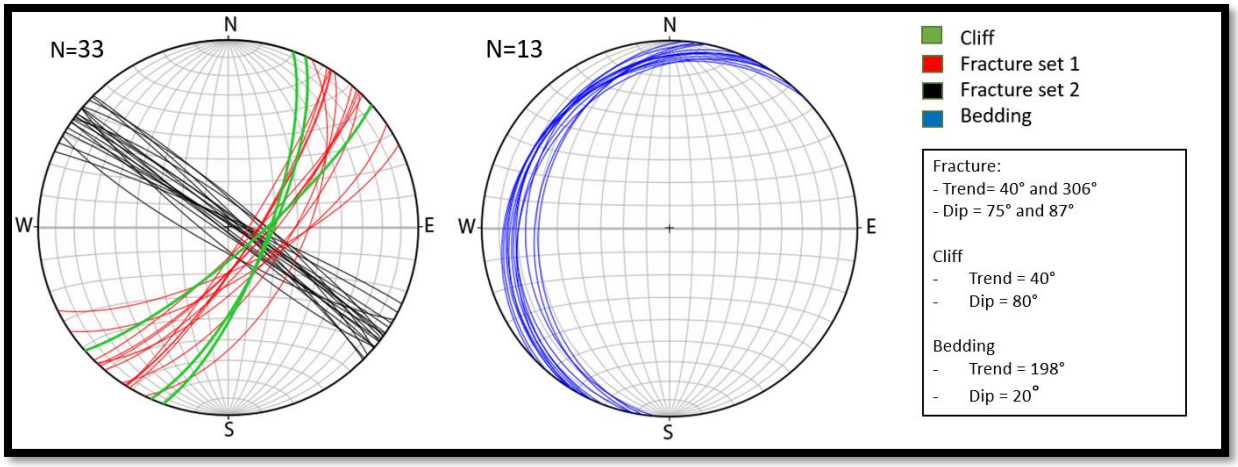

Figure 5-10: Stereonet showing fractures and bedding planes. The left stereonet shows fracture planes from fracture set 1 (red), fracture set 2 (black) and the cliff (green). The right stereonet shows bedding planes (blue)

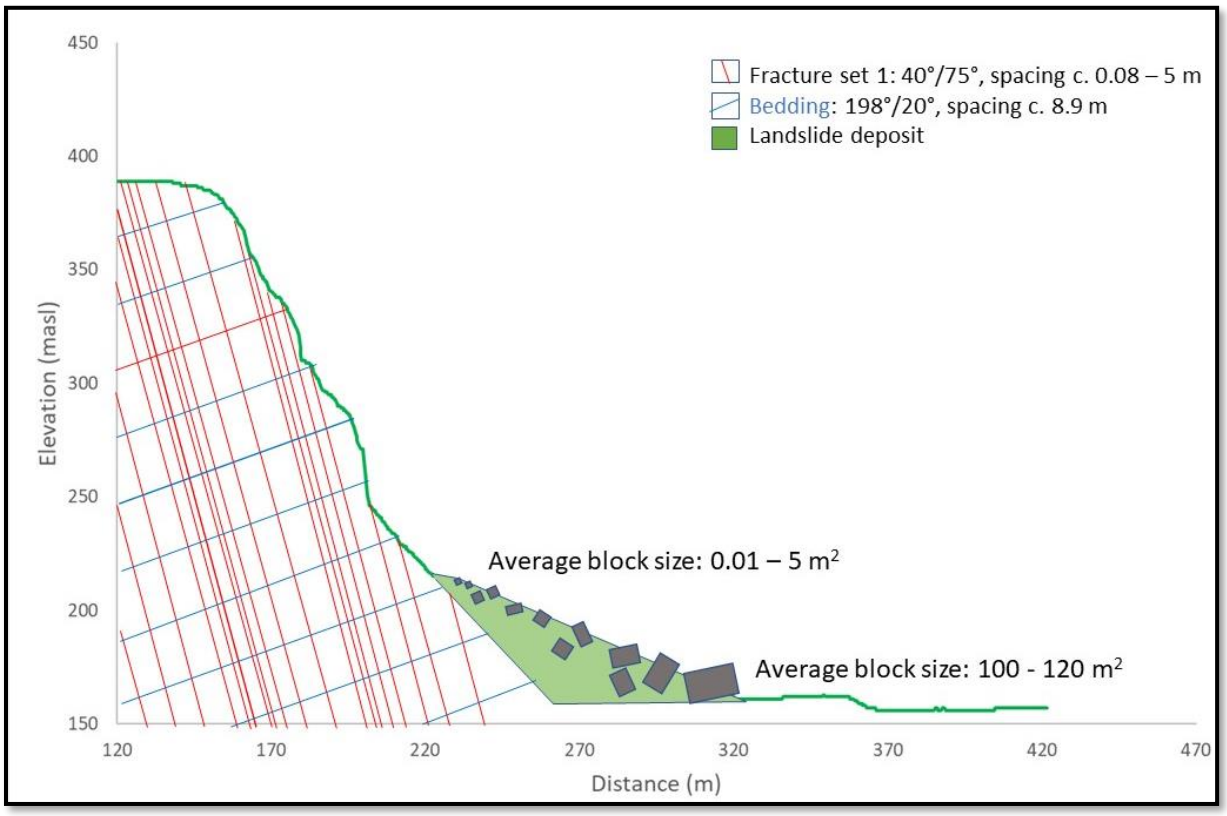

Figure 5-11: Side view of the cliff showing fracture set 1 and bedding relative to the cliff. Fracture set 2 is not illustrated as the planes are oriented parallel to the view. The figure is not to scale, but shows relative spacing of fracture and beddings, and trends in block size.

A total of 8 scan lines sample the fracture population in order to provide a spatial analysis of their frequency and spacing (e.g. Table 5-2). Fracture intensities and fracture spacings vary between scan line localities, ranging from 0.1–1 N/m and 1.0–13.4 m respectively. This is illustrated by the scatter of data in figure 5-12A, which compares fracture intensity against the coefficient of variance (CV) for fracture spacing. As explained in sub-chapter 5.1.2, this

variation between scan line localities can be explained by differences in the resolution of the 3-D model rather than spatial variations. The scan lines from the right and the left cliff section exhibit lower intensities (~0.2 N/m) coinciding with a low image resolution (100). Whereas the scan lines from the mid cliff section exhibit the greatest fracture intensities and coinciding with higher image resolutions (30 cm). Thus, the scan lines from the mid cliff section are more representative of the fracture population. These indicate an average fracture intensity of ~0.1 m^{-1} with an average fracture spacing CV of ~1.5, suggesting a clustered fracture distribution (CV > 1), or in simpler terms, less regular (figure 5-11) (explained in chapter 4.2.2).

The datasets from the mid part of the cliff are further presented in figure 5-12B, which plots normalized cumulative frequency against distance along the scan line, and illustrate the spatial distribution of fracturing. As the fracture frequency is proportional to the slope of the distribution, zones of higher frequency are recognized by steeper slopes. The plot shows a stair-stepped curve along the scan lines, indicating several clustered zones of varying fracture frequencies. Furthermore, the maximum departure above ($D^+ = 0.02$) and below ($D^- = -0.36$) the line is used to calculate the heterogeneity parameter ($V= |D^+| + |D^-|$), resulting in a V value of 0.4. This value is quite high indicating a non-uniform (heterogeneous) distribution, thus supports the fracture CV spacing values (CV=1.3 and 1.7).

Tabell 5-2: Corrected values for the fracture analysis of each scan line. Green areas represent the scan lines that are the most representative of the fracture population.

Scan line	Cliff side	elevation (masl)	Resolution (cm)	Total frequency	Average fracture spacing (m)	Fracture intensity (N/m)	CV
1	Right	150	100	46.4	3.0	0.3	0.6
2	Right	130	100	32.3	5.1	0.2	1.1
3	Middle	150	30	48.6	1.0	1.0	1.3
4	Middle	130	30	38.8	1.0	1.0	1.7
5	Left	150	100	4.6	2.3	0.4	0.7
6	Left	140	100	5.8	3.3	0.3	1.4
7	Left	130	100	31.0	13.4	0.1	0.3
8	Left	120	100	32.2	12.3	0.1	1.2

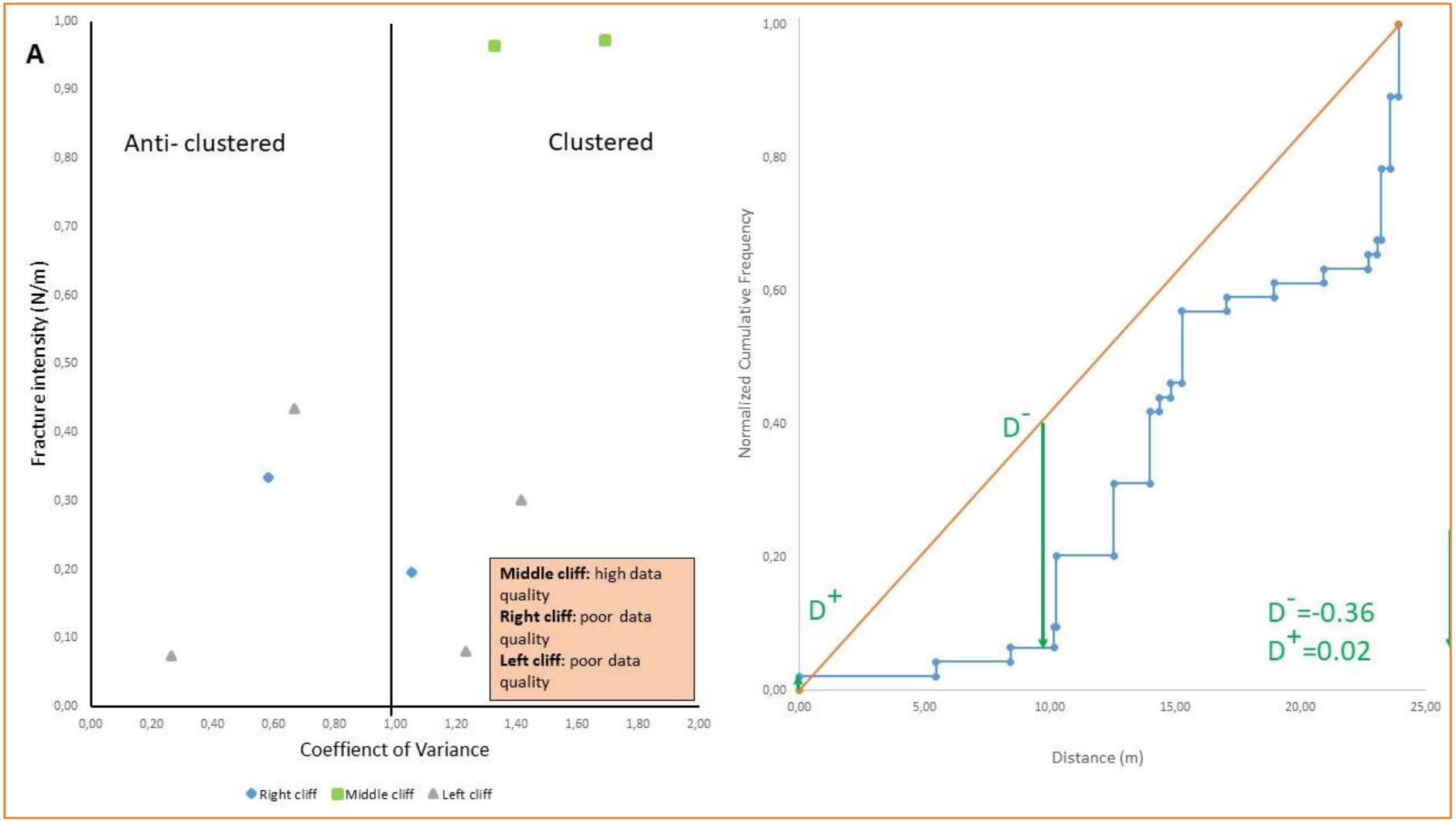

Figure 5-12: (A) The intensity versus coefficient of variance plot from scan lines in Taulen. The scatter plot shows, based on the most reliable data (scan lines from the mid cliff), a clustered fracture distribution (green squares). (B) Normalized cumulative frequency diagram of the most reliable data (scan lines from the mid cliff), showing curve with several big variations in scale, thus indicate clustering. *D+ and D-* represent *the maximum departure above* and below the line.

5.2.2.1 Block Size vs Fracture Spacing

The box plots in figure 5-13 compare the fracture spacing data from the mid cliff sections with the calculated block dimensions (square root of block size area) of the digitized rock in the avalanche deposits. In this case, both datasets show comparable data ranges and averages. In particular the range of data between the 25th and 75th percentiles. Furthermore, the mean values (marked by X) are very similar, with means of 1.3 m and 1.2 m for fracture spacings and block dimensions, respectively. The whiskers (vertical lines), showing the minimum and maximum values, is also quite close. The decreased in average and maximum size for blocks can likely be explained by fragmentation (i.e. breaking) of blocks during impacts when falling. Additional. the slightly higher minimum size for blocks is likely explained by that small (< 5 cm) rocks are easily covered by vegetation or larger rocks.

Various frequency-size plots are presented in Figure 5-14 for both the block dimensions and fracture spacings, where a straight line fit to the data indicates whether they conform to a negative exponential (figure 5-14A and D), a power-law (figure 5-14B and E) or log-normal distribution (figure 5-14C and F). In Taulen, both the fracture- and the block populations appear to conform best to a power law distribution. Deviations from the straight-line fit are due to truncation and censoring effects. The exponents (i.e. the gradients) of the power-law fits are very similar and low (<2) for both the fracture spacings and block dimensions. A low exponent indicating a wider range of fracture spacings and block dimensions present, thus the mean values are not representative of their populations.

Overall the fracture spacings and block dimensions show similar size ranges, averages and frequency-distribution. These similarities indicate that fracture spacings are a major controlling factor on the block sizes within the avalanche deposits at Taulen.

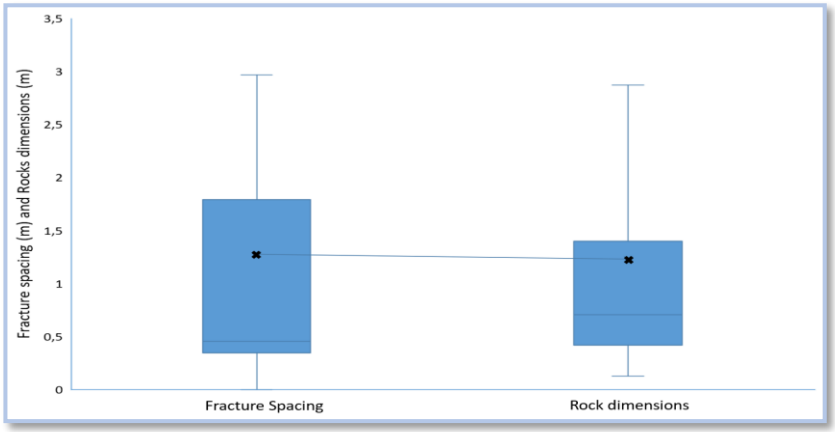

Figure 5-13: Box plot of the fracture spacings and rock dimensions form Taulen. Middle line in the box = the median, x in the box = the mean, vertical lines = the whiskers (minimum and maximum value). The maximum value is only 95th percentile.

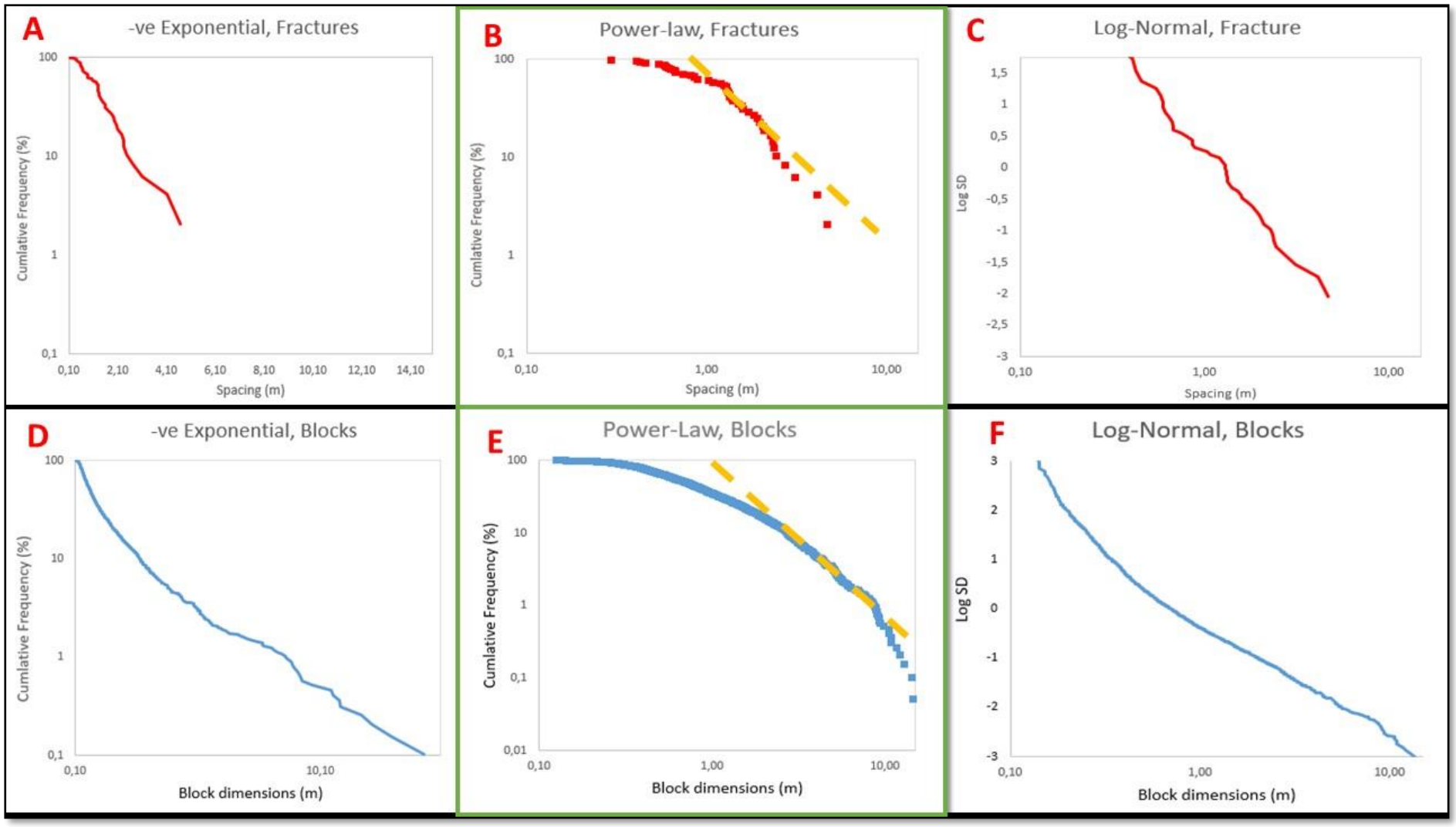

Figure 5-14: Three frequency-size plots for block dimensions and fracture spacings at Taulen; negative exponential (A,D), a power-law exponential (B,E) or log-normal distribution (C,F). The distributions with a green frame are considered the best fit distribution.

5.3 Case study 3: Mundal

5.3.1 Spatial mapping of the avalanche

The case study at Mundal consist of a NE facing steep slope with a prominent 30 m wide, 350 m deep valley that hosts a steep fan. The fan consists of coarse rock fragments, which have accumulated through gravitational processes. A total number of 13069 rocks has been digitized in this locality (figure 5-15). The rocks deposited form a fan with small variation in block sizes, where smaller rocks (0.1 – 1 m^2) dominates. Analysis of the spatial distribution of the surface blocks shows that block intensity (number of blocks per m^2) is varying throughout the fan (figure 5-16B). The red areas in the contour plot indicates high intensity areas with up to 31 blocks per m^2. The spatial distribution of the average block size shows no specific trend, but rather a uniformly distribution of small rock (green) (figure 5-16A). However, there is a small area in the NW part of the fan that shows a prominent downslope coarsening. The overall distribution of the surface indicate that water have an important impact on the fan deposits and thus explain the lack of sorting and the uniformly distribution of smaller rocks. The small area showing distal coarsening is interpreted as fall-sorting and might indicate rocks descending from the cliff.

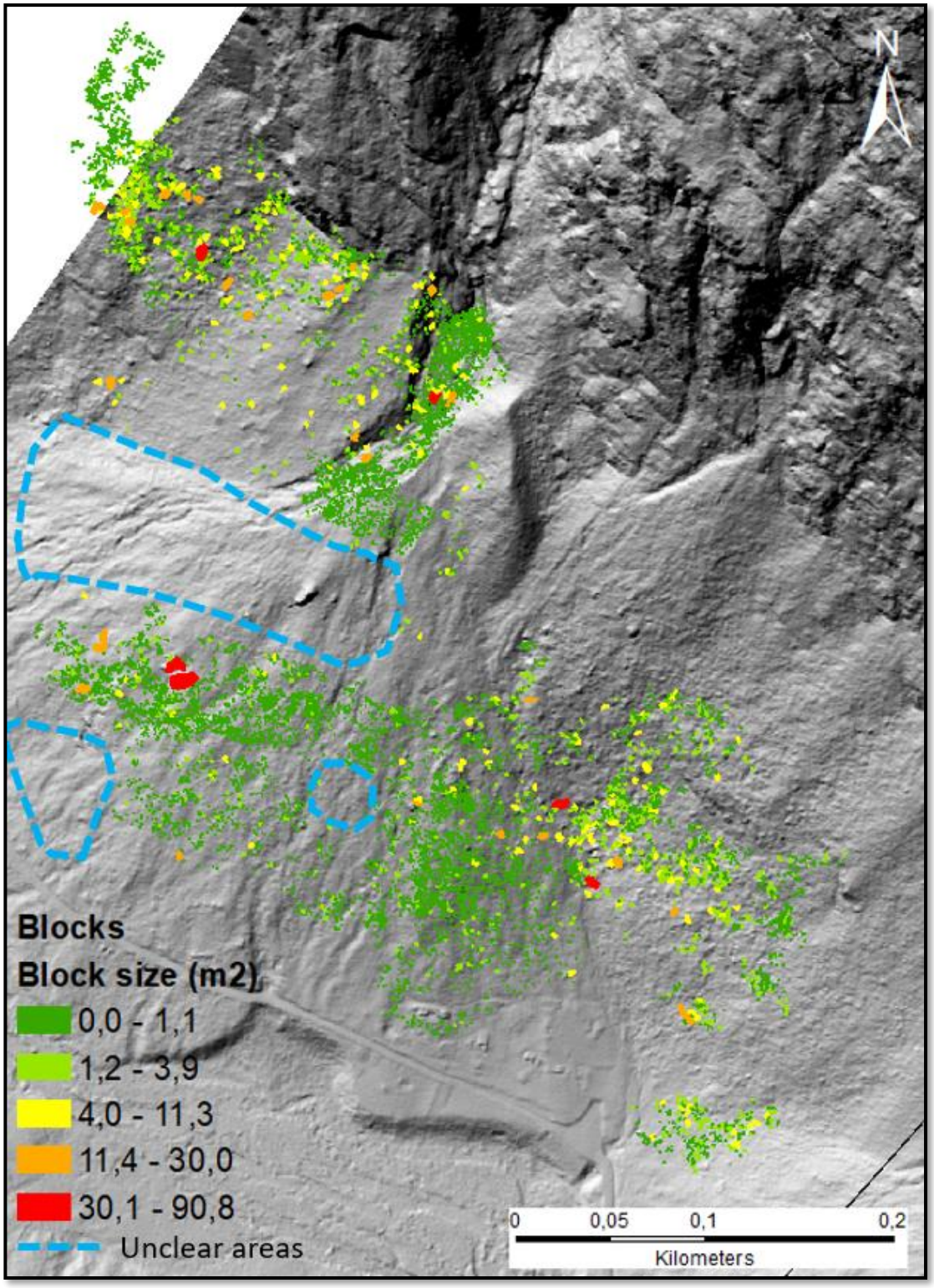

Figure 5-15: Hillshade map and all the 13069 digitized rocks. The blocks are color coded based on their size (m^2). The areas within the dotted lines are inaccessible areas du to vegetation.

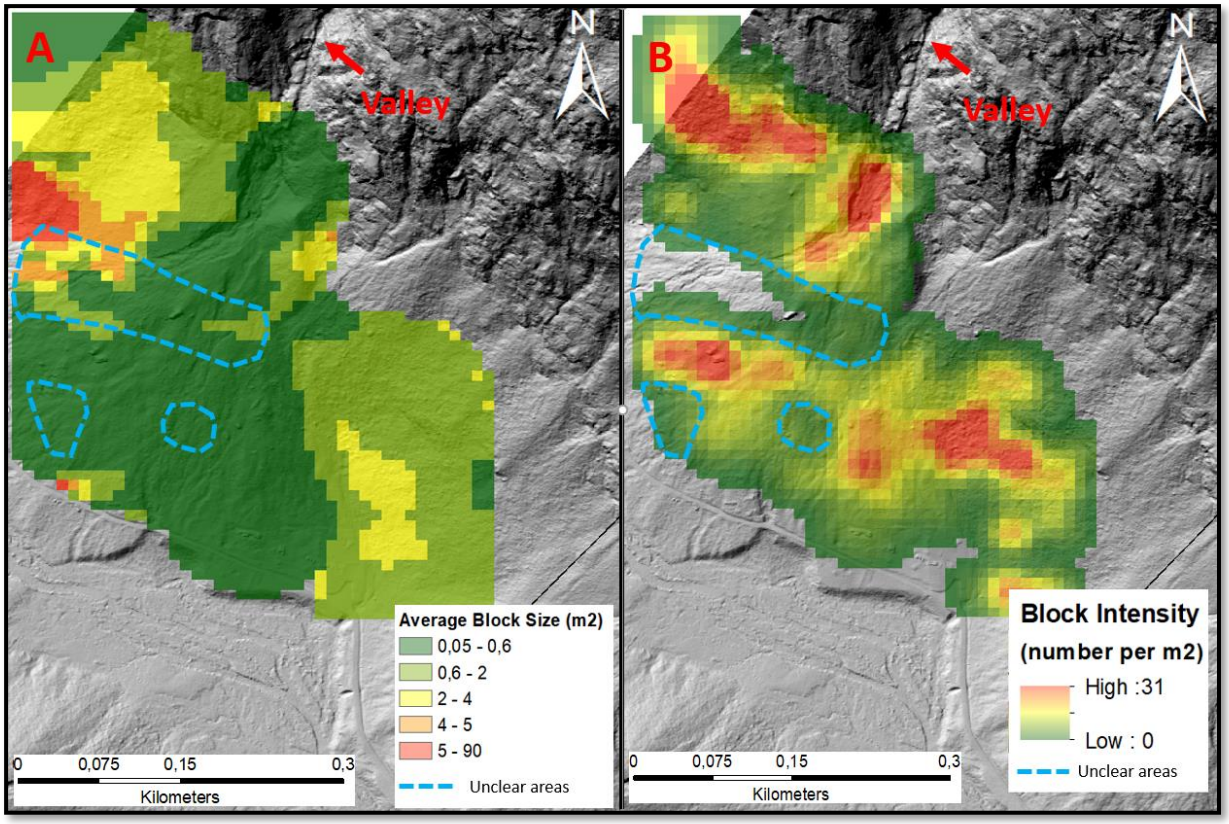

Figure 5-16: Ddistribution maps from the ArcGIS model of Mundal. A: Block size distribution (average block size per m^2) where the largest blocks = red, and the smallest = green. B: Intensity distribution (number per m^2) where: high intensity area = red, low intensity area = green. The areas within the dotted lines are inaccessible areas du to vegetation.

5.3.2 Fracture population characteristics

The fracture population at Mundal was mapped on the cliff sections and sampled using a series of line scans. The dip and strike of 37 fractures and 21 bedding planes were measured (data in appendix) and plotted in a stereonet (figure 5-17). Measured fracture orientations indicates two almost orthogonal of near vertical fracture sets, trending ~NNE-SSW and ~NW-SE. Fracture set 1 has an average trend at N195°E and a steep dip of approximately 75° towards E. Fracture set 2 has an average trend at N130°E and a dip of approximately 70° towards NE. The fractures cut through moderate dipping (~50°) bedding that strikes N40°E with a relatively consistent bed thicknesses averaging 1.9 m. The cliff itself (green plane) has an ~N-S orientation, parallel to the trend of fractures in set 1, almost perpendicular to the trend of fractures in set 2 and slightly oblique to the bedding trend (figure 5-18).

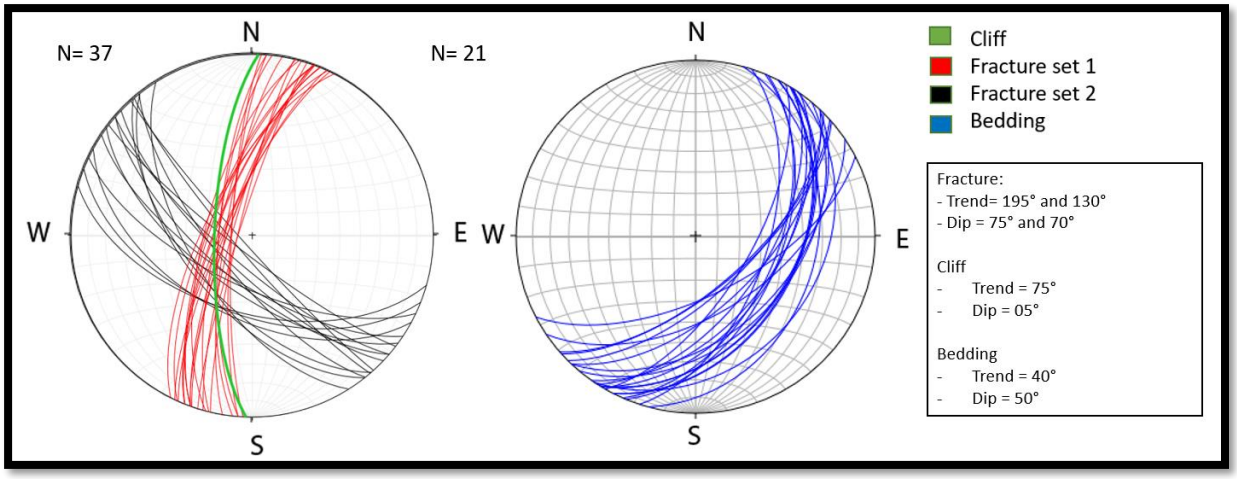

Figure 5-17: Stereonet where fractures and bedding planes are potted. The left stereonet shows fracture planes from fracture set 1 (red), fracture set 2 (black) and the cliff (green). The right stereonet shows bedding planes (blue).

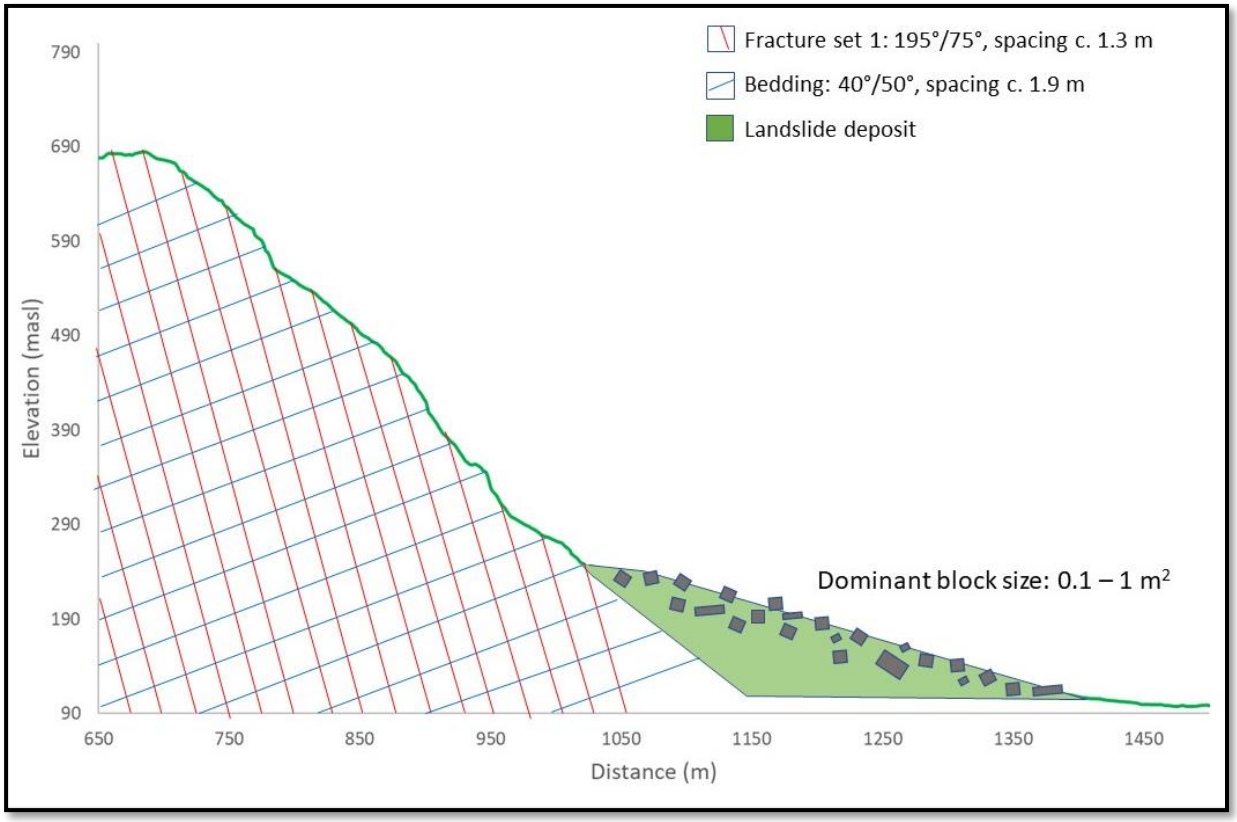

Figure 5-18: Side view of the cliff showing fracture set 1 and bedding relative to the cliff. Fracture set 2 is not illustrated as the planes are oriented parallel to the view. The figure is not to scale, but shows relative spacing of fracture and beddings, and trends in block size.

A total of 9 scan lines sample the fracture population in order to provide a spatial analysis of their frequency and spacing (e.g. Table 5-3). Fracture intensities and fracture spacing vary between scan line localities, ranging from 0.5–72.9 N/m and 1.1–4.8 m respectively. This is illustrated by the scatter of data in figure 5-19A, which compares fracture intensity against the

coefficient of variance (CV) for fracture spacing. This variation between scan line localities can be explained by differences in the resolution of the 3-D model rather spatial variations. The scan lines from the left cliff section exhibit lower intensities (~18.5 N/m) coinciding with a low image resolution (100 cm). Whereas the scan lines from the right cliff section exhibit the higher image resolutions (30 cm). Of the four scan lines, three (marked with a green) represent the scan lines with highest fracture intensities and are thus considered the best representative of the fracture population. These indicate fracture intensities of ~41.1 m^{-1} with a fracture spacing CV of ~0.9, suggesting a random fracture spacing (CV = 1) with no clustering of fractures (figure 5-18) (explained in chapter 4.2.2).

The datasets from the mid part of the cliff are further presented in figure 5-19B, which plots normalized cumulative frequency against distance along the scan line and illustrates the spatial distribution of fracturing. As the fracture frequency is proportional to the slope of the distribution, zones of higher frequency are recognized by steeper slopes. The plot shows no stair stepped curve, indicating a lack of clustering and a more regular distribution of fractures. Furthermore, the maximum departure above ($D^+ = 0.19$) and below ($D^- = -0.05$) the line is used to calculate the heterogeneity parameter ($V= |D^+| + |D^-|$), resulting in a V value of 0.2. This value is quite low indicating a uniform (homogenous) distribution, thus supports the fracture CV spacing values (CV= ~0.9).

Tabell 5-3 Corrected values for the fracture analysis of each scan line. Green areas represent the scan lines that are the most representative of the fracture population.

Scan line	Cliff side	Elevation (masl)	Resolution (cm)	Total frequency	Average fracture spacing (m)	Fracture intensity (N/m)	CV
1	Right	160	30	78.4	2.0	0.5	0.9
2	Right	200	30	72.9	1.8	72.9	0.9
3	Right	240	30	51.0	2.3	51.0	0.9
4	Right	270	100	42.3	2.9	42.3	1.0
5	Right	320	100	35.0	1.1	35.0	0.8
6	Left	200	100	12.6	4.8	12.6	1.0
7	Left	240	100	20.9	2.6	20.9	0.3
8	Left	270	100	19.8	3.8	19.8	0.6
9	Left	320	100	23.5	1.5	23.5	0.6

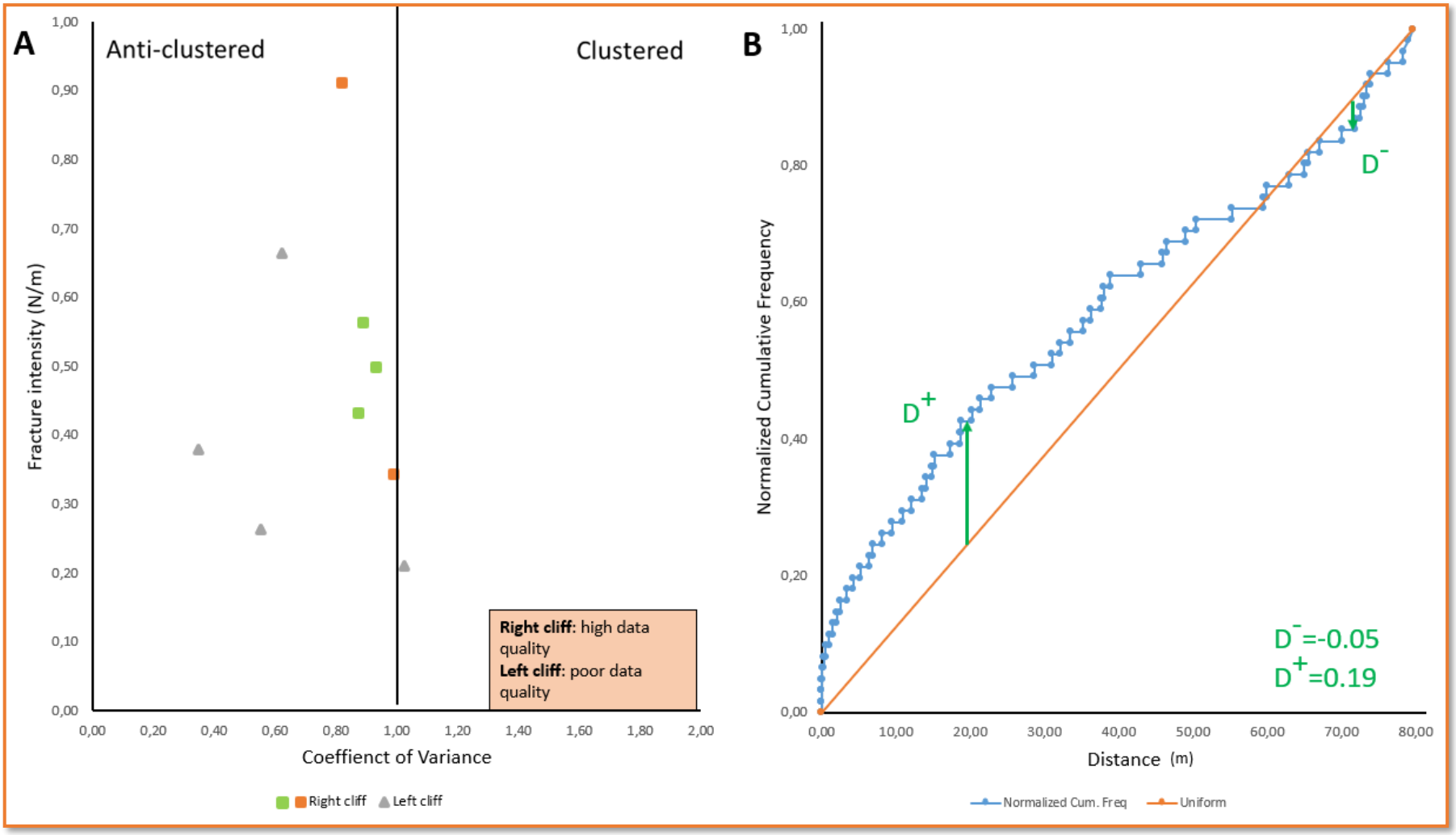

Figure 5-19: A) The intensity versus coefficient of variance plot from scan lines in Mundal. The scatter plot shows, based on the most reliable data (right cliff), that the fractures are randomly distributed (green squares). (B) Normalized cumulative frequency diagram of the most reliable data, showing a curve with no big variations in scale, thus indicate a random fracture distribution. D+ and D- represent *the maximum departure above* and below the line.

5.3.2.1 Block Size vs Fracture Spacing

The box plots in figure 5-20 compare the fracture spacing data from the mid cliff sections with the calculated block dimensions (square root of block size area) of the digitized avalanche deposits. In this case, the two datasets show no comparable data ranges or averages. The mean values (marked by X) are different with average fracture spacings of 1.3 m and average rock dimensions at 0.5 m. Thus, the rocks deposited in the avalanche fan is a lot smaller than the spacings between fractures.

Various frequency-size plots are presented in figure 5-21 for both the block dimensions and fracture spacings, where a straight line fit to the data indicates whether they conform to a negative exponential (figure 5-21A and D), a power-law (figure 5-21B and E) or log-normal distribution (figure 5-21C and F). In this case, the distribution between block dimensions and fracture spacings are different. The fracture populations appear to conform best to a log-normal distribution, while the block populations appear to conform best to power-law distribution. However, the exponents (i.e. the gradients) of the log-normal and the power-law fits are both very high, indicating that there is a limited scale range in fracture spacings and block dimensions. Thus, the mean values for the block dimensions or the fracture spacings are representative of their populations.

Overall the fracture spacings and block dimensions has different size ranges, averages and frequency-distribution. These differences can be explained by the water activity in Mundal. The main control on the block sizes is not the fracture spacings in the cliff, but rather the waters ability to transport fragments from other areas and deposit them on the avalanche fan.

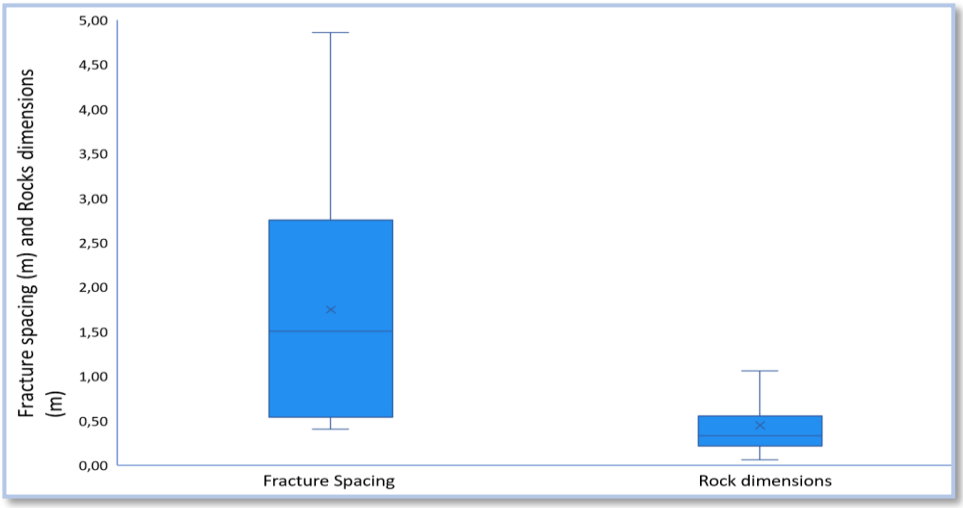

Figure 5-20: Box plot of the fracture spacings and rock dimensions form Mundal. Middle line in the = median, x in the box = the mean, vertical lines = the whiskers (minimum and maximum value). The maximum value is only 95th percentile.

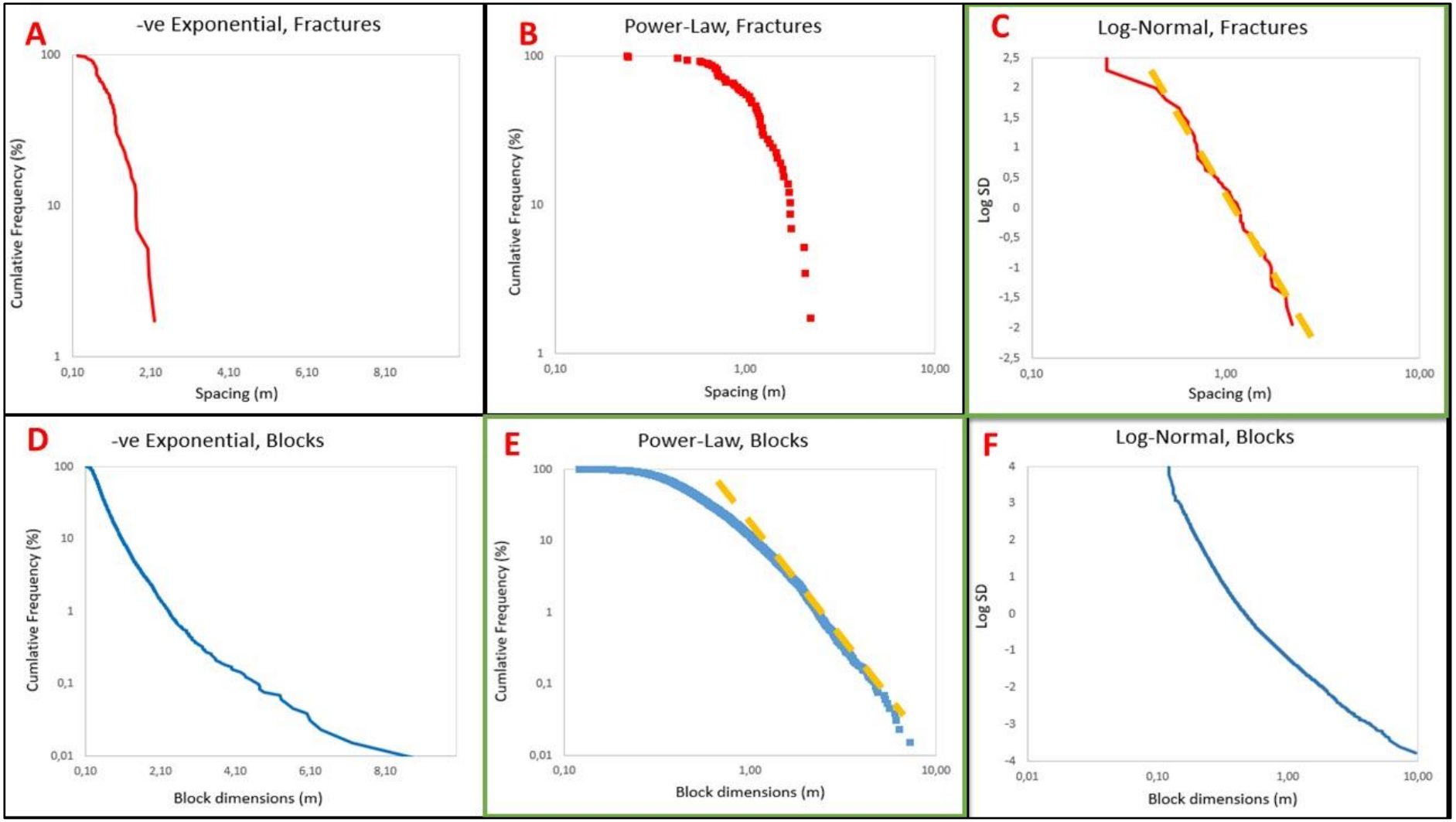

Figure 5-21: Three frequency-size plots for block dimensions and fracture spacings at Mundal; negative exponential (A,D), a power-law exponential (B,E) or log-normal distribution (C,F). The distributions with a green frame are considered the best fit distribution...

5.4 Temporal analysis of the avalanches

5.4.1 Age constraints from graveyards

In total, the dimensions of 70 lichens has been measured, 20 green lichens, 25 white lichens and 25 gray lichens, on 30 different gravestones (data in appendix). Eight representative gravestones, that has been investigated, showing coverage with increasing age are presented in figure 5-22A. The coverage measurements plotted in the graph in figure 5-22B is based on an approximate values and observations done in the field. The coverage values in the age span between 10 and 40 years show a great variation, where some rocks, after 20-30 years, have 90-100 % coverage, while others have only 20-30 % coverage. These various results can be due to many factors such as sunlight, shadow, rock type, visual investigation, cleaning of gravestones etc. Accordingly, this plot should only be used to tell if the rock is younger than 10 years (>2% cover) or older than 40 years (80-100% cover), and in combination with other dating methods.

All the lichen measurements are presented in scattered charts showing year vs lichen diameter. As illustrated in figure 5-23 the lichen growth rate in Bergen between granite, granitic gneiss and gneiss was very similar, resulting in one graph showing the measurements independent of rock types. This was also done for the results from Voss, as the same observations was seen in the measurements from Oppheim kyrkje. Further, when comparing the results from Voss and Bergen, there were no significant difference between the growth patterns of the lichens (figure 5-24A and B). Consequently, the measurements from Bergen and Voss was pooled, resulting in one plot for each lichen, showing years vs lichen diameters (figure 5-25, 5-26 and 5-27). These plots were further developed by plotting an estimated trendline, and boxes showing the approximate lichen size within different time intervals. The trendlines are based on the largest lichen measured as the measurements of the diameter on the largest lichen gives the minimum age of the rock. The amount of data in these plots are limited and should therefore only be used for a qualitative dating purpose. However, there is a clear overall trend in each plot, thus the trendlines are considered to be reasonable.

Moreover, by combining lichenometry plots, the coverage measurements plots and a vegetative analysis, a quantitative estimation of rock ages in the field can be acquired and thus an analysis of the avalanche potential.

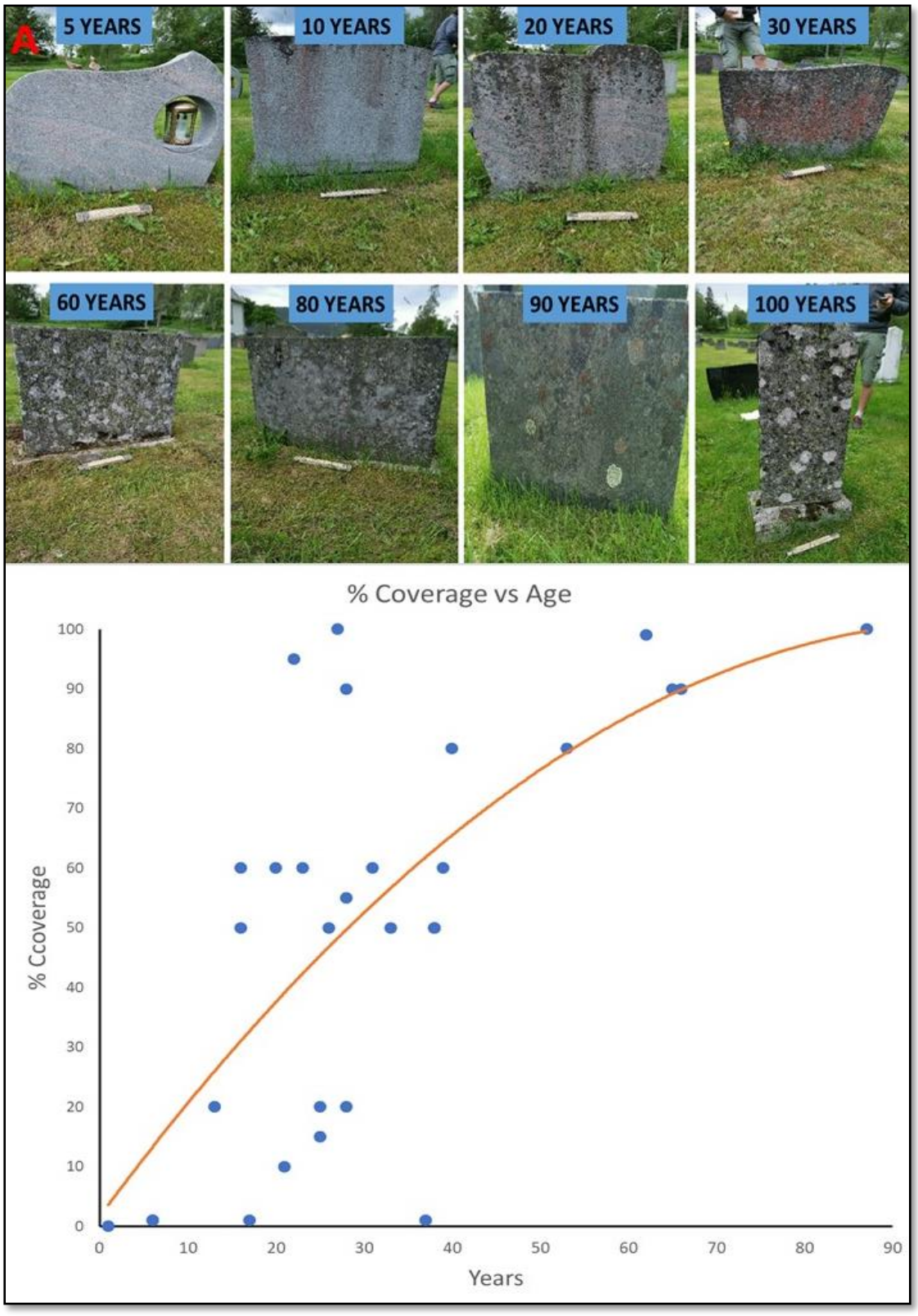

Figure 5-22: A) Backside of gravestones investigated with different ages showing increase in lichen cover. B) A graph showing coverage (%) vs age, based on observation in the field.

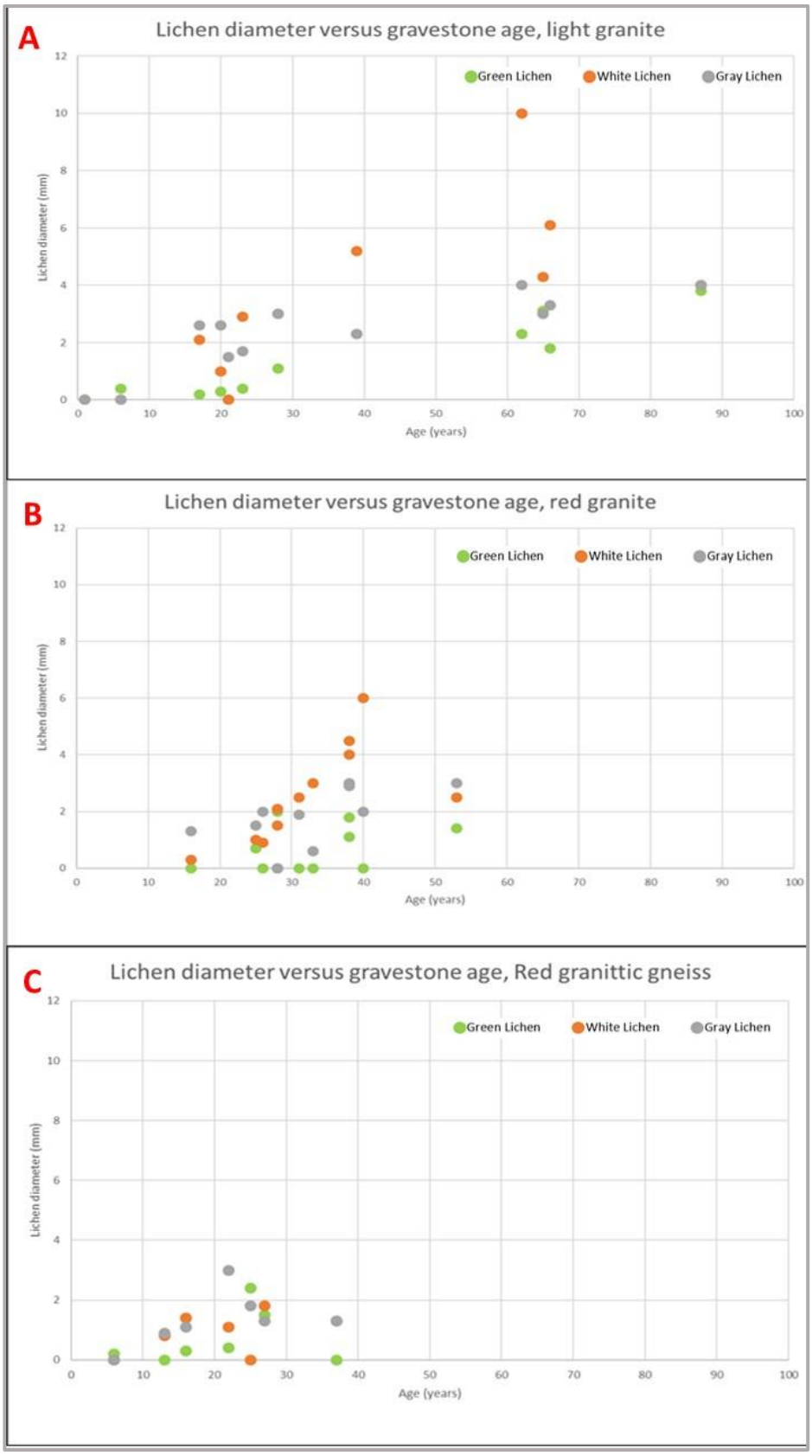

Figure 5-23: Rock dependent charts of lichen measurement from Bergen showing diameter vs age. From top to bottom; light granite, red granite and red granittic gneis

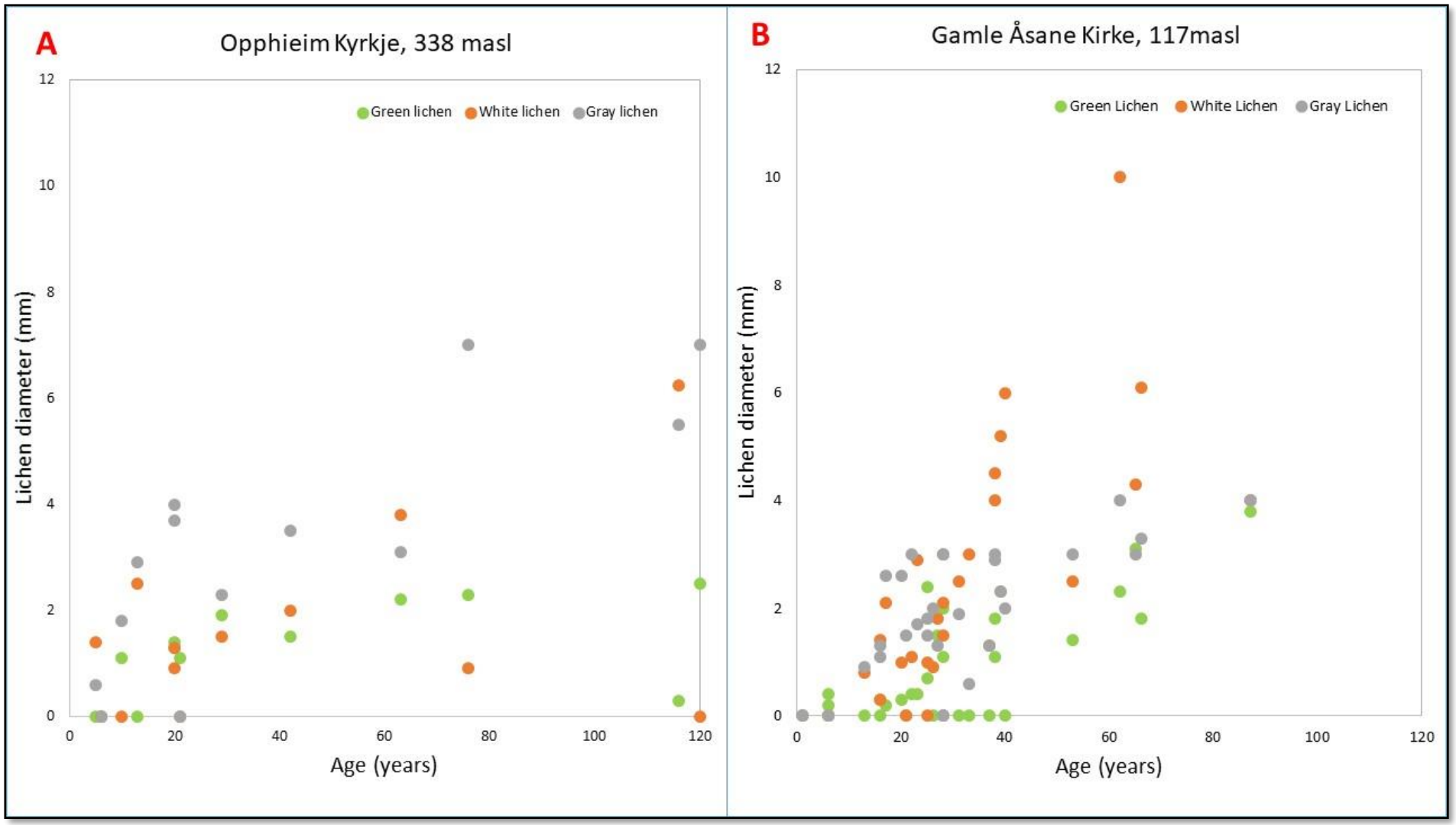

Figure 5-24: Lichen measurements plot independent of the rock type for (A) Oppheim Kyrkje and (B) Åsane Gamle kyrkje.

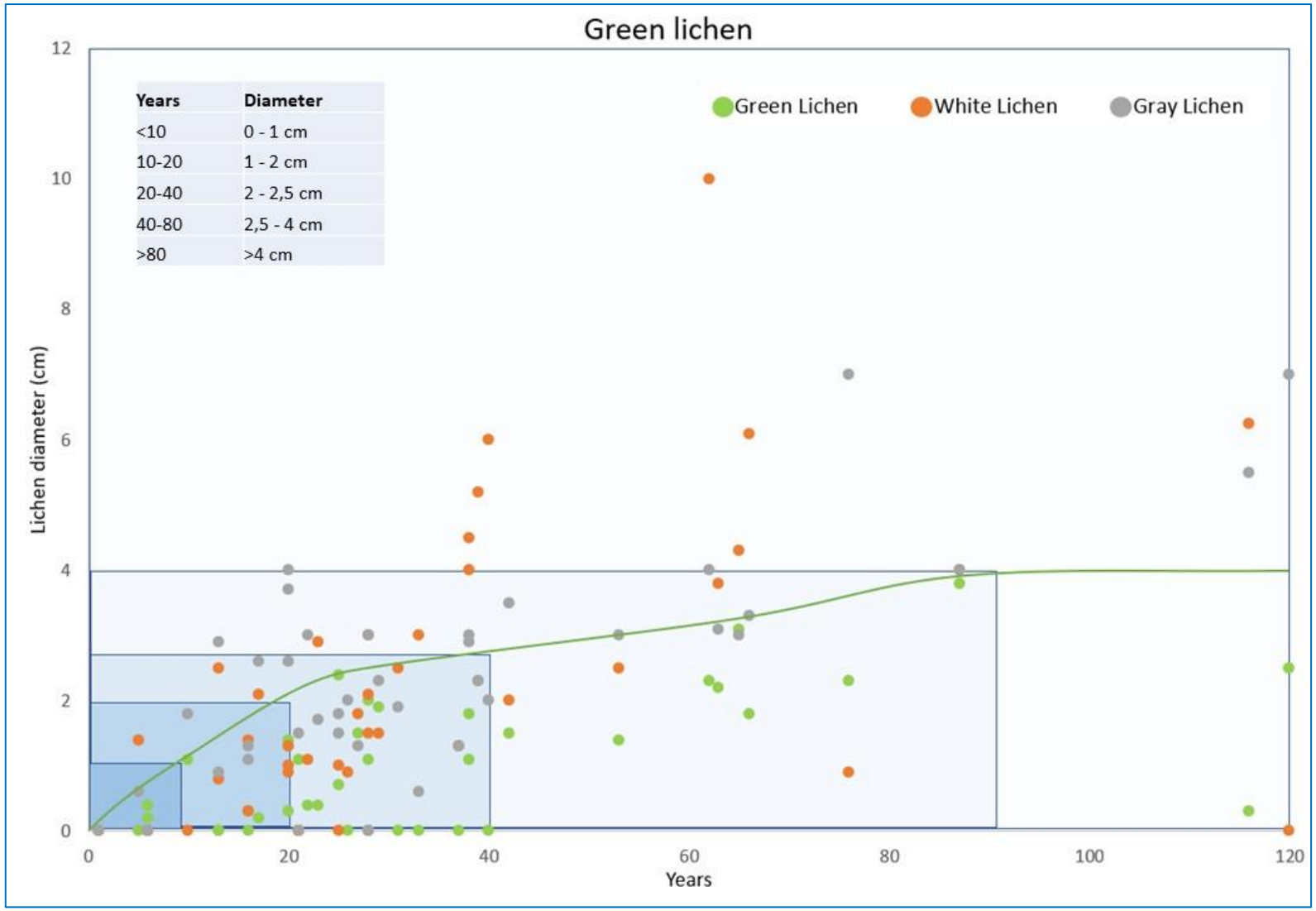

Figure 5-25: Result from lichen measurements done on green lichen from Oppheim kyrkje and Åsane gamle kyrkje, showing lichen diameter vs years. Each color box represents lichen size within different age intervals. Green line represents envelope of largest lichen of green lichen type at a certain age, excluding outliers.

Figure 5-26:Result from lichen measurements done on gray lichen from Oppheim kyrkje and Åsane gamle kyrkje, showing lichen diameter vs years. Each color box represents lichen size within different age intervals. Grey line represents envelope of largest lichen of grey lichen type at a certain age, excluding outliers.

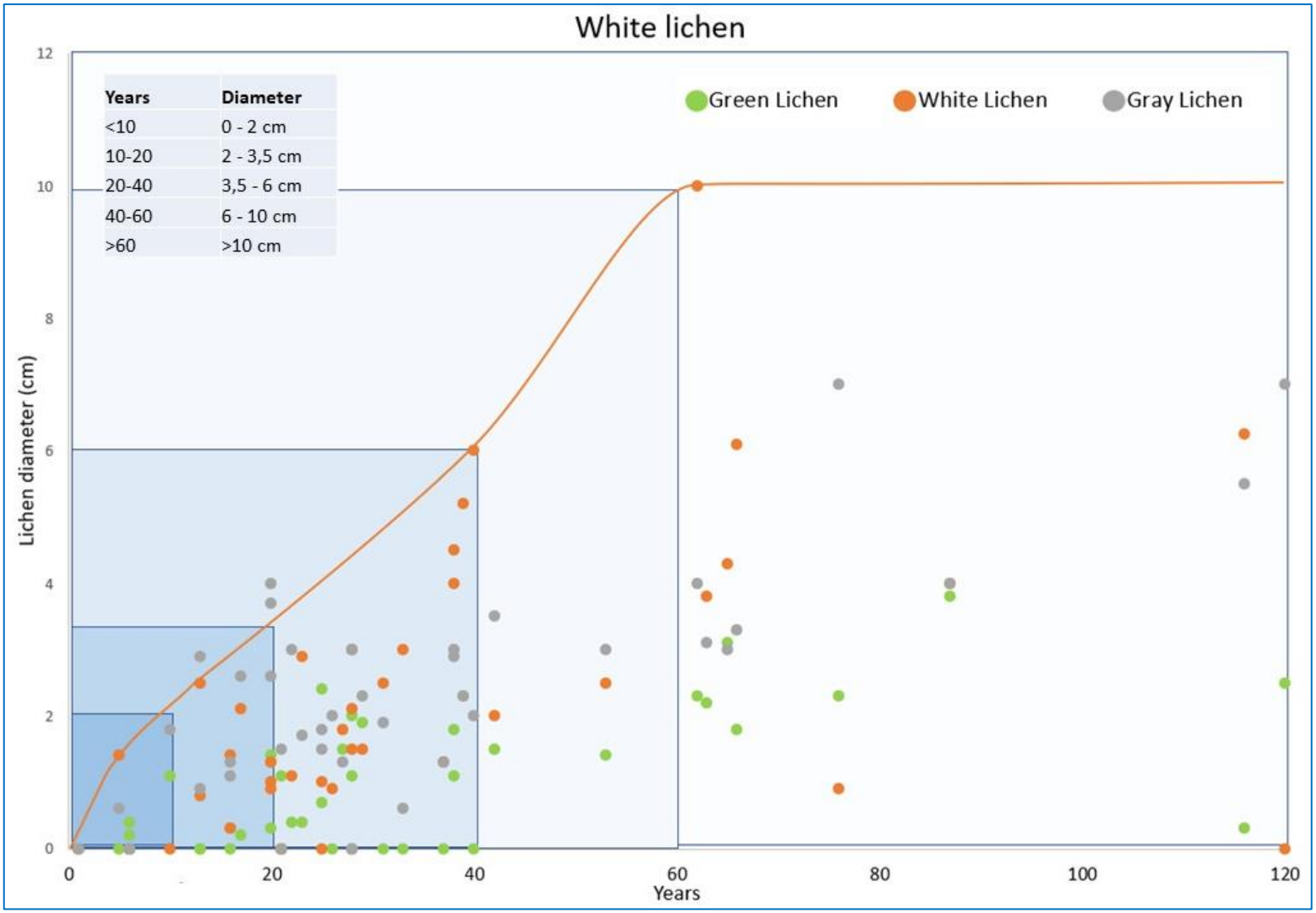

Figure 5-27:Result from lichen measurements done on white lichen from Oppheim kyrkje and Åsane gamle kyrkje showing lichen diameter vs years. Each color box represents lichen size within different age intervals. Orange line represents envelope of largest lichen of white lichen type at a certain age, excluding outliers.

As illustrated in the three plots above (figure 5-25, 5-26, 5-27), every lichen has a different growth pattern. The green lichen is, overall, the slowest grower. During the first 10 years it has its maximum diameter at 1 cm. This growth is close to linear until 20 years where it starts to decrease. After 90 years the growth stabilizes. Thus, if a green lichen is larger than 4 cm it is probably older than 90 years (figure 5-25). The growth rate for the white and gray lichen are quite similar the first 20 years, where the gray lichen has a diameter at 4 cm and the white a diameter at 3.5 cm. At this point the growth rate for the gray lichen gradually decrease until it stabilizes after 80 years. Accordingly, a gray lichen larger than 7 cm it is probably older than 80 years (figure 5-26). Unlike the gray lichen, the white lichen increases its growth rate after 20 years. This trend continues until it stabilizes after 60 years, reaching a diameter of 10 cm (figure 5-27).

This subchapter only investigates the observed trends in lichen diameter versus age. The validity of these observations, to which degree they can be trusted, and how they can be used, will be discussed in subchapter 6.1.

5.4.2 Colonization of vegetation

As described in chapter 2.5, the colonization of a rock can be divided into three successional stages. Each of these stages are dominated by a different species assemblage, suggesting directional replacement of species in the succession (Irene et.al 2011). The first stage, called the pioneer stage, is dominated by lichens. After about 50-80 years the development of a moss matt marks the transition from the pioneer to the second stage, called the mid-successional stage. Throughout this stage the moss matt expands and after about 140 years forms an almost continuous, thick (ca 15 cm) matt. The last stage, called the late-successional stage, is characterized by the development of vascular plants (Irene et.al 2011). Table 5-4 gives a short summary of expected development of lichens, moss matts and vascular plants within different time intervals.

Tabell 5-4 Colonization of a rock divided into three stages with estimated ages. First, lichen development, followed by moss and at last, development of vascular plants

Plants		Year	Cm
Lichen	Green lichen	<10	0 – 1 (Diameter)
		10-20	1 – 2 (Diameter)
		20-40	2 – 2,5 (Diameter)
		40-80	2,5 – 4 (Diameter)
		>60	>4 (Diameter)
	Gray lichen	<10	0 – 2 (Diameter)
		10-20	2 – 4 (Diameter)
		20-40	4 – 5 (Diameter)
		40-80	5 – 7 (Diameter)
		>80	>7 (Diameter)
	White lichen	<10	0 – 2 (Diameter)
		10-20	2 – 3,5 (Diameter)
		20-40	3,5 – 6 (Diameter)
		40-60	6 – 10 (Diameter)
		>60	>10 (Diameter)
Moss matt		50-80	Appearance of moss
		80-110	1-15 (thickness)
		>110	>15 (thickness)
		140	Continuous moss mat
Vascular plants		>140	Start developing

5.5 Field observation

5.5.1 Field work in Vinddal

Before conducting fieldwork, a map, showing areas that needed and should be investigated, was created and brought. In addition, an outcrop of the 3-D model created in ArcGIS, showing the avalanche area, was used to keep track of where different measurements and observations were conducted during the field work. This resulted in the map, shown in figure 5-28, where the letters A-F illustrate areas where detailed observations and measurements were conducted. Further, at each pitstop, pictures were taken as shown in figure 5-29, where the letter on each picture (A-F) correspond with the letters in figure 5-28.

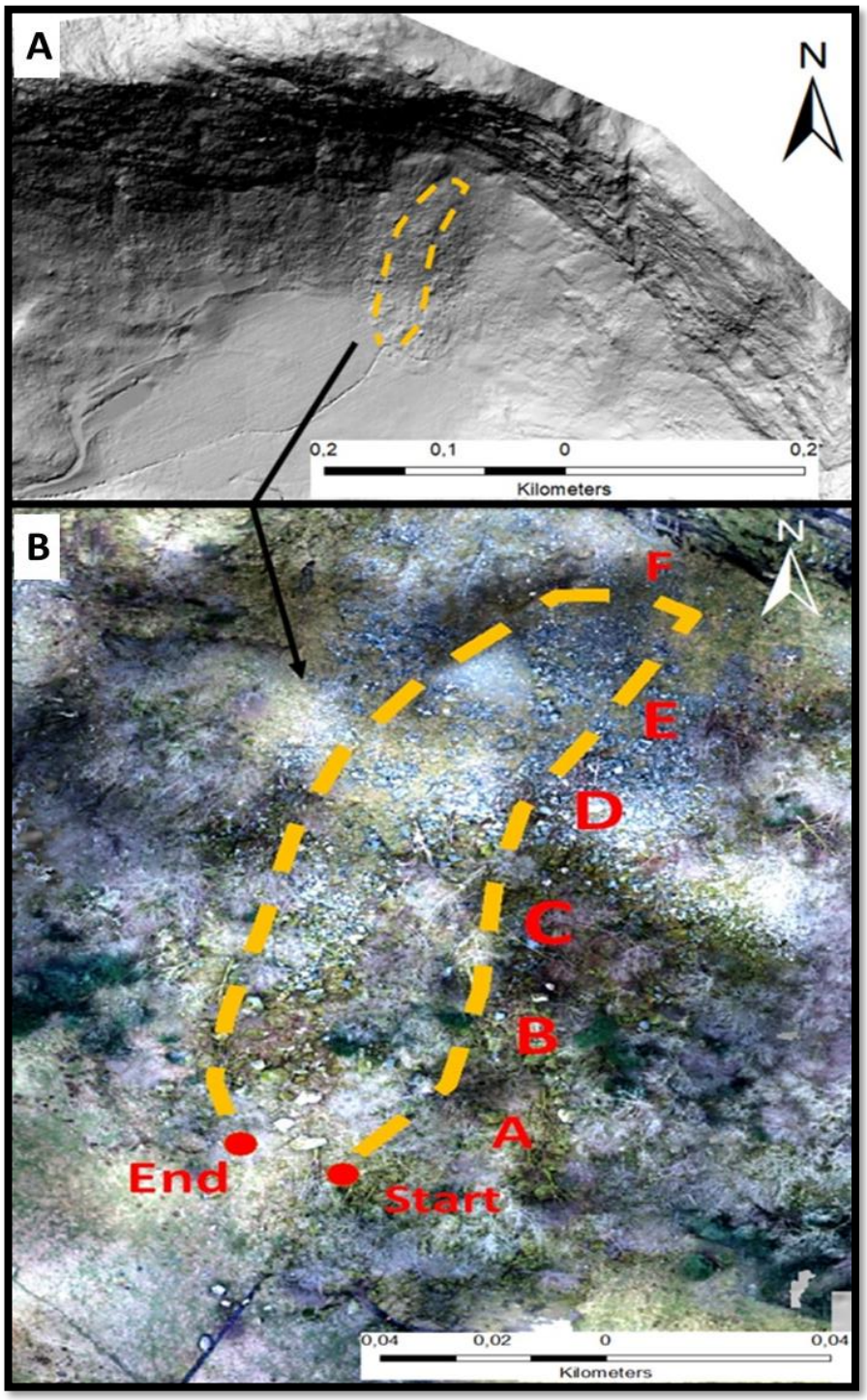

Figure 5-28: A) A hillshade map and B) an orthomosaic map showing the field work route from Vinddal. The letters A-F represent some of the stops where closer investigation was conducted. For each letter a picture from the stop is shown in figure 5-29.

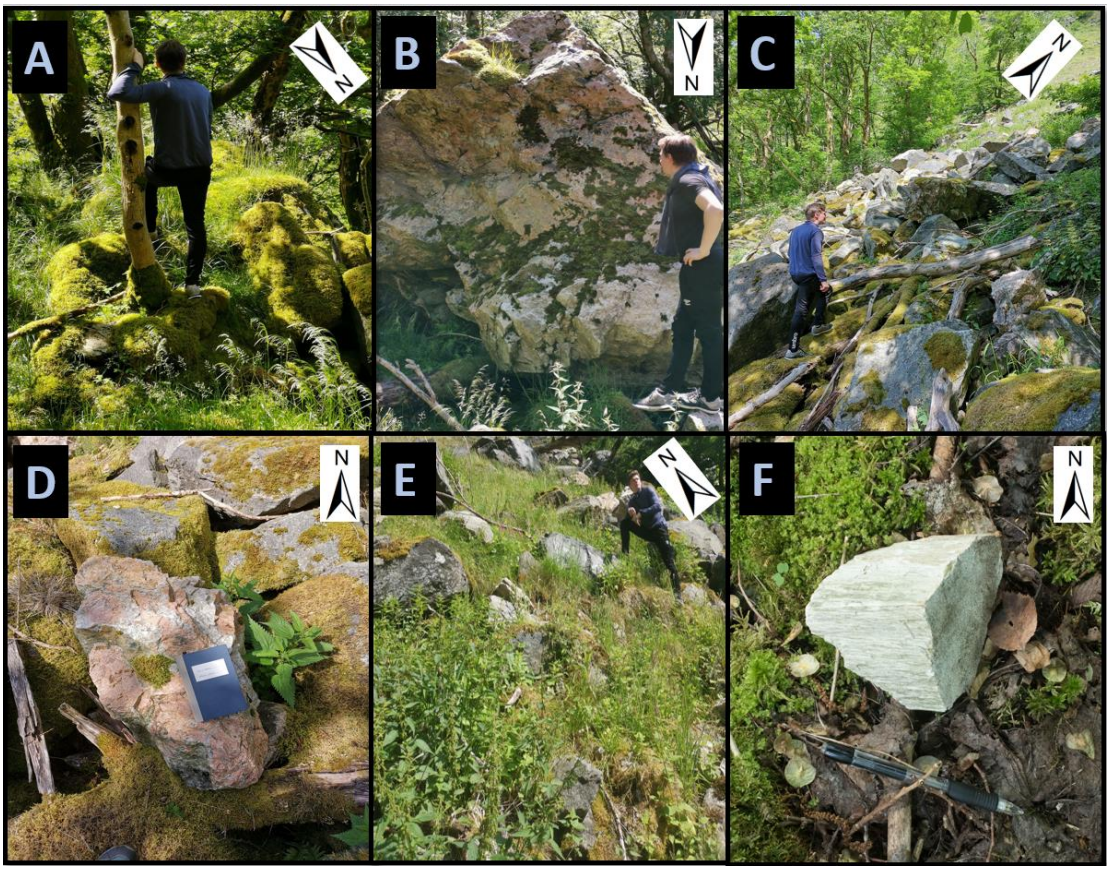

Figure 5-29 :Field work in Vinddal. (A) Large block with vascular plants growing on top it, (B) Block with spots of moss and lichen, (C) Several fresher looking rocks and broken trees, (D) Fresh rock origination from the vain (diorite/trondhjemite), (E) close to the cliff: decrease in amount of rocks and increase in vegetation, (F) Fresh rock without lichen or moss. The location where each picture was taken is illustrated in figure 5-28.

In the distal and middle part of the fan (A and B in figure 5-28) medium to large (0.25 m^2 – >4 m^2) sized blocks covered by continuous moss matts with an average thickness of 7 cm, was dominating. Three large blocks between 50 m^2 – 100 m^2 (10x5 m – 10x10 m) were observed with approximately 4-meter-high trees growing on them (figure 5-29A). Additionally, a few fresher looking medium to large (0.25 m^2 – >4 m^2) sized blocks were observed (figure 5-29B). These rocks contained small spots of moss with an average thickness of 1.2 cm and green lichen with a 4.0 cm diameter. Overall, the rocks in this part of the fan can be dated at least 140 years back. The fresher looking rocks indicating an age estimate at 50-80 years, thus in the transition from the pioneer stage to the mid-successional stage.

In the middle part of the cliff (C and D in figure 5-28), the amount of fresher looking rocks, dominated by white (8 cm), green (2-3 cm) and gray (1 cm) lichens, increased (figure 5-29C). Still, there were a few rocks covered with continuous moss matt at about 1-5 cm, present. The variety of rocks sizes (0.25 – 15 m^2) and rock types also increased, and rocks originating from the prominent "vein" of diorite/trondhjemite (figure 3-5), became more frequent (figure 5-29D).

According to the lichenometry result (chapter 5.4.1), the age of the dominating fresher rocks is in the range of 5-60 years. The moss-covered rocks are estimated to be in the age range of 60-80 years. The increased present of diorite/trondhjemite rocks, may indicate that the margin of this vein is a weakness zone in the cliff.

At the apex of the fan, closest to the cliff (location E and F in figure 5-28), the rock size and amount of rocks decreased and vegetation (grass, plants and ferns) increase (figure 5-29E). Fresher looking small to medium (1 cm^2 – 1 m^2) sized rocks dominated. Some was without any lichen or moss (figure 5-29F), and some with green (1 cm), white (2-4 cm) and gray (1) lichen growing on them. Additionally, some rocks with green vegetation underneath was observed. The appearance of moss-covered rocks had in this part decreased, but were still present. Overall, the decrease in size and amount of rocks provides better growth conditions, thus explain the increase in vegetation. The dominant fresher looking rocks has, based on the lichenometry study (chapter 5.4.1), an estimated age of 5-20 years. The green vegetation underneath some rocks, indicate activity the last 1-2 years.

Along the avalanche track (A - F in figure 5-28), among all the rocks, vegetation, such as plants, bushes and a few trees, were present. In addition, several broken trees lied on the ground (figure 5-29C). All of them was either completely rotten or covered in moss, indicating that these trees most likely broke during a period of high activity for at least 140 year ago.

As a summary, the general age of rocks increases from the apex to the distal part of the fan. Based on the variation in the rock ages, one can assume that the area has been exposed to several rockfalls and rockslides for a much more than 140 years. For the last 60 years the largest avalanche events (where 30 – 125 m^3 large blocks descend), with runout distance to the distal part of the fan, has probably been absent, and thus explains the present of vegetation along avalanche track. However, based on the small to medium sized fresher looking rocks observed from location C to F in figure 5-28, there is reason to believe that smaller events, such as rockfalls (where <0.25 m^3 sized rocks descend), younger than 10 years has happened (maybe even younger than 1 year). This is probably an area that might still be active, and to assume that smaller rockfalls still frequently happens, is likely.

5.5.2 Fieldwork in Taulen

Like the field trip in Vinddal, a map showing areas that needed and should be investigated was created and brought. Also, an outcrop of the 3-D model created in ArcGIS, showing the avalanche area, was brought to keep track of where detailed measurements and observations were conducted during the field work. In the resulting map (figure 5-30), areas marked by the letters A-F illustrate where the different observations and measurements were conducted. Further, at each pitstop, pictures were taken and are shown in figure 5-31, where the letter on each picture (A-F) correspond with the letters in figure 5-30.

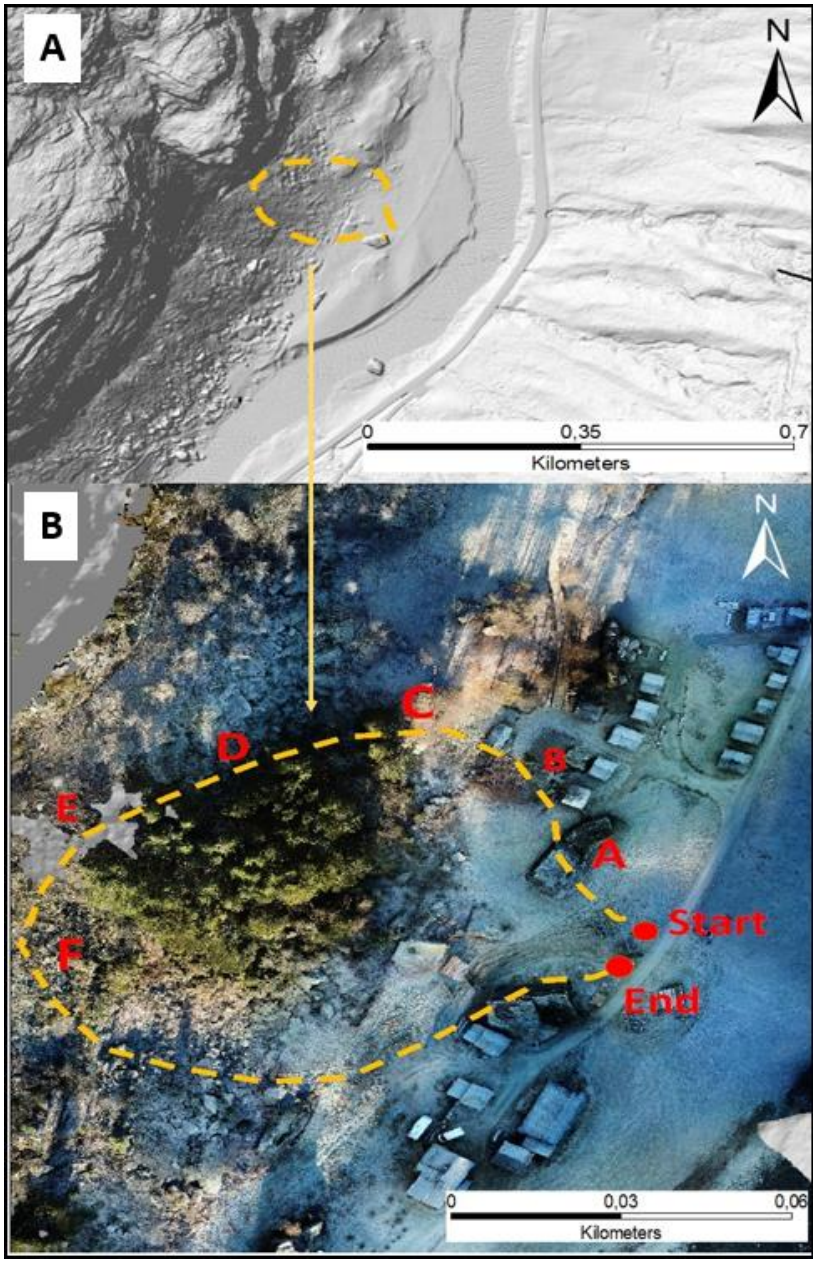

Figure 5-30: A) A hillshade map and B) an orthomosaic map showing the field work route from Taulen. The letters A-F represent some of the stops where closer investigation was conducted. For each letter a picture from the stop is shown in figure 5-31.

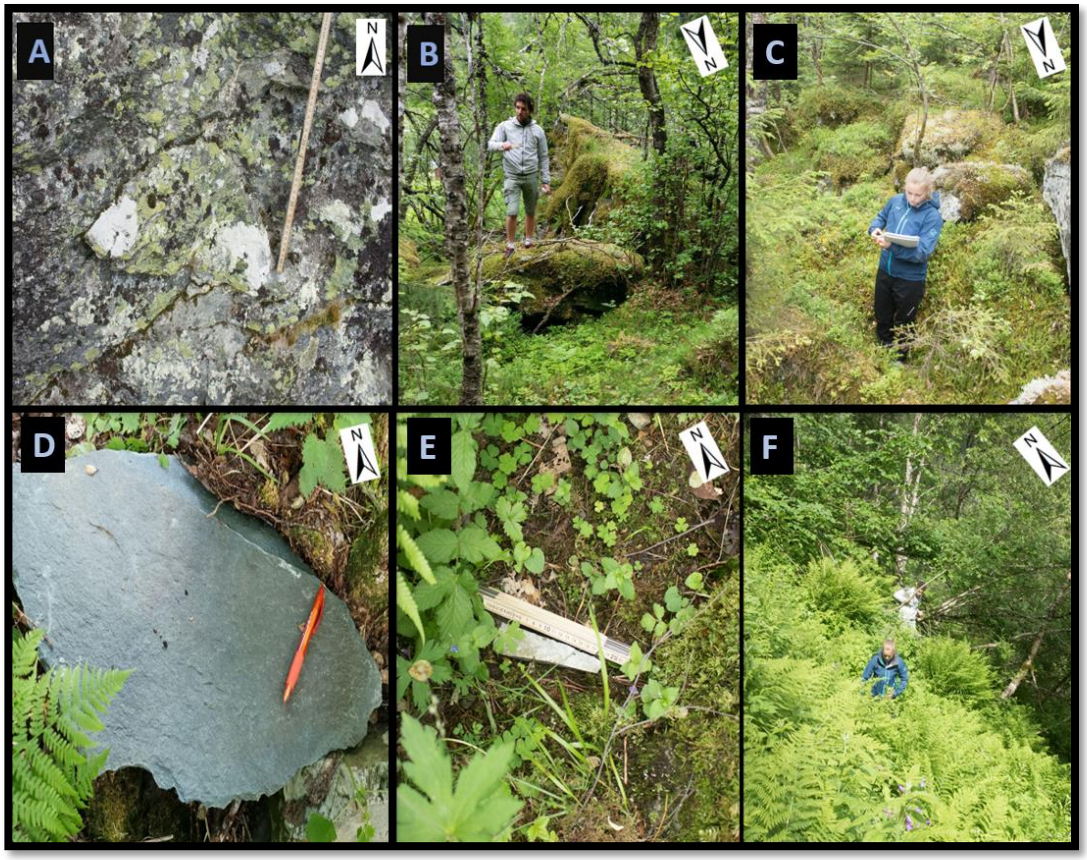

Figure 5-31: (A) Moss covered rocks, (B) High diversity and lichens between 17-20 cm, (C) Ground covered by moss covered rocks, (D)Fresh rock with no lichen or moss development, (E) Fresh rock with green underneath, (F) In general, a great amount of vegetation in the avalanche area. The location where each picture was taken is illustrated in figure 5-30.

In the distal part of the fan (A and B in figure 5-30), medium to large ($2m^2$ - $>4m^2$) blocks covered by a continuous thick moss matt at about 5-10 cm, were dominating (figure 5-31B). On rocks not covered by moss, 17-20 cm large lichens dominated the rock surface (~90% coverage) (figure 5-31A). These observations suggest an age estimate of over 140 years for moss covered rocks, and over 60 years for lichen covered rocks.

In the middle and upper part of the cliff (C, D, E and F in figure 5-30), the terrain was steep, and rock density increased. The ground was covered by small to medium ($0.25\ m^2 – 4\ m^2$) sized rocks. Most of the rocks in location C was covered by a continuous moss matt of ~7 cm (figure 5-31C), while in location D the rocks only had spots of moss on them. There were also observed a few fresh-looking rocks with no development of lichen or moss (figure 5-31D). Closest to the cliff, at location E and F in figure 5-30, fresh rocks with green vegetation underneath was observed (figure 5-31E). Accordingly, the mid and upper fan contains rocks with a high variety of ages, ranging from moss cover rocks estimated to over 140 years, rocks with spots of moss estimated to be 60-80 years, and fresh rocks estimated to be 1-10 years.

Overall, there were a great amount of vegetation covering all parts of the fan, where a thick layer of bushes, ferns, trees and plants dominated (figure 5-31F). Some of the trees were bent, but without any scars from a falling rock. Thus, makes it difficult to determine if the trees has been bent as result of dominating wind direction, soil creep or a major rockfall event several years ago. The large amount of vegetation in the avalanche track indicated that it is probably over 140 years since the last large rockslide event (where 30 – 125 m^3 large blocks descend).

Based on the above, there is a general increase in rock ages down the slope. The significant variation in the degree of vegetative colonization on the rocks leads to the assumption that several rockfalls and rockslides events has happened for more than 140 years. The vascular plants and large trees present in the avalanche track has had a long time to grow, indicating that the last major rockslide event (where 30 – 125 m^3 large blocks descend) happened for much more than 140 years ago. The fresher looking rocks, located in the middle and upper part of the fan, indicate that small to medium avalanche event, such as rockfalls or rockslide (where <0.25 - 8 m^3 large blocks descend), has happened for less than 60 years, maybe even the last years. If that is the case, the vegetation and trees has probably limited the run-out distances. Though, some uncertainties are still valid as the vegetation and the rough steep terrain made it difficult to access certain part of the fan.

6 Discussion

The goal of this study was to evaluate a workflow using photogrammetric models acquired using a drone, field investigation and lichenometry to investigate the avalanche potential in three different areas. Based on experience and the results from this study, three aspect of this workflow will be discussed.

6.1 Validity of age assessment data to study avalanche frequency and activity

In order to estimate avalanche frequency and activity in the three studied areas, field investigations, including lichenometry and a vegetative analysis, was conducted. The main purpose was to understand the size, frequency and runout distance of rockfalls or rockslides, in an avalanche prone area. Close to the cliff, fresh rock fragments indicate recent smaller rockfall events, but do not pose a high risk, while large fresh blocks observed far from the cliff indicate a recent large rockslide and poses a high risk. The goal of this investigation is then to estimate how often these small to large avalanche events happen, within time intervals of once every tenth, fiftieth or hounded year. Thus, the age estimates of rocks only have to be grouped in ages of 1, 10, 50, 60, 100, 140 and >140 years. The validity of this method, using lichenometry and vegetative analysis to study avalanche frequency and activity, will be further discussed.

The lichenometry was completed by measuring the largest lichen diameter on rock surfaces with known ages, in this case gravestones, in order to create a graph showing lichen diameter vs age. The resulting three plots automatically contains three important advantages: 1) they automatically include colonization time, 2) the effect of the regional climatic change is accounted for, and 3) it can be prepared in a single field season (James, 2009). However, there are some sources of error that might affect the resulting plots and must be considered when conducting a lichenometry study.

Firstly, there are great uncertainty related to if and when the gravestones were cleaned. Secondly, lichens are sensitive to climate, where factors, such as day length, snow cover, precipitation and air temperature, can affect the growth rate. Consequently, growth curves that has been developed in one area will not necessarily be valid in other areas (Walker, 2005).

Another issue is related to the importance of identifying and recognizing different types of lichens. As illustrated in the lichenometry results, the growth rate differs depending on lichen type, thus the calibrated growth curves must also distinguish between different lichen types (Walker, 2005). Accordingly, it is important to be able to identify lichens and be consistent on

which types of lichens that are used throughout the study. However, this can be problematic because lichens are normally microscopic, thus can only be distinguished chemically. An example is the *Aspicilia cinereal* (the gray lichen), investigated in this thesis, which can only be reliably differentiated from *A. caesiocinerea* based on their chemical reaction with potash lye *(*Jochimsen, 1973).

According to Ten (1977), another source of error worth considering is competition among lichens. Certain species dominate others, and the weakest growing lichen will be overgrown and sacrificed in favor for the dominant lichen. This is particularly relevant for lichens growing on gravestones, because on smaller surfaces, less space is available, and thus the competition increases (Ten, 1977). Consequently, there are uncertainties related to the validity of correlation between a graveyard and an avalanche area, due to great differences in both amount of vegetation and size of exposed surfaces. An example is the avalanche area in Taulen compared to the graveyard at Oppheim kyrkje. Taulen has a wide variety of vegetation where vascular plants, trees, moss and lichens are all competing for nutrient and space. The gravestones at Oppheim kyrkje, on the other hand, are placed in an open area without any free growing vegetation except for lichens.

Complimentary to the lichenometry, vegetative analysis, where observations such as fallen or bent trees, scars or damages, vegetation beneath rocks (fresh or rotten), is used to estimate how long a rock has been exposed to the surface. The age estimates are based on the study done on rocky environments in south Africa, by Irene et.al (2011). Accordingly, the climate conditions are quite different, and thus using these results to estimate ages in western Norway can be questioned. Accordingly, an examine of the literature and see if such work has been done in the western country should be done.

Furthermore, as the lichenometry and the vegetative analysis are performed in an avalanche area, one important factor has to be considered. Both, the vegetative analysis and the lichenometry provide a minimum value of how long the rock has been exposed to the surface, assumed that the rock surface has been immobile and undisturbed. In an avalanche area, this is not always the case, due to a constant risk of new avalanches. Hence, the lichen- and vegetation growth may be terminated or interrupted by sudden slope movements or an impact that can break off parts of a rock already deposited, making a fresh surface. Accordingly, it is important to be selective when choosing rocks and rock surfaces to be investigate in the field.

Based on these uncertainties discussed above, the age assessment can contain some errors.

The resulting lichen plots do not differ between measurement from Voss and Bergen, due to comparable results (figure 5-25, 5-26, 4-27). Thus, there might be an issue related to climate sensitive lichens. As illustrated in table 3-1 and 3-2, the climate in Bergen and Voss is different, where it is an average annual temperature difference at 2.4°, a precipitation difference at 1300 mm (Hanssen-Bauer et al., 2015), and an elevation difference of 222 masl. However, the climate in Voss and Bergen also has several common features, such as amount of sunshine, bedrock and a general wet climate. Whether the climate between Voss and Bergen is comparable enough that the measurements can be pooled and presented in the same lichen diameter vs age plots is uncertain. Accordingly, the following measures should be done; 1) examine the literature and see if such work has already been done, and 2) make more measurements at several burial sites around the western country.

Furthermore, the data set in the lichenometry plots is largest for ages younger than 40 years and shows a clear trend for all of the three lichens. Measurements of age older than 40 years, has fewer data points, but nevertheless a clear trend for the gray and green lichen continues. The measurements of the white lichen, on the other hand, show a more scattered result after 40 years. These scattered results can be due to the many uncertainties mentioned above, such as wrong identification, environmental conditions, cleaning of gravestones etc. In order to increase validity, a larger dataset is needed, especially for older gravestones.

Nevertheless, by complimenting the lichenometry results with the vegetative analysis, several factors were considered. For rocks older than 40, other age indications where useful, such as moss and the surrounding vegetation. After 60, the lichens were often overgrown by moss, thus the vegetative analysis became more beneficial. Accordingly, lichenometry provided a great tool for estimating rock ages younger than 60, and vegetative analysis for ages older than 60.

As mentioned above the main purpose of lichenometry and vegetative analysis, was to estimate avalanches frequency within different time intervals of once every tenth, fiftieth or hounded year. Accordingly, the level of precision in the age assessment does not necessarily have to be high. It is therefore uncertain if whether the mentioned problems are relevant enough to have a crucial effect on the results, thus the estimated rock ages (within ages of 1, 10, 50, 100, 140, and >140 years) is considered to be valid.

As a conclusion, using lichenometry in combination with vegetative analysis to estimate avalanche activity and frequency within time intervals, contains some errors that must be considered, but overall is believed to be a valid and recommended method.

6.2 Avalanche potential in the different studied areas

The avalanche hazard in Vinddal, Taulen and Mundal will be discussed based on the results from the lichenometry- and vegetative analysis preformed during field work, spatial analysis of the avalanche areas and the fracture analysis.

6.2.1 Vinddal

The case study at Vinddal consist of a steep (35°), short (215x110 m) fan with fall-sorted coarse and angular fragments of rocks. Analysis of the spatial distribution of the surface blocks (size and intensity) and field observations, indicates that Vinddal is mainly exposed to rockfalls and rockslides (figure 6-1B).

The cliff in Vinddal has an E-W orientation with an 80° dip (figure 6-1A). The fracture analysis shows a single fracture set trending ~SE-NW, with a moderate dip of approximately 60° towards SW, resulting in fractures slightly oblique relative to the cliff face. These data coincide with measurements done by Bertelsen (2009) in a report about geohazards in Bergen. Bertelsen (2009) state that the dominating fracture system in Bergen has an SE-NW orientation, which also correspond with the schistosity or foliation/layering in Bergen. Further, the analysis of the fracture distribution suggests a random fracture spacing (CV=0,83) with no clustering and a uniform (homogeneous) distribution (V=0.1).

The box plot (figure 5-6) and the various frequency plots (figure 5-7), show equal results between the spatial distribution of the fracture spacings and rock dimensions. Both datasets show similar averages (block dimensions = 0.45, fracture spacing =0.50), frequency distribution (power-law) and the exponent of the power-law fits (high: >2). Overall, there is a limited scale range in fracture spacings and block dimensions, thus the mean values are representative of both populations. All these observed similarities indicate that the fracture spacings is a major controlling factor on the block sizes within the avalanche deposit at Vinddal.

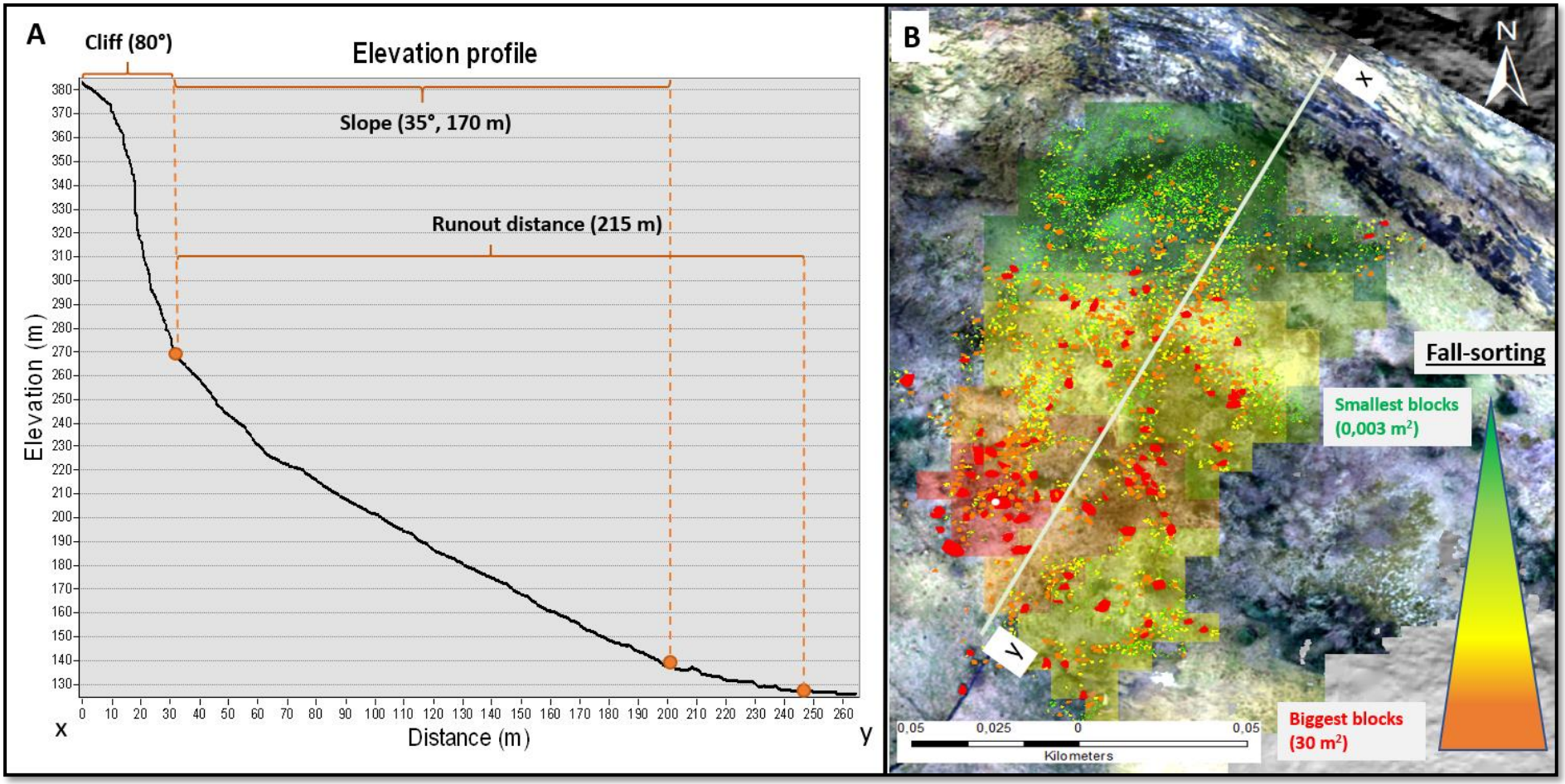

Figure 6-1: A) Elevation profile of Vinddal showing cliff area, slope area and runout area. B) Image from the ArcGIS model of the avalanche area in Vinddal, showing the rocks interpreted, the size distribution and a figure indicating fall-sorting.

The results from the field investigation reveals a great variety in the degree of colonization on the blocks, where the general age of rocks increases from the apex to the distal part of the fan. Some blocks are estimated to be much older than 140 years, while others may be only a year or two old. In the distal part of the fan, very old rocks indicate that large avalanches (where 30 – 125 m^3 large blocks descend), with runout distance to this part of the fan, has not happened for decades and is rather unlikely to happened in any near future. However, based on the small to medium sized fresher looking rocks observed in the middle and upper part of the fan, there is reason to believe that smaller events, such as rockfalls (where >0.25 m^3 large blocks descend), younger than 10 years have happened, maybe even younger than 1 year. Accordingly, Vinddal is probably an area that might still be active, and to assume that smaller rockfalls still frequently happens, is likely. However, the vulnerability in this area is low because no constructions or human activity are close enough to be affected by even a large avalanche event.

6.2.2 Taulen

An analysis of the avalanche potential in Taulen is particularly important due to the camp site and farm located close to the cliff. Recently, Heggen et.al. (2019) did a report on avalanche hazards in Voss, including Taulen camping. This report will further be used as a comparison to the results from this study.

The case study at Taulen consist of a steep (30°) talus with coarse angular shaped rock fragments that are fall-sorted. Analysis of the spatial distribution of the surface blocks (size and intensity) and field observations, indicate that Taulen is mainly exposed to rockfalls and rockslides (figure 6-2B).

The cliff in Taulen is very steep (80°) (figure 6-2A) and consist of several large overhanging areas (figure 3-8). In addition, the results from the fracture analysis preformed in this study and by Heggen et.al. (2019), shows two fracture sets that creates a dangerous fracture pattern. One fracture set is nearly parallel with the cliff face and the other one is nearly perpendicular to the cliff face. These fractures, especially the fracture set parallel to the cliff, can generate large areas of the cliff to detached, even in areas that appear to be stable.

The results from the spatial analysis of the fracture system suggest a clustered fracture spacing (CV=1.5) and a non-uniform (heterogeneous) distribution (V=0.4). The box plot (figure 5-13) and the various frequency plots (figure 5-14), shows equal results between the spatial analysis of fracture spacings and rock dimensions. Both dataset shows similar averages (fracture spacing =1.30 m, block dimensions = 1.2 m), frequency distribution (power-law) and the exponent of

the power-law fits (low: <2). The low exponent, indicating a wide range of fracture spacings and block dimensions present. This coincide well with the results showing a clustered, heterogeneous, fracture distribution, where the fracture spacing is varying. Overall, the similarities between size ranges, averages and frequency-distributions indicate that fracture spacings are a major controlling factor on the block sizes within the avalanche deposits at Taulen.

However, one issue with assuming that the fractures are controlling the avalanche deposit, is that the largest blocks observed (15x10x5 m), correspond badly with the fracture spacings (largest spacing is 2 m from reliable data set). The bedding, on the other hand, with an average thickness of 8.9 m and the thickest bed registered at 13m, can explain these blocks. Another possibility, based on the fracture orientations, is toppling, where large areas/blocks detach along the fracture set parallel to the cliff. Either way, as the falling rocks hit the slope, it probably breaks up along the fracture planes, thus explains both the similar results from the spatial analysis and the origin of the large blocks. Furthermore, there is also a possibility that these rocks have been transported by the glacier and deposited in Taulen, thus do not originate from the cliff.

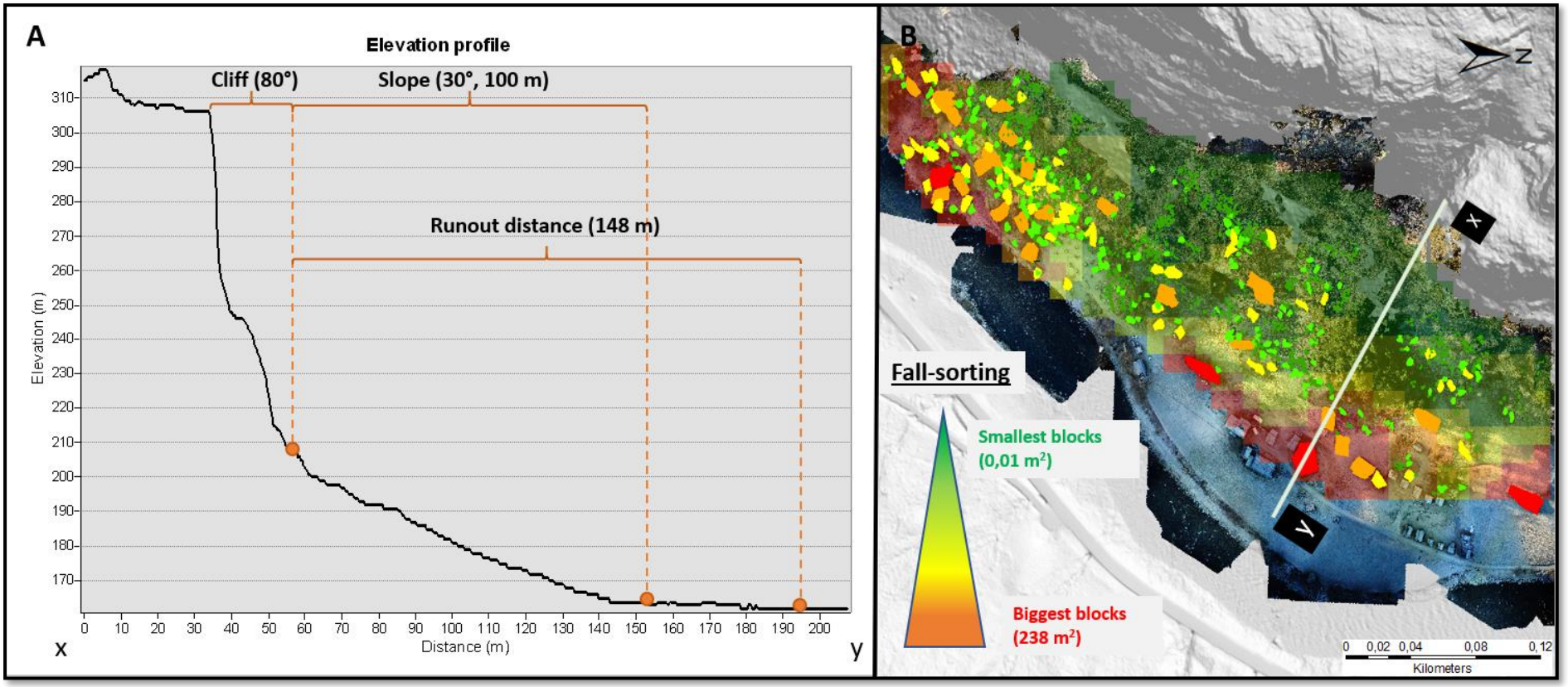

Figure 6-2: A) Elevation profile of Taulen showing cliff area, slope area and runout area. B) Image from the ArcGIS model of the avalanche area in Taulen, showing the rocks interpreted, the size distribution and a figure indicating fall-sorting.

Based on field observations, there is a reason to believe that the last large avalanche (where 30 – 125 m^3 large blocks descend) with runout distance to the distal part of the fan, can be dated at least 140 years back, maybe even back to the early postglacial time according to Heggen et.al. (2019). Thus, the possibility of a large avalanche happening today or in any near future, is rather unlikely. Although, closer to the cliff, where some fresh rocks are observed, smaller rockfalls (where >0.25 m^3 large blocks descend) can still occur.

These field observations correspond well with observation done by Heggen et.al. (2019), which have resulted in a danger zone map. Three zones with a repeat interval for rockfalls at 1/100, 1/1000 and 1/5000, are estimated (figure 6-3). The likelihood for an avalanche large enough to affect the farm and most of the camp site is estimated to be 1/5000. The danger zone corresponding to 1/1000 is affecting a garage and the back row of the cabins, while the most active area, closest to the cliff is within the danger zone of 1/100 (Heggen et.al 2019).

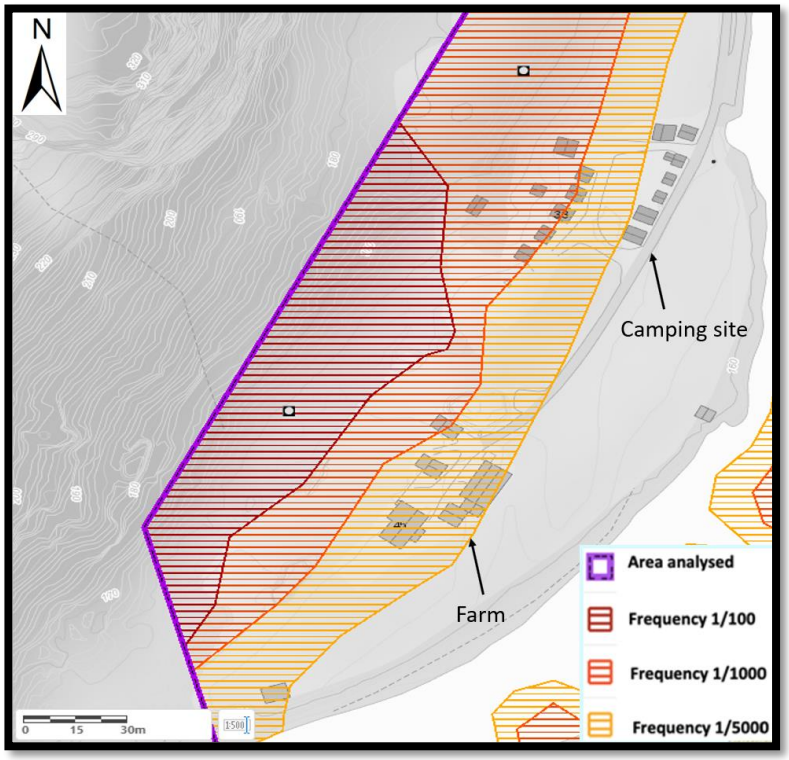

Figure 6-3: Danger zone map of Taulen Camping. Modified from NVE Atlas (2019)

6.2.3 Mundal

A second field investigation in Mundal was not conducted due to insufficient funds. Accordingly, the avalanches frequency and activity estimations are based on a spatial analysis of the avalanche area, the fracture analysis, and a report done by Grue et.al. (2017) about hazard mapping in Sogndal.

Mundal is in a valley consisting of several avalanche fans along both sides of the valley. The fan studied is steep (30°), facing NE and consist of coarse rock fragments (figure 6-5A). There is a dominant distribution of smaller rocks (0.1 – 1 m^2). However, there is a small area in the NW part of the fan that shows a prominent downslope coarsening (figure 6-5B). It is possible that several other medium to large blocks (4 m^2 – 90 m^2) is deposited in this part of the fan, but has been buried by smaller rocks. Drone pictures from Mundal, shows clear sign of water (and snow) activity in the area, where figure 6-4A shows water running from the valley, and figure 6-4B shows fallen and bent trees.

The overall distribution of the blocks on the surface of the fan and the drone pictures, indicate that water related processes, such as debris flow and snow avalanches, are dominating in Mundal. According to Grue et.al. (2017), the fan investigated, is only one of several fans that shows clear signs of mass transport with water related avalanches in this area. The small area showing distal coarsening is interpreted as fall-sorting and might indicate rockfall or rockslide activity. Accordingly, the rockfall and rockslide deposits are probably restricted to the upper part of the fan, while, with a fan extend of 450 m, deposits in the distal part originate from the water related avalanches.

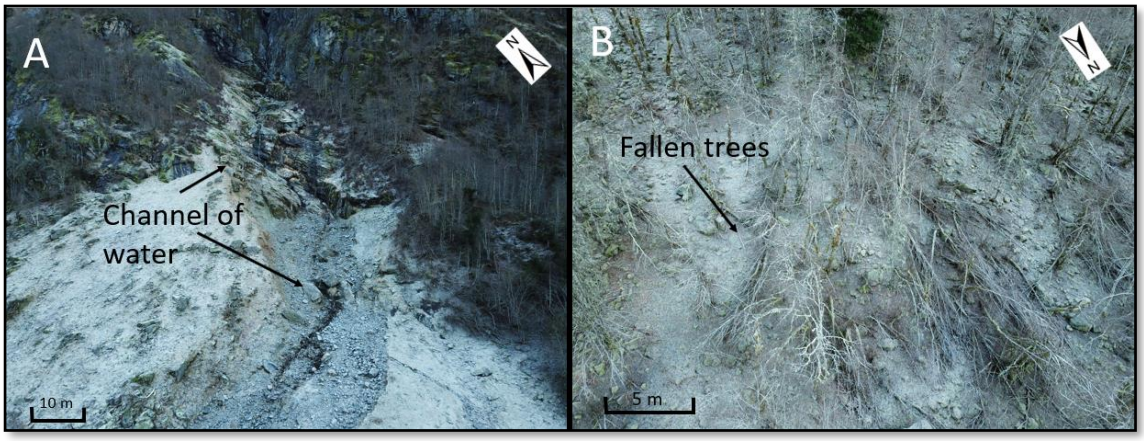

Figure 6-4: Drone pictures from Mundal showing A) water running from the valley and B) fallen trees indicating snow avalanches

The fracture analysis shows two fracture sets, where one set is parallel oriented to the cliff face, and one almost perpendicular oriented to the cliff face (figure 5-18). This fracture pattern can be dangerous as it can generate large areas of the cliff to detached. Additionally, as the slope has an inclination of 30° and that climate conditions in Sogndal can generate large amount of snow within a short period of time, the snow avalanche risk can in some periods be high (Grue et.al., 2017).

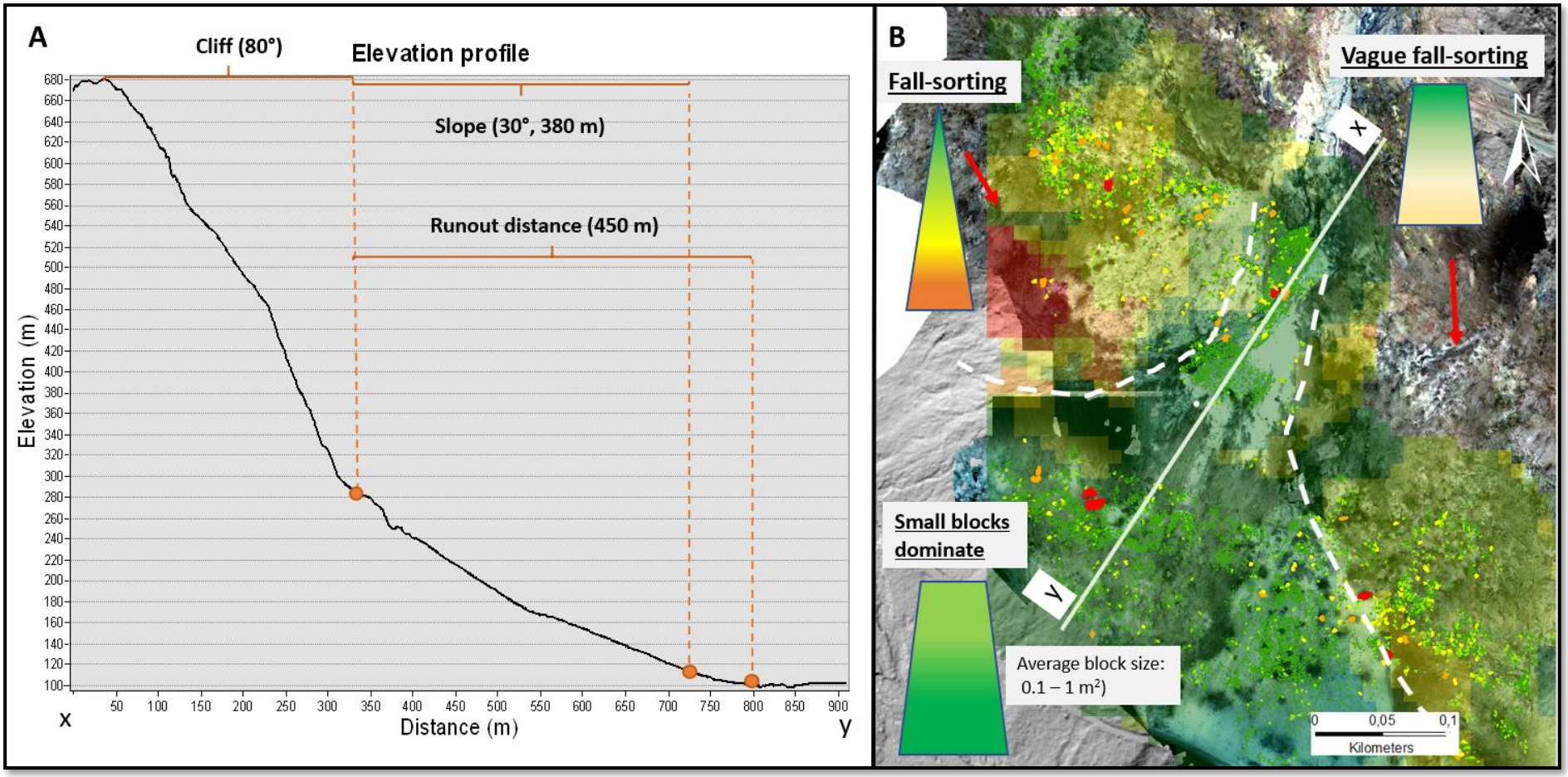

Figure 6-5: A) Elevation profile of Mundal showing cliff area, slope area and runout area. B) Image from the ArcGIS model of the avalanche area in Mundal, showing the rocks interpreted, the size distribution and three figures indicating fall-sorting, vague sorting and no sorting.

Further, the fracture distribution analysis suggests a random fracture spacing (CV=0,9) with no clustering and a uniform (homogeneous) distribution (V=0.2). When comparing the fracture spacings and the block dimensions no comparable data ranges or averages are observed. The mean values are very different with average fracture spacings at 1.3 m and average rock dimension at 0.5 m. For the frequency plots, the fracture populations conform best to a log-normal distribution, while the block populations conform best to power law distribution. However, the exponents (i.e. the gradients) for both datasets are high, indicating a limited scale range for both the fracture spacings and the block dimensions. These differences are not unexpected, and is explained by the water activity in Mundal. The main control on the block sizes is not the fracture spacing in the cliff, but rather the waters ability to transport fragments from other areas and deposit them on the avalanche fan. Depending on the season it is likely that, avalanche hazards, such as snow avalanches, debris flows, rockfalls and rockslides, can be active in this area. As for Vinddal, the avalanche activity in Mundal do not compose any danger to humans or constructions.

6.2.4 Summary

As a summary, Taulen and Vinddal is mainly prone to rockslides and rockfalls. Even though Taulen can still experience smaller rockfall events, Vinddal is considered the most active area with an overall higher amount of fresher rocks and less vegetation in the fan. However, the vulnerability in Vinddal is much lower than in Taulen, where a large avalanche (where 30 – 125 m^3 large blocks descend) can cause great consequences for the camp site and the farm located close to the cliff. Additionally, the cliff in Taulen is more dangerous, with several large overhanging areas and a dangerous fracture pattern. Mundal differs from both Vinddal and Taulen. This area is, depending on the season, prone to rockfalls, rockslides, snow avalanches and debris flow. However, the avalanche activity in this area do not compose any danger to humans or constructions.

Further, the fracture distribution in Vinddal and Mundal is randomly distributed, while the cliff in Taulen is clustered. In both Vinddal and Taulen the fractures are considered to control the avalanche deposit. Thus, with a random distributed fracture system and low fracture spacing, the deposit in Vinddal consist of smaller and less variable rock sizes (0.003 m^2 (0.012x0.25 m) to 30 m^2), compared to Taulen (0.01 m^2 - 210 m^2). The avalanche deposit in Mundal, on the other hand, is mainly controlled by the water flow, thus the fracture distribution is irrelevant

for the fan deposit. As the water manage to transport smaller blocks, the fan mainly consists of smaller rocks (0.1 - 1 m^2).

6.3 Usability of method and potential for improvement

A complete detailed analysis of three different areas prone to avalanches has been achieved by combining drones to collect data, photogrammetric models and field investigation, including lichenometry dating and vegetative analysis. A summary of the process in step by step is shown as a flow chart in figure 4-1 (chapter 4).

6.3.1 Field work

In order to gain a complete analysis of the studied areas, two separate field trips were performed in each area. In the first field trip a drone was used to collect data, and in the second field trip a more detailed field investigation was conducted in two of the study sites (Vinddal and Taulen).

It may be argued that in order to do this in a more efficient and economical way, both procedures should have been performed during the first field trip. However, by collecting drone data first, a 3-D model could be created, making it possible to get an overview of the studied area. Also, areas where the model presented limited or no information (e.g. vegetation) was identified. Accordingly, for the second field trip, these areas were known and mapped, thus less time was used to find the best and most relevant places to investigate. Additionally, a picture from the ortomosaic model in ArcGIS, showing the avalanche area, provided a great tool to keep track of where in the field thorough measurement and analysis were preformed (figure 5-28, 5-30). Consequently, by conducting fieldwork in two separate instances, instead of one, a more organized and effective field trip and data acquiring were conducted.

On the other hand, the lichenometry measurements complete in the graveyards and in the fields, were performed in the same day. As discussed above, this may not have been the most effective way. If the collecting and interpreting of all the lichenometry data from the graveyard were done before conducting the field measurements, a more thorough and informative analysis may have been performed. Knowledge about the relationship between the lichen types, and the diameter vs age intervals, would provide a better understanding of the most representative and relevant data that needed to be collected in the field.

Furthermore, the lichenometry data were collected by using the indirect method, which means measuring the size of lichen colonies with known dates of origin. This was a simple,

inexpensive and effective method. However, as discussed in 6.1, the lichenometry might contain some errors due to a relatively small data set. Hence, in order to improve the validity of the result, more than two graveyards could have been investigated.

6.3.2 Using drones to collect data

Using drones to map avalanche prone areas, was an informative, uncomplicated and effective approach. Within a few hours, including time for preparations and discussions, the drone had acquired data from large areas of both the cliff and the slope. Compared to manned air-crafts, a drone acquisition is safer, less expensive and has low operating costs (Eisenbeiss, 2009). The drone, including extra batteries and the software, costs about 20 000 NOK, while a helicopter costs about 25 000 NOK/hour (Christian Haug Eide, personal communications, October 28, 2019)

The development of the technology where photogrammetry can be used to create high quality 3-D models, has enhanced the mapping efficiency and can capture exceptional detailed geographical data. In this study, models in Lime and ArcGIS have provided important information about many features of both the cliff and the avalanche deposit. Nevertheless, to achieve a full detailed analysis, the traditional field work methods are unavoidable and should therefore be complemented with the new modern techniques.

One disadvantage by using drone is that it requires fair weather; no precipitation, no fog and wind not stronger than fresh breeze (8-10 m/s). Additionally, cold temperature can cause batteries to lose charge faster and a ground covered in frost. Also, the survey should be conducted during daylight. All these factors can have an important impact on the quality of the collected data. For instance, during the survey in Vinddal the weather changed, it started to rain, and wind increased. The wind caused sudden movements of the drone (figure 6-6A) and raindrops covered the lens (figure 6-6B). This resulted in lower quality of the pictures, and several unsharp and bad pictures had to be deleted. Consequently, the 3-D model created for Vinddal, has slightly reduced resolution (20 cm in ArcGIS and 50 cm in LIME) compared to the 3-D models made for Taulen and Mundal (10-20 in ArcGIS and 30 in LIME). However, as the survey in Taulen and Mundal was conducted in November, the temperature was low, and the ground was covered in frost (figure 6-7).

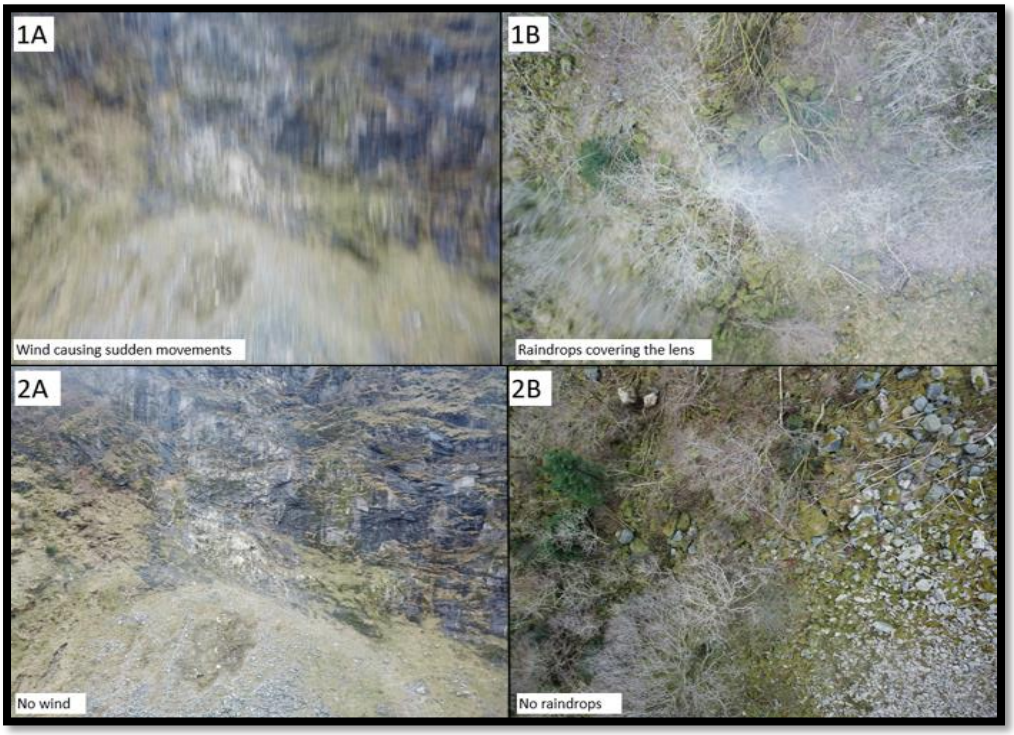

Figure 6-6: Two pictures from Vinddal showing how wind and rain affect the quality of the data. Picture 1A) Picture affected by wind and 2A) Not affected by wind. Picture 1B) picture with a raindrop on the lens, picture 2B) clean lens.

Figure 6-7: Pictures of Taulen and Mundal, showing frost covered grounds.

The process from drone images to finished 3-D models in ArcGIS (Orthomosaic and DEM) and LIME (Texture and Mesh) contains four stages: (1) alignment, (2) dense cloud construction, (3) mesh construction for LIME and DEM construction for ArcGIS, and (4) texture generation for LIME and ortomosaic construction for ArcGIS (figure 4-2). When performing this procedure, a step by step recipe was followed making the 3-D models easy to create without any advanced training. However, as the amount of the collected data is very large, it requires a high computer capacity and the processing can be extremely time consuming. In this study. the processing took 1-2 weeks, but as this process only requires input from the user 5 times, for

about 10 minutes to 1 hour, it did not prevent any further work. Hence, even though the processing is time-consuming, it only needs 2-4 hours work by the user.

Overall, using drones to investigate avalanche prone areas is an informative, simple and effective approach. It provides a detailed analysis within a short period of time, and is highly recommended, especially when mapping high risk, steep mountain areas with limited field access. Still, planning according to weather conditions are important. This can be challenging as there are several factors that have to be accounted for. However, despite some weather challenges, most of the data collected in this study has high quality, thus prove that it is possible to acquire good data even with challenging weather.

6.3.3 Using ArcGIS to analyze avalanche deposits

The spatial distribution of the avalanche fans in Vinddal, Taulen and Mundal was analyzed in ArcGIS by using a combination between Orthomosaic, DEM, a hillshade map and a slope map. These models provided a high-resolution image (10-20 cm) of the fan area and enable a detailed mapping of the surface geomorphology. Further, by creating polygons to distinguish different features (e.g. blocks) useful information, such as the spatial patterns, rock intensity and fan extent, were acquired. This information was further used to get indications of which geomorphological process that was present and a following avalanche hazard analysis.

There were some challenges related to the models in ArcGIS. Issues with areas covered by vegetation were an overall trend in all the studied areas. As the data collected by the drone did not show areas covered by vegetation, several parts of the avalanche fans could not be interpreted, thus became areas without data. Also, areas where the resolution was bad (20-50 cm versus a resolution c.10-20 cm in most places), recognizing rocks or estimating the outline of the rock became difficult. These resolution issues might have been a result of challenging weather during the drone survey (wind and rain in Vinddal, and frost in Taulen and Mundal)

However, these problems did not have a major impact on the final results and is considered to be insignificant compared to the many advantages gained by using the model in ArcGIS. Information about several important features are achieved, which allowed a detailed analysis. Accordingly, using ArcGIS to analyze avalanche areas, is a highly recommended method.

6.3.4 Using LIME to analyze the cliff

The spatial distribution of fracture patterns in the cliff was analyzed in LIME by using photogrammetric models. Fractures and beddings were mapped, providing an overview of the fracture patterns and information about dip, dip directions and strike.

Like the models in ArcGIS, some challenges were also experienced when using LIME. The main problem was resolution issues (100-200 cm versus a resolution c. 30-50 cm in most paces) in some parts of the cliff faces. Additionally, vegetation in certain areas of the cliffs also caused some difficulties. As an example, the model in Taulen contains high resolution data in the mid part of the cliff (30 cm), while in the right and left cliff the resolution is lower (100 cm) (figure 6-8). Also, the left cliff is disturbed by abundant vegetation. Consequently, the interpretation from these low-resolution areas was difficult and is illustrated by the scattered results in the fracture intensity vs the coefficient of variance plot (figure 5-12A).

Nevertheless, these problems did not have a major impact on the final results and are considered to be insignificant compared to the many advantages gained by using LIME to conduct a fracture analysis. LIME provides a useful tool when analyzing the structural characteristics of the cliff face and is highly recommended.

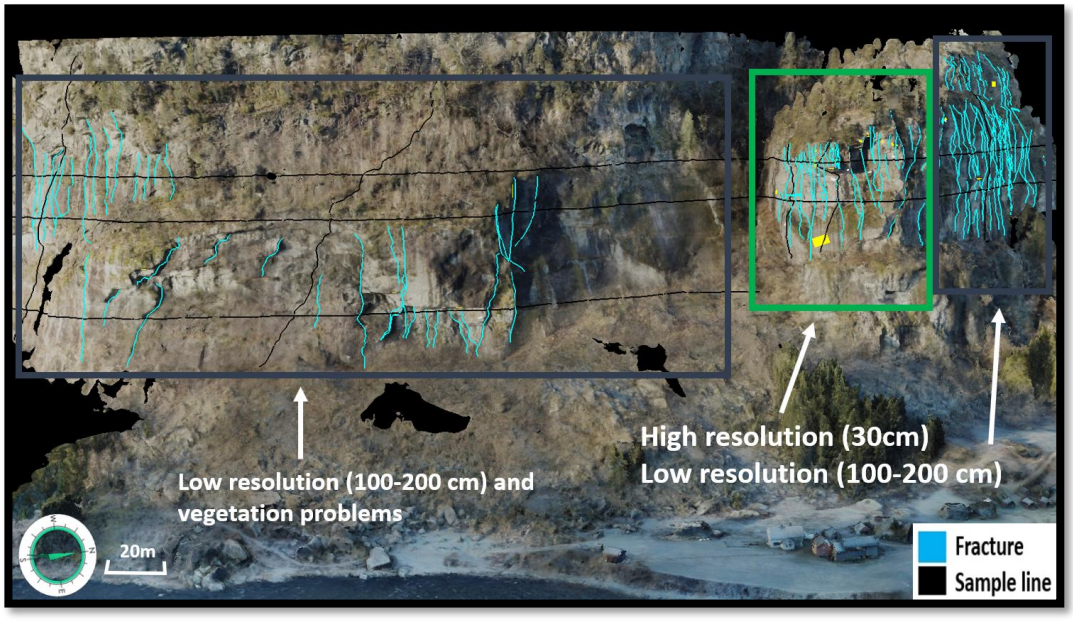

Figure 6-8: Image of the model from Taulen in LIME showing the mid cliff with high resolution data, the right cliff with low resolution data and the left cliff disturbed by vegetation and low resolution data.

7 Conclusions

Based the discussion in chapter 6.1, the following conclusion has been made.

- Lichenometry is a widely applicable and inexpensive tool for estimating ages on rock surfaces. The indirect method is quite straightforward, and does not need any intensive training.
- The resulting lichen plots are simple, useful and valid when preforming a quantitative dating survey to estimate rock ages. The measurements that differs from the overall trend are probably due to uncertainties related to cleaning of the measured gravestones, environmental conditions and identification of lichens.
- By combining the lichenometry results and a vegetative analysis, a more thorough and valid analysis of the rock ages was achieved. This analysis was further used to perform a quantitative estimation of the avalanche frequency and activity. Based on the experience throughout the study and the results, it is concluded that this is a recommended method that is simple, inexpensive and informative.
- Moreover, there are some challenges associated with this method, but with awareness and caution these issues can be minimized. Accordingly, three key points that will minimize these errors is presented: 1) proximity and comparable environments between the area where lichenometry measurements is collected (e.g. cemetery) and the area where the lichenometry result and vegetative analysis is conducted (e.g. avalanche area), 2) acquire some background knowledge about the chosen lichens and how to identify them, and 3) avoid rocks where competition between lichen species is high, 4) be selective when choosing rocks and rock surfaces to investigate in the field.

The evaluation of avalanche potential in Vinddal, Taulen and Mundal (chapter 6.2) is based on lichenometry- and vegetative analysis preformed during field work, spatial analysis of the avalanche areas and the fracture analysis.

- Vinddal is mainly prone to rockfalls and rockslide, where the fractures act as the main control on the deposits. The results from the fracture analysis show a random distribution of fractures, where fracture spacings correlate well with the dimensions of the block deposited in the fan. Further, the spatial analysis of the deposit shows a fan that is fall-sorted, with a low variety in block sizes (0.003 m^2 – 30 m^2). Field observation reveals a general increase in age from the apex to the distal part of the fan. Several fresh

rocks indicate that smaller rockfalls still frequently happens, but large avalanches are rather unlikely. Of the three areas studied, Vinddal is the most active area. However, the vulnerability is quite low because no constructions or human activity are close enough to be affected by an avalanche event.

- Taulen is mainly prone to rockfalls and rockslides. A fall-sorted fan, with high variety of block sizes (0.01 m^2 – 210 m^2) is deposited in the area. The results from the fracture analysis show a clustered fracture distribution, where the average fracture spacings correlate well with the average block dimensions. However, based on larger blocks present, both the fractures and the beddings are considered to control on the deposits. Further, the cliff shows several large overhanging areas and a dangerous fracture pattern. However, the estimated frequency and activity in Taulen is low, thus large areas will probably not detach from the cliff in the near future. Although, a large avalanche event poses a great risk, as there is a camp site and a farm located close to the cliff.
- Mundal differs from the two other study sites due to high water activity. The area is prone to rockfalls, rockslides, snow avalanches and debris flows. The fan is dominated by smaller rocks (0.1 – 1 m^2). There is no sorting, except a vague fall-sorting close to the cliff. The results from the fracture analysis shows a random distribution of fractures and no correlation between the fracture spacings and block dimensions. Mundal may still be an active area, where the type of avalanche and activity level are highly depending on the season (weather). However, the avalanche activity in this area do not pose any danger to humans or constructions.

The evaluation of the method used in this study (chapter 6.3) has resulted in the following conclusion.

- The results from this study show that using photogrammetric models acquired by drone are a useful and a safe tool when investigating avalanche prone areas. Drones are especially important when exploring inaccessible and dangerous areas where it is difficult to obtain information.
- Additional, geological mapping has in the past been complex, time-consuming and an expensive process. By using drone in geological mapping, large areas can be mapped in a short period of time at a low cost.
- When preforming drone data acquisition two factors should be considered. Firstly, the weather, as it can have a large effect on the data quality. Secondly, vegetation in the

study site, whereas in areas with abundant vegetation the drone is not able to collect any data. This also applies to seasons, whereas in the summer vegetation is dominating in many areas.

- The drone data processing procedure is relatively easy, but time consuming. However, as the process only requires input from the user 5 times, for about 10 minutes to 1 hour, it did not prevent any further work.
- The 3-D models created provides high quality data and are proven to be beneficial when preforming a detailed analysis. Several important features were interpreted and important information was acquired in both ArcGIS and LIME.
- Overall, this is an easy, informative and recommended method to understand avalanche potential in steep cliffs exposed to avalanches.

7.1 Proposed further work

This study provides a lichenometry analysis, performed by using the indirect method on a graveyards in Voss and Bergen. These measurements from Voss and Bergen were pooled, and presented as three plots, showing lichen diameter vs age, for three different lichens. Complementing the lichenometry data, from this study, with more lichen measurements from Voss and Bergen would increase the validity of the data. Moreover, with sufficient data, two plots separating Voss and Bergen can be achieved.

Moreover, these lichenometry results are used in combination with vegetative analysis to provide an avalanche recurrence time estimation. In order to improve this analysis, NVE Atlas, which has registered several avalanche events throughout time, can be used. Lichen and vegetation measurements of several avalanche deposits in western Norway, with known age can be collected. Thus, offers a more detailed and relevant analysis of colonization in avalanche areas, and provides a better foundation in understanding the avalanche potential. Additionally, as a higher amount of avalanche areas are investigated, the dominating avalanche processes will vary, thus the relevance of the data will increase. For instance, areas where snow avalanches are a dominating process would be interesting to investigate.

Additionally, a more thorough field analysis of each area is recommended, where a better analysis of the fan area and the cliff can be achieved. More lichen and vegetation measurements and observation of fractures, bedrock and other characteristic of the cliff, will provide a better analysis of the area and increase the accuracy of the avalanche potential estimations.

8 References

- Aa, A. R. and Sønstegaard, E. (1995). Fjærland – 1317 I. Kvartærgeologisk kart M 1:50 000 med beskrivelse. Norges geologiske undersøkelse.
- Aasbrenn, K. (2017). *Lav- Høyt og Lavt: en lavsafari* [photo]. Available at: https://docplayer.me/52723126-Lav-hoyt-og-lavt-en-lavsafari-tekst-og-bilder-kristian-aasbrenn.html
- Abellán, A., Oppikofer, T., Jaboyedoff, M., Rosser, N. J., Lim, M. and Lato, M. J. (2014) Terrestrial laser scanning of rock slope instabilities. *Earth Surface Processes and Landforms*, *39*(1), 80-97.
- Andersen, B. G. (1980). The deglaciation of Norway after 10,000 B.P. *Boreas*, *9*(4), 211-216
- Armstrong, R. A. (2002). The effect of rock surface aspect on growth, size structure and competition in the lichen Rhizocarpon geographicum. *Environmental and Experimental Botany*, *48*(2), 187-194.
- Armstrong R. A. (2004). Lichens, lichenometry and global warming. *The Microbiologist*, *5*, 32- 35.
- Askheim, S. (2016) Bergensfeltet. In Store Norske Leksikon. Available at: https://snl.no/Bergensfeltet.
- Aune, B. (1993). Nedbørsnormaler (02/93). Oslo: Det norske meterologiske institutt
- Bakke, J., Lie, Ø., Nesje, A., Dahl, S.O. and Paasche, Ø. (2005) Utilizing physical sediment variability in glacier-fed lakes for continuous glacier reconstructions during the Holocene, northern Folgefonna, western Norway. *The holocene*, *15*(2), 161-176.
- Bellwald, B., Hjelstuen, B. O., Sejrup, H. P., Stokowy, T. and Kuvås, J. (2019). Holocene mass movements in west and mid-Norwegian fjords and lakes. *Marine Geology*, *407*, 192-212.
- Bemis, P. S., Micklethwaiteb, S., Turnerc, D., Jamesd, R. M., Akcize, S., Sam, T. T. and Bangash, H. A. (2014). Ground-based and UAV-Based photogrammetry: A multi-scale, high-resolution mapping tool for structural geology and paleoseismology. *Journal of Structural Geology*, *69*, 163–178.
- Benedict, J. B. (2009). A review of lichenometric dating and its applications to archaeology. *American Antiquity*, *74*(1), 143-172.
- Bertelsen, G (2009). ROS II – SKREDFARE / PILOT I – SALHUS (2/5). Bergen: Etat for byggesak og private planer.
- Beschel, R. E. (1961). Dating Rock Surfaces by Lichen Growth and Its Application to Glaciology and Physiography. In Rassch, G. O (ed.), *Geology of the Arctic* (*2, 1044–1062*). Toronto: University of Toronto Press
- Blikra, L. H., Hole, P. A. and Rye, N. (1989). Hurtige massebevegelser og avsetningstyper i alpine områder, Indre Nordfjord. *Skred I Norge*, *92*(1-17), 11.
- Blikra, L.H., Anda, E., Braathen, A., Stalsberg, K. and Longva, O. (2002). *Rock avalanches, gravitational bedrock fractures and neotectonic faults onshore western Norway: Examples, regional distribution and triggering mechanisms* (2002.016). Oslo: Norges geologiske undersøkelse.
- Blikra, L. H and Nemec, B. (2002a) Postglacial colluvium in western Norway: depositional processes, facies and palaeoclimatic record. *Sedimentology*, *45*(5), 914
- Blikra, L. H and Nemec, B., (2002b). Postglacial colluvium in western Norway: depositional processes, facies and palaeoclimatic record. *Sedimentology*, *45*(5), 915

- Bohme, M., Oppikofer, T., Longva, O., Jaboyedoff, M., Hermanns, R.L. and Derron, M. H. (2015). Analyses of past and present rock slope instabilities in a fjord valley: Implications for hazard estimations. *Geomorphology*, *248*, 464-747
- Braathen, A., Blikra, L.H., Berg, S.S. and Karlsen, F. (2004). Rock-slope failures in Norway; type, geometry and hazard. *Norwegian Journal of Geology*, *84*, 67-88.
- Bryhni, I (2018). Geologi og landformer i Norge. In *Store norske leksikon.* https://snl.no/Geologi_og_landformer_i_Norge
- Buckley, S. J., Ringdal, K., Naumann, N., Dolva, B., Kurz, T. H., Howell, H. A. and Dewez, T. J. B (2019). LIME: Software for 3-Dvisualization, interpretation,and communication of virtual geoscience models. *Geosphere*, *15*(1), 222–235. doi:https://doi.org/10.1130/GES02002.1
- Bull, W. B., King, J., Kong, F. C., Moutoux, T. and Phillips, W. M. (1994). Lichen dating of coseismic landslide hazards in alpine mountains. *Geomorphology, 10*(1), 253–264.
- Burrows, C. V. and Burrows V. L. (1976*).* Procedures for the study of snow avalanche chronology using growth layers of woody plants. *Institute of Arctic and Alpine Research*, *23*, 54
- Bøe, R., Longva, O., Lepland, A., Blikra, L. H., Sonstegaard, E., Haflidason, H., Bryn, P. and Lien, R. (2004). Postglacial mass movements and their causes in fjords and lakes in western Norway. *Norsk Geologisk Tidsskrift*, *84*(1), 35-55.
- Campbell, C. S. and Gong, A. (1986). The stress tensor in a two-dimensional granular shear flow. *J. Fluid Mech*, *164*, 107-125.
- Carrara, P. E. (1979). The determination of snow avalanche frequency through tree-ring analysis and historical records at Ophir, Colorado. *Geological Society of American Bulletin Part I 90*, 773-780
- Colleuille, H and Engen, I. K. (2009). *Utredning om overvåking og varsling av løsmasse- og snøskredfare på regionalt nivå* (16/2009), Oslo: Norges vassdrags- og energidirektorat
- Cox, D. R. and Lewis, P. A. (1966). *The Statistical Analysis of Series of Events*. London: Methuen.
- Dahl, S. O. and Nesje, A. (1993). Late glacial and Holocene glacier fluctuations and climate variations in western Norway; a review. *Quaternary Science Reviews*, *12*(4), 255-261.
- Dahl, S.O. and Nesje, A. (1996). A new approach to calculating Holocene winter precipitation by combining glacier equilibrium-line altitudes and pine-tree limits: a case stud from Hardangerjokulen, central southern Norway. *The holocene*, *6*(4), 381-394
- David, M. (2019) *Lecanora rupicola Arzon 1* [Photo]. Available at: http://www.lichensmaritimes.org/index.php?task=fiche&lichen=87&lang=en
- DJI (2019). Mavic PRO specs. Available at: https://www.dji.com/no/mavic/info
- Domaas, U. and Grimstad, E. (2014). Fjell- og steinskred. In: Høeg, K. (ed.*) Skred: skredfare og sikringstiltak - praktiske erfaringer og teoretiske prinsipper* (45-77*)* Oslo: NGI Universitetsforl.
- Dorren, L. (2003). A review of rockfall mechanics and modelling approaches. *Prog. Phys. Geogr. 27*(1), 69-87.
- Douglas, G.R. (1980). Magnitude frequency study of rockfall in Co. Antrim, North Ireland. *Earth Surface Processes and Landforms 5*(2), 123–129.

- Droker, R. (2019). *ASPICILIA CAESIOCINEREA (NYL. EX MALBR.)* ARNOLD [Photo]. Available at: https://www.waysofenlichenment.net/lichens/Aspicilia%20caesiocinerea
- Eisenbeiss, H. (2009). *UAV photogrammetry* (Ph.D), University of Technology Dresden, Germany
- Evans, S and Hungr, O (1993). The assessment of rockfall hazard at the base of talus slopes. *Can Geotech J, 30,* 620–636
- Evans, I. S. and Slaymaker, O. (1996). Steepland geomorphology. *Geographical Journal 162*(3), 336
- Farfaglia, S., Lollino, G., Iaquinta, M., Sale, I., Catella, P., Martino, M. and Chiesa, S. (2015). The use of UAV to monitor and manage the territory: perspectives from the SMAT project. *Eng Geol Soc Territory, 5*, 691–695.
- Fischer, L., Purves, R. S., Huggel, C., Noetzli, J. and Haeberli W. (2012). On the influence of topographic, geological and cryospheric factors on rock avalanches and rockfalls in high-mountain areas. *Nat Hazards Earth Syst Sci, 12*, 241–254.
- Fossen. H (2014). The bedrock of the Bergen-Geiranger area. In Husås A. M (ed.). *West Norwegian fjords: Guide to geological excursion from Nærøyfjord to Geirangerfjord* (Level 3, Research and professional geologists, p.5). Trondheim: Geological Society of Norway
- Førland, J. F. (1993). *Nedbørsnormaler* (39/93). Oslo: Det norske meterologiske institutt
- Gardner, J.S. (1983). Rockfall frequency and distribution in the Highwood Pass area, Canadian Rocky Mountains. *Zeitschrift für Geomorphologie, 27*(3), 311–24.
- Garibotti, I.A., Pissolito, C.I. and Villalba, R. (2011). Vegetation Development on Deglaciated Rock Outcrops from Glaciar Frías. *Argentina, Arctic, Antarctic, and Alpine Research, 43*(1), 35-45.
- Gillespie, P. A., Howard, C., Walsh, J. J. and Watterson, J. (1993). Measurement and characterization of spatial distributions of fractures. *Tectonophysic,s 226*, 113-141.
- Gillespie, P. A., Johnston, J. D., Loriga, M. A., Mccaefrey, K. J. W., Walsh, J. J. and Watterson, J. (1999). Influence of layering on vein systematics in line samples, In. Mccaffrey, K. J. W., Lonergan, L. and Wilkinson, J. J. (eds) *Fractures, fluid flow and mineralization* (35-56*)*. London: Geological Society, Special Publications, 155.
- Gillespie, P. A., Walsh, J. J. Watterson, Bonson, C. G. and Manzocchi, T. (2001). Scaling relationships of joint and vein arrays from The Burren, Co. Clare, Ireland. *Journal of Structural Geology, 23*(9), 183-201.
- Goodman, R.E. and Bray. J.W. (1976). Toppling of Rock Slopes. *Proceedings of the Specialty Conference on Rock Engineering for Foundations and Slopes, 2*, 201-234.
- Google Earth (2019). Pictures of Vinddal [photo]. Available at: https://earth.google.com/web/@61.41461017,6.6861124,209.5914679a,780.41443141d,35y,-3.02068646h,81.7534895t,360r/data=ChUaEwoLL2cvMXB2MHBuMHIYASABKAI
- Gosse, J.C. and Phillips, F.M. (2001). Terrestrial in situ cosmogenic nuclides: theory and application. *Quaternary Science Reviews, 20*(14), 1475- 1560.
- Grue, G. H., Henriksen, H. and Kronholm, K. (2017). *Skredfarekartlegging i Sogndal kommune* (35/2017). Oslo: The Norwegian Water Resources and Energy Directorate.
- Gudmundsson, A. (1999). Postglacial crustal doming, stresses and fracture formation with application to Norway. *Tectonophysics, 307*(3), 407-419.
- Guzzetti, F. (2015). Forecasting natural hazards, preformance of scientists, ethics and the need for transparency. *Toxicological and Environmental Chemistry, 98*(9), 1-17

- Hale, M. (1961). Lichen Handbook. A guide to the lichens of eastern North America. *Science, 134*(3492), 1746
- Hale, M. (1967). *The Biology of Lichens* (3rd ed., 226). London: Edward Arnold.
- Hanssen-Bauer, I., Førland, E.J., Haddeland, L., Hisdal, H., Mayer, S, Nesje, A., Nilsen, J.E.Ø., Sandven, S., Sandø, A.b, Sorteberg, A. and Ådlandsvik, B. (2015). *Klima i Norge 2100* (2/2015). Oslo: Miljødirektoratet
- Heggen, H. P., Øystese, A., Lemme, A., Pihlainen, M., Krogh, K. and Johannesen, F. (2019). *Faresonekartlegging i Voss kommune* (44/2019). Oslo: Norges vassdrags- og energidirektorat
- Hermanns, R. (NGU), Devoli, G. (NVE), Eikenæs, O. (NVE), Taurisano, A. (NVE), Fischer, L. (NGU), Oppikofer, T. (NGU) and Bunkholt, H. (NGU) (2011). *Delrapport steinsprang, steinskred og fjellskred* (15/2011). Oslo: Norges vassdrags- og energidirektorat.
- Hermanns, R. L., Blikra, L. H. and Anda, E. (2012). Systematic mapping of large unstable rock slopes in Norway. In Margottini C. (ed.), *Landslide Science and Practice* (1). Trondheim, Geological Survey of Norway
- Hudson, J. A. and Priest, S. D. (1983). Discontinuity frequency in rock masses. *International Journal of Rock Mechanics and Mining Sciences & Geomechanics Abstracts, 20*(2), 73-89.
- Hughes, A. L. C., Gyllencreutz, R., Lohne, Ø. S., Mangerud, J. and Svendsen, J. I. (2016). The last Eurasian ice sheets – a chronological database and time-slice reconstruction, DATED-1. *Boreas, 45*(1), 1-45.
- Hungr, O., Evans, S. G., Bovis, M. J. and Hutchinson, J. N. (2001). A review of the classification of landslides of the flow type. *Environmental & Engineering Geoscience, 7*(3), 221-238
- Hutchinson, J. N. (1968). Mass Movement. In Fairbridge R. W. (ed.). *Encyclopedia of Geomorphology* (688-695). New York: Reinhold.
- Hutchinson, J.N. (1988). General Report: Morphological and Geotechnical Parameters of Landslides in Relation to Geology and Hydrogeology. In Bonnard, C. (ed.). *Fifth International Symposium on Landslides (1, 3-35)* Netherland: Rotterdam.
- Iden, K., Isaksen, K., Kristiansen, S., Mamen, J. and Bartnicka, S.H. (2009). *Været i Norge. Klimatologisk oversikt året 2009* (13/2009). Oslo: Meterologisk institutt
- Innes, J. L. (1984). The optimal sample size in lichenometric studies. *Arctic and Alpine Research 16*, 233–244.
- Innes, J. L. (1985). Lichenometry. *Progress in Physical Geography 2*, 187-254.
- IPCC (2014). *Climate Change 2014 - Impacts, Adaption, and Vulnerability* (5). Genève: Working Group II. Intergovernmental Panel on Climate Change.
- Irene A. Garibotti, Clara I. Pissolito and Ricardo Villalba (2011). Vegetation Development on Deglaciated Rock Outcrops from Glaciar Frías, Argentina. *Arctic, Antarctic, and Alpine Research, 43*(1), 35-45
- Jaedicke, C., Solheim, A., Blikra, L. H., Stalsberg, K., Sorteberg, A., Aaheim, A., Kronholm, K., Vikhamar-Schuler, D., Isaksen, K., Sletten, K., Kristensen, K., Barstad, I., Melchiorre, C., Høydal, Ø. A. and Mestl, H. (2008). Spatial and temporal variations of Norwegian geohazards in a changing climate, the GeoExtreme Project. *Natural Hazards and Earth System Sciences, 8*(4), 893-904.
- James, B. B. (2009). A Review of Lichenometric Dating and Its Applications to Archaeology. *American Antiquity, 47*(1), 143-172

- Jenkins, M. .J. and Hebertson, E.G. (1994). *USING VEGETATIVE ANALYSIS TO DETERMINE THE EXTENT AND FREQUENCY OF AVALANCHES IN LITTLE COTTONWOOD CANYON, UTAH* (thesis). Utah State University: Logan, Utah
- Jochimsen, M. (1973). Does the size of lichen thalli really constitute a valid measure for dating glacial deposits? Arctic and Alpine Research, *5*(4), 417-424.
- Johnson, E. A. (1987). The relative importance of snow avalanche disturbance and thinning on canopy plant populations. *Ecology, 68*(1), 43-53.
- Jones, J. H and Handcock, M. S. (2003) An assessment of preferential attachment as a mechanism for human sexual network formation. *Proc Biol Sci, 7(270), 1123-1128.*
- Joyce, K. E., Samsonov, S. V., Levick, S.R., Engelbrecht, J. and Belliss, S. (2014). Mapping and monitoring geological hazards using optical, LiDAR, and synthetic aperture RADAR image data. *Nat Hazards, 73*, 137–163.
- Kartverket (2019). *Modified map of Western Norway*, accessed 23 juli 19. Available at: https://www.norgeskart.no/?_ga=2.227791901.1239431260.1556188777-964008503.1556188777#!?project=norgeskart&layers=1002&zoom=4&lat=7197864.00&lon=396722.00
- Kvale, A. and Ingdahl, S.E. (1985). Voss – 1316 III. Berggrunnsgeologisk kart – 1:50 000. Norges geologiske undersøkelse
- Lal, D. (1991): Cosmic ray labeling of erosion surfaces: in-situ nuclide production rates and erosion models. *Earth and Planetary Science Letters, 104*(2-4), 424-439.
- Lied, K. and Kristensen, K. (2003). *Snøskred: håndbok om snøskred*. Oslo: Vett & Viten.
- Lied, K., Høeg, K., Karlsrud K. and Gregory, T. (2014). Innledning og historikk. In: Karlsrud, K. (eds.), *Skred: skredfare og sikringstiltak - praktiske erfaringer og teoretiske prinsipper* (10). Oslo: NGI Universitetsforl.
- Liljequist, G. (1970). *Klimatologi*. Stockholm, Gencralstabens Litografiska Anstall.
- Luckman, B. H. (1977). The geomorphic activity of snow avalanches. *Physical Geography, 59*(1/2), 31-48.
- Mangerud, J., Gyllencreutz, R., Øystein, L. and Svendsen, J. I. (2011). Glacial History of Norway. In: Hughes, P. D., Gibbard, P. L. and Ehlers, J. (eds.), *Quaternary Glaciations - Extent and Chronology: A Closer Look* (279-298). Amsterdam, Elsevier.
- Martinelli, M. Jr. (1974). Snow avalanche sites: their identification and evaluation. *Journal of travel research, 14*(1), 26
- McCaffrey, K. J. W., Sleight, J.M., Pugliese, S. and Holdsworth, R., E. (2003). *Fracture formation and evolution in crystalline rocks: Insights from attribute analysis* (109-124). London: Geological Society, Special Publications, 214.
- McCarroll, D. (1994). A new approach to lichenometry: Dating single-age and diachronous surfaces. *Holocene, 4*(4), 383-396
- McClung, D. M. (2003). Magnitude and frequency of avalanches in relation to terrain and forest cover. *Arctic, Antarctic, and Alpine Research, 35*(1), 82-90.
- Mottershead D. N. (1980). Lichenometry – some recent applications. In Davidson, R. A., Lewin, J. (eds), *Timescales in Geomorphology* (95-108), Chichester: Wiley & Sons Ltd.
- Nash, T. H., Ryan, B. D., Gries, C. and Bungartz, F. (2004*). Lichen Flora of the Greater Sonoran Desert Region* (2). Arizona: Arizona State University
- Nash, T. H., Ryan, B. D., Gries, C. and Bungartz, F. (2007*). Lichen Flora of the Greater Sonoran Desert Region* (3). Arizona: Arizona State University
- Nelson, S.A. (2015). Mass movements. *Physical Geology*. USA: Tulane University

- Nemec, W. (1990). Aspects of sediment movement on steep delta slopes. In Colella, A. and Prior, D.B. (eds.) *Coarse-Grained Deltas* (29-73). Oxford: Blackwell scientific publicaiton.
- Nesje, A., Blikra, L. H. and Anda, E. (1994). Dating rockfall-avalanche deposits from degree of rock-surface weathering by Schmidt-hammer tests: a study from Norangsdalen, Sunnmøre, Norway. *Norsk Geologisk Tidsskrift, 74*, 108-113.
- NGI (2019a) Successful protection against avalanches. Available at: https://www.ngi.no/eng/News/NGI-News/Successful-protection-against-avalanches
- NGI (2019b). Rockslides. Available at: https://www.ngi.no/eng/Services/Technical-expertise/Rock-slides
- NGU (2014). Skred. Available at: https://www.ngu.no/emne/skred
- NGU (2015). TERRESTRIAL COSMOGENIC NUCLIDE DATING. Available at: https://www.ngu.no/en/topic/terrestrial-cosmogenic-nuclide-dating
- NGU (2019a), ROCK AVALANCHES IN NORWAY. Available at: https://www.ngu.no/en/topic/rock-avalanches-norway
- NGU (2019b), HAZARD AND RISK CLASSIFICATION OF UNSTABLE ROCK SLOPES. Available at: https://www.ngu.no/en/topic/hazard-and-risk-classification-unstable-rock-slopes
- NGU (2019c*). Quaternary geological map of Vinddal, Taulen and Mundal*. Available at: http://geo.ngu.no/kart/losmasse/
- Noller, J. S. and Locke, W. W. (2000). Lichenometry. In Noller, J. S., Sowers, J. M. and Lettis, W. R. (eds). *Quaternary Geochronology: Methods and Applications* (261-272). American Geophysical Union: Washington.
- Norang, R. L. (2016). *Lidarskanning av skredutsatte skråninger i Hardanger* (thesis), The University of Bergen, Bergen.
- NVE Atlas (2019). *Map of avalanche events*. Availale at: https://gis3.nve.no/link/?link=SkredHendelser
- NVE Atlas (2019). *Map of danger zones in Taulen*. Avalaible at : https://atlas.nve.no/Html5Viewer/index.html?viewer=nveatlas#
- NVE. (2014). *Sikkerhet mot skred i bratt terreng - Kartleggingav skredfare i arealplanlegging og byggesak* (8/2014), Oslo: Norges vassdrags- og energidirektorat
- NVE (2016*). NVE – Skredfarekartlegging*. Available at: https://www.nve.no/Media/3408/kravspesifikasjon_nve_generelt.pdf
- NVE (2017*). Skredfarekartlegging i Sogndal kommune* (35/2017). Sogndal: Norges vassdrags- og energidirektorat
- NVE (2019a). Identifisering, vurdering og kartlegging av skredfare i bratt terreng ved utarbeiding av arealplanar. *Rapportmalar, adapted 03.07.2019 URL:* https://www.nve.no/Media/4952/rapportmaler-prosedyrebeskrivelse.pdf
- NVE (2019b). *Map showing where Åsane Gamle kirke is located compared to the studied area in Vinddal.* Modified from NVE 2019.
- NVE (2019c). *Aktsomhetskart for steinsprang*. Aktsomhetskart for steinsprang Mundal. 04.07.19. Available at: https://gis3.nve.no/link/?p=aktsomhetskartmundal
- Ochs, S. I. and Kober, F. (2008). Surface exposure dating with cosmogenic nuclides. *Eiszeitalter und Gegenwart Quaternary Science Journal*, *57*(1-2), 157-189
- Parsons, A. J. and Abrahams, A. D. (1987). Gradient particle size relations on quartz monzonite debris slope in the Mojave Desert. *Journal of Geology, 95*, 423-432
- Patten, R. S. and Knight, D. H. (1994). Snow avalanches and vegetation pattern in Cascade Canyon, Grand Teton National Park, Wyoming, USA. *Arctic and Alpine Research*, *26*(1), 35-41.

- Ritchie, A.M. (1963). Evaluation of rockfall and its control. *Highway Research Record, 17*(2), 13–28.
- Rocscience (2019). Terzaghi Weighting. Available at: https://www.rocscience.com/help/dips/dips/Terzaghi_Weighting.htm
- Sadeghipoor, K. Z., Lu, Y. and Susstrunk, S. (8–12 February, 2015). *Gradient-based correction of chromatic aberration in the joint acquisition of color and near-infrared images.* Proceedings of IS&T; SPIE EI: Digital Photography and Mobile Imaging XI. San Francisco, California, USA
- Sandersen, F., Bakkehoi, S., Hestnes, E., and Lied, K. (17–21 June 1996). *The influence of meteorological factors on the initiation of debris flows, rockfalls, rockslides and rockmass stability*. Proceedings of the 7th International Symposium on Landslides, Trondheim, Norway.
- Sanderson, J.D and Peacock, C. P. D. (2019). Line sampling of fracture swarms and corridors. *Journal of Structural Geology 122*(2019), 27-37.
- Schumm, S. A. and Chorley, R. J. (1964). The fall of endangering rock. *American Journal of Science, 262(*1), 1041–1054.
- Selby, M. J. (1982). Hillslope materials and processes. *Earth Surface Processes and Landform,s 9*(1), 264.
- Selby, M. J. and Hodder, A. P. W. (1993). Rock slope processes. *Hillslope materials and processes* (249) Oxford: Oxford University Press.
- Shi, B. and Liu, C. (9. December, 2015). *UAV for landslide mapping and deformation analysis.* International Conference on Intelligent Earth Observing and Applications. Guilin.
- Sigmond E. M. O., Bryhni I. and Jorde K. (2013). *Norsk geologisk ordbok* (1), Trondheim: Akademika forl.
- Skaar, E. (2004). Nedbør. *Grind – kunnskap om landskap*. Universitetet I Bergen, Bergen
- Statham, I. and Francis, S.C. (1986). Influence of scree accumulation and weathering on the development of steep mountain slopes. In Abrahams, A.D. (ed.). *Hillslope processes* (245-267). Winchester: Allen and Unwin Inc.
- Sulebak, J. R. (2007). Skråninger og massebevegelse. In Sulebak J.R. (eds.), *Landformer og prosesser: En innføring i naturgeografiske tema* (89-90), Bergen: Fagbokforlaget.
- Ten Brink, N. W. (1977). Colonisation, growth, succession and competition. In Seward, M. R. D (ed). *Lichen Ecology (31-68)*, London: Academic Press.
- Terzaghi, R.D. (1965). Sources of errors in joint surveys. *Geotechnique, 15*(3), 287-304.
- Torrero, L., Seoli, L., Molino, A., Giordan, D., Manconi, A., Allasia, P. and Baldo, M. (2015). The use of micro-UAV to monitor active landslide scenarios. *Eng Geol Soc Territory, 5,* 701–704
- Tveit, J. R. and Helliksen, D. (1997). *Geologisk kart over Norge*, berggrunnskart over Bergen – M 1:250 000: Norges geologiske undersøkelse
- Varnes, D. J. (1978). Slope movement types and proceses. In: Schuster, R. L., Krizek, R. J (eds.). *Landslides: Analysis and Control* (11-33). Washington D. C: Transportation and Road Research Board, National Academy of Science.
- Vasuki, Y., Holden, E. J., Kovesi, P. and Micklethwaite, S. (2014). Semi-automatic mapping of geological structures using UAV based photogrammetric data: an image analysis approach. *Comput Geosci, 69,* 22–32.

- Vasskog, K. (2011). *Continuous and episodic sedimentation in western Norwegian fjord lakes: a Holocene climatic perspective* (PhD). University of Bergen, Bergen
- Vidrih, R., Ribicv, M. and Suhadolc, P. (2001). Seismogeological effects on rocks during the 12 April 1998 upper Soca Territory earthquake (NW Slovenia). *Tectonophysics, 330*(3), 153–175.
- Vorren, T. O. and Mangerud, A. J. (2007). Norge trer fram. In: Ramberg I. B., Bryhni I., Nøttvedt A. (eds.), *Landet blir til: Norges geologi (2).* Trondheim: Geological Society of Norway.
- Walker, M. (2005). *Quaternary Dating Methods*. Antony Rowe Ltd, Chippenham: John Wiley & Sons Ltd
- Wang, X. and Mauldon, M. (2006). Proportional error of the Terzaghi correction factors. *American Rock Mechanics Association, 6(1055), 1-2*
- Wieczorek, G.F., Nishenkod, S.P. and Varnes, D.J. (1995). Analysis of rockfalls in the Yosemite Valley, California. In Daemen, J. J. K. and Schultz, R. A. (eds). *Rock mechanics: proceedings of the 35th US symposium (85-89).* Rotterdam: Balkema.
- Wieczorek, G. F., Snyder, J. B., Waitt, R. B., Morrissey, M. M., Uhrhammer, R.A., Harp, E. L., Norris, R. D., Bursik, M. I. and Finewood, L. G. (2000). Unusual July 10, 1996, rock fall at Happy Isles, Yosemite National Park, California. *Geological Society of America Bulletin, 112*(1), 75–85.
- Zellmer, J.T. (1987). The unexpected rockfall hazard. *Bulletin of the Association of Engineering Geologists, 24*(2), 281–83.